UNIVERSITY OF BIRMINGHAM

TOXICITY OF SILVER NANOPARTICLES IN THE BACTERIUM *PSEUDOMONAS PUTIDA*

by

FENG DONG

A thesis submitted to the

University of Birmingham

for the degree of

DOCTOR OF PHILOSOPHY

School of Biosciences

College of Life and Environmental Sciences

The University of Birmingham

November 2016

Abstract

This thesis investigated the toxicity of silver nanoparticles (AgNPs) in an environmental model bacterium *Pseudomonas putida*.

It is unclear whether the antimicrobial activities of AgNPs are exclusively mediated by the release of silver ions (Ag^+) or, instead, are due to combined nanoparticle and silver ion effects. Therefore, it is essential to quantify dissolved Ag in nanosilver suspensions for investigations of nanoparticle toxicity, but it is difficult to distinguish Ag^+ from AgNP effects during toxicity tests. A method to measure dissolved Ag in Ag^+/AgNPs mixtures was first developed by combining aggregation of AgNPs with centrifugation. Silver nanoparticles can be quickly aggregated by 2 mM Ca^{2+}, forming large clusters that can be sedimented in a low speed centrifuge. The sedimentation time of AgNPs was markedly reduced to 30 min due to Ca^{2+} mediated aggregation, which provides a convenient and inexpensive way to separate dissolved Ag from AgNPs, avoiding the long ultracentrifugation times to sediment small nanoparticles.

The discrepancy in the physicochemical properties of different AgNPs and their transformation under different conditions combine to contribute to the complexity of toxicity tests. The systematic and time-resolved characterization of AgNPs is required for toxicity assays. In this thesis, AgNPs were characterized at synthesis, during storage and after addition to microbial media. Stable, uncoated AgNPs were synthesized by a reproducible method. The long-term stability of AgNP stocks exposed to ambient air or under nitrogen atmosphere was compared. Silver nanoparticles underwent different

degrees of aggregation in Davis minimal media (DMM). Compared to the fast Ag^+ release in H_2O, uncoated AgNPs dissolved much slower in DMM.

The minimum inhibitory concentrations of Ag^+ and AgNPs for *Pseudomonas putida* steadily increased with increasing initial cell densities, suggesting that Ag was titrated away by the cells, decreasing the effective Ag concentration. Silver nanoparticles acted as a Ag reservoir, releasing new Ag^+ to add to the Ag stress. Silver ions had stronger toxicity than AgNPs and the toxicity of AgNPs was dominated by dissolved Ag.

However, whether AgNPs directly contribute to bacteria killing is controversial. Experimental evolution was used to ask whether bacteria respond differently to Ag^+ and AgNPs. It is hypothesized that bacteria will evolve differently in the presence of Ag^+ and AgNPs if these have different antibacterial activities. A *P. putida* population that has pre-evolved in DMM was treated with Ag^+ or AgNPs for 75 d. These populations evolved for ~500 generations, adapted to the presence of Ag^+ and AgNPs, and gained fitness. The mutations in the evolved populations stressed by Ag^+ and AgNPs displayed different patterns, indicating different toxicity mechanisms. The nonsynonymous mutations in AgNP-stressed populations were mostly associated with cell surface proteins. In contrast, Ag^+ stress selected for mutations in cytoplasmic proteins linked to metal metabolism. This suggests the existence of direct AgNP effects targeting the bacterial cell surfaces.

Acknowledgements

There are many people I would like to thank who have involved in my PhD. First, I need to thank my supervisors Dr Jan-Ulrich Kreft and Prof Eva Valsami-Jones. From scholarship application to every progress that I have achieved to make this thesis possible, Jan has given me kind help with great efforts. Under your supervision, I understand what are essential for an academic researcher. The inspiration from your attitude and enthusiasm for scientific research leads me to continue my academic career. I would like to extend my gratitude to Eva. Your generous support makes the laboratory life in FENAC productive. I have fortune of working with Dr Pablo Fuentes-Utrilla in the same laboratory. Not to mention your great help with the genome sequencing, your humour make the laboratory more enjoyable. I would like to thank Dr Emily Jane Richardson for help with the sequencing data analysis. Thanks must go to Dr Timothy Wells. I will not forget your precious time teaching me confocal microscopy and flow-cell. I am very grateful for the financial support from the Darwin Trust of Edinburgh, allowing me this precious opportunity of doing PhD research at the University of Birmingham.

I am lucky to study alongside with Dr Robert Clegg. I would like to thank your advice for my settlement in UK, especially your help for my English improvement. I think I will keep in deep memory about the four years in the same office. Special thanks must go to you for your help with the codes. I am thankful to Huey How. Your help for my early experiment are valuable. Big thanks go to Dr Christine Elgy and Marie-France

Belinga in FENAC for helping me with the instruments for nanoparticle analysis. I would like to thank Paul Stanley and Theresa Morris from the Centre for Electron Microscopy. I am thankful for the help with many valuable data from Nurul Mohd Zaidi. A big thank you goes to Joanna Summers for language help in this thesis.

All the support and encouragement outside of laboratory are important to help me go through the PhD. I need to thank all my friends and housemates enjoying the life out of sciences. Finally, I must say a huge thank you to my parents and sister. Words definitely cannot describe your love in my life. The confidence and courage in my PhD come from your endless support. I am really grateful.

TABLE OF CONTENTS

List of Tables ..... **vii**

List of Figures ..... **viii**

List of Abbreviations ..... **x**

1 Chapter One Introduction **1**

1.1 Nanomaterials and silver nanoparticles 2

1.1.1 Nanomaterials 2

1.1.2 Silver nanoparticles 4

1.2 Environmental impact of AgNPs 7

1.3 Synthesis of AgNPs 10

1.4 Characterization of nanomaterials 14

1.5 Physical and chemical transformations of AgNPs 18

1.5.1 Dissolution 18

1.5.2 Surface chemistry 21

1.5.3 Aggregation 22

1.6 Toxicity of Ag^+ and AgNPs to microorganisms 24

1.6.1 Toxicity of Ag^+ 24

1.6.2 Bacterial resistance to Ag 27

1.6.3 Toxicity of AgNPs 32

1.7 Overview of the thesis 36

2 Chapter Two New, Rapid Method to Measure Dissolved Silver Concentration

in Silver Nanoparticle Suspensions by Aggregation Combined with Centrifugation 39

2.1 Introduction 40

2.2 Materials and methods 42

2.2.1 Synthesis of uncoated AgNPs 42

2.2.2 Characterization of uncoated AgNPs 42

2.2.3 Determining aggregation kinetics of AgNPs in $Ca(NO_3)_2$ solutions 44

2.2.4 Centrifugation of AgNPs in $Ca(NO_3)_2$ 44

2.2.5 Measurement of AgNP content in supernatant after centrifugation of AgNPs in $Ca(NO_3)_2$ 45

2.2.6 Measuring dissolved Ag in AgNPs suspension with aggregation-centrifugation or ultrafiltration 46

2.3 Results 47

2.3.1 Synthesis of uncoated AgNPs 47

2.3.2 AgNPs aggregate in $Ca(NO_3)_2$ solutions 49

2.3.3 Concentration dependence of aggregation of AgNPs in $Ca(NO_3)_2$ 51

2.3.4 Time required to sediment AgNPs after aggregation 54

2.3.5 Sedimentation of Ca^{2+}-aggregated AgNPs is complete 55

2.3.6 Measuring dissolved Ag in AgNP suspensions by aggregation or ultrafiltration 57

2.4 Discussion 60

2.4.1 Formation of stable, uncapped AgNPs 60

2.4.2 Aggregation of AgNPs in $Ca(NO_3)_2$ solution 60

2.4.3 Efficiency of AgNP sedimentation in $Ca(NO_3)_2$ solution by centrifugation 61

2.4.4 Comparing the aggregation-centrifugation method with ultrafiltration. 63

2.5 Conclusions 65

3 Chapter Three A Real-time Toxicity Study Reveals the Dynamic Interactions between Uncoated Silver Nanoparticles and Bacteria 66

3.1 Introduction 67

3.2 Materials and methods 69

3.2.1 Synthesis of uncoated AgNPs 69

3.2.2 Characterization of AgNPs 69

3.2.3 Storage of AgNPs 69

3.2.4 Aggregation of AgNPs in defined medium 70

3.2.5 Dissolution of AgNPs 71

3.2.6 Bacterial strain and culture conditions 72

3.2.7 Measurement of growth rate 72

3.2.8 Determination of MICs 74

3.2.9 AgNP and Ag^+ kill kinetics 75

3.3 Results 77

3.3.1 Synthesis and characterization of uncoated AgNPs 77

3.3.2 Stability of AgNPs during long-term storage 78

3.3.3 Aggregation of AgNPs in a mineral medium 80

3.3.4 Dissolution of AgNPs in a mineral medium 81

3.3.5 Growth rates of *P. putida* 84

3.3.6 Effect of cell density on inhibition 85

3.3.7 Growth rate depends on Ag^+ or AgNP concentration 86

3.3.8 Inhibition kinetics 87

3.3.9 High-resolution inhibition kinetics 90

3.4 Discussion 94

3.4.1 Formation and stability of uncapped AgNPs 94

3.4.2 Aggregation of AgNPs in mineral growth medium 94

3.4.3 Dissolution of AgNPs in H_2O and mineral growth medium 95

3.4.4 Cell density effects 96

3.4.5 Inhibition kinetics of Ag^+ and AgNPs 97

3.4.6 Quantifying the toxicity of Ag^+ and AgNPs 97

3.5 Conclusions 99

4 Chapter Four Experimental Evolution of *Pseudomonas putida* under Silver Ion and Nanoparticle Stress 100

4.1 Introduction 101

4.2 Materials and methods 103

4.2.1 Preparation of AgNPs 103

4.2.2 Characterization of AgNPs 103

4.2.3 Bacterial strains and media 105

4.2.4 Evolution experiment 105

4.2.5 Fitness assay 108
4.2.6 Whole genome sequencing 109
4.2.7 Variant calling 110
4.2.8 Association of mutations with selective pressures 111
4.3 Results 112
4.3.1 Synthesis and stability of AgNPs 112
4.3.2 Fitness of evolved populations 114
4.3.3 Mutations during the pre-evolution experiment 118
4.3.4 Mutations during the main evolution experiment 119
4.3.5 Mutations that differ between exposure to Ag^+ or AgNPs 121
4.4 Discussion 124
4.4.1 Silver nanoparticles for the evolution experiment 124
4.4.2 Pre-evolution experiment 124
4.4.3 Fitness improvements 125
4.4.4 Differential mutation profiles 126
4.4.5 Differential mutations in response to AgNP versus Ag^+ stress 127
4.4.6 Functions of mutated genes 128
4.5 Conclusions 131
5 Chapter Five Conclusions and Future Work 132
5.1 Conclusions 133
5.2 Future work 134
6 References 137

7 Appendices.....156

Appendix 1 Mutations in population in the pre-evolution experiment.....157

Appendix 2 Mutations in populations in main evolution experiment.....159

Appendix 3 List of mutations in the coding regions for the populations in main evolution experiment.....176

List of Tables

Chapter One

Table 1.1 Standard reduction potential of different chemicals (pH = 7)..... 13

Table 1.2 Comparison of different techniques for characterizing the size of nanomaterials 17

Chapter Two

Table 2.1 Characteristics of AgNPs 47

Chapter Three

Table 3.1 Characteristics of uncoated AgNP suspensions……...77

Table 3.2 Dissolution rates of AgNPs in DMM salts solution and H_2O 82

Table 3.3 Cell viability and dissolved Ag concentration…….…….89

Table 3.4 Specific death rate 93

Chapter Four

Table 4.1 Mid-p-values calculated with a modified Fisher's exact test for association between mutation and condition 111

List of Figures

Chapter One

Figure 1.1 Morphologies of different nanomaterials 4

Figure 1.2 Concentration of Ag in environment 10

Figure 1.3 Schematic diagram of the formation of AgNPs 14

Figure 1.4 Antibacterial activities of Ag (Gram-negative bacterium as the model) 27

Figure 1.5 Bacterial resistance to Ag 32

Chapter Two

Figure 2.1 Characterisation of uncoated AgNPs and reproducibility of synthesis 48

Figure 2.2 Aggregation of AgNPs in 2 mM $Ca(NO_3)_2$ solution 50

Figure 2.3 Calibration of UV-Vis absorption against concentration for AgNPs 51

Figure 2.4 Aggregation kinetics of AgNPs in $Ca(NO_3)_2$ solution 53

Figure 2.5 TEM images of AgNPs aggregates 54

Figure 2.6 The time required to sediment AgNPs 55

Figure 2.7 Sedimentation of AgNPs in $Ca(NO_3)_2$ by centrifugation 57

Figure 2.8 Comparison of aggregation-centrifugation with ultrafiltration 58

Figure 2.9 Adsorption of Ag^+ to ultrafiltration units during ultrafiltration 59

Figure 2.10 Simulation of sedimentation of AgNPs by centrifugation 62

Chapter Three

Figure 3.1 Flow-cell system 74

Figure 3.2 Characteristics of uncoated AgNPs 78

Figure 3.3 Stability of uncoated AgNPs stored in ambient air or under nitrogen 79

Figure 3.4 TEM images of AgNPs stored under nitrogen or in ambient air over time 80

Figure 3.5 Aggregation kinetics of AgNPs in DMM salts solution 81

Figure 3.6 Dissolution or adsorption kinetics of AgNPs in H_2O or DMM salts solution 83

Figure 3.7 Growth rate of *P. putida* KT2442 84

Figure 3.8 MICs of Ag^+ and AgNPs increase with initial cell densities 86

Figure 3.9 Effect of Ag^+ and AgNPs on specific growth rate 87

Figure 3.10 Toxicity kinetics of Ag^+ or AgNPs to *P. putida* 89

Figure 3.11 High-resolution inhibition kinetics 91

Figure 3.12 Dependence of death rates on silver concentrations 92

Chapter Four

Figure 4.1 Schematic diagram of evolution experiment 106

Figure 4.2 Properties of AgNPs for evolution experiment 113

Figure 4.3 Evolved and reference cells on the same LB plate 115

Figure 4.4 Reproducibility of the fitness assay and relative fitnesses of the evolved populations 118

Figure 4.5 Number of mutations in populations in main evolution experiment 121

Figure 4.6 Mutations in the populations of the main evolution experiment 123

Figure 4.7 Different adaption models in *Pseudomonas putida* under the stress of Ag^+ or AgNPs 130

List of Abbreviations

Asymmetric flow field-flow fraction	AF4
Asymmetrical flow field-flow fractionation coupled with inductively coupled plasma mass spectrometry	AF4-ICP-MS
Atomic force microscopy	AFM
Borohydride	BH_4^-
Bovine serum albumin	BSA
Branched polyethyleneimine	BPEI
Coding region	CDS
Critical coagulation concentration	CCC
Davis minimal medium	DMM
Deionized	DI
Derjaguin-Landau-Verwey-Overbeek	DLVO
Differential centrifugal sedimentation	DCS
Dynamic light scattering	DLS
Electron transport chain	ETC
Extracellular polymer substance	EPS
Field-flow fraction	FFF
Gold nanoparticle	AuNP
Graphite furnace atomic absorption spectrometry	GFAAS
Green fluorescent protein	GFP
Hydrogen peroxide	H_2O_2
Ion-selective electrode	ISE
Localized surface plasmon resonances	LSPR
Lysogeny broth	LB
Minimum inhibitory concentration	MIC

Mercury	Hg	
Nanomaterial	NM	
Nanoparticle tracking analysis	NTA	
Optical density	OD	
Poly(3-(6-(1-methylimidazolium-3-yl)hexyl)thiophene-2,5-diyl bromide		PMHT
Poly(vinyl pyrrolidone)	PVP	
Proton motive force	PMF	
Quantum dot	QD	
Reactive oxygen species	ROS	
Scanning electron microscopy	SEM	
Silver	Ag	
Silver ion	Ag^+	
Silver nanoparticle	AgNP	
Single nucleotide polymorphism	SNP	
Single particle inductively coupled plasma mass spectrometry		SP-ICP-MS
Sodium borohydride	$NaBH_4$	
Solubility constant	K_{sp}	
Standard deviation	SD	
Standard error	SE	
Superoxide dismutase	SOD	
Transmission electron microscopy	TEM	
Tricarboxylic acid	TCA	
Wastewater treatment plant	WWTP	

1 Chapter One

Introduction

1.1 Nanomaterials and silver nanoparticles

1.1.1 Nanomaterials

Nanomaterials (NM) have obtained increasing attention owing to their distinctive physicochemical properties. Nanomaterials are defined as materials that have one or more dimensional size in the nanoscale (1-100 nm) [1]. The components of nanomaterials include metal, metal oxide, semiconductor, carbon, silicon and organic substances with different shapes such as spheres, cubes, rods, plates and tubes (Figure 1.1). Most of the inorganic NMs have a solid core that is capped with various chemicals (e.g. ligand, surfactant, polymers and biomolecules) on the surface for stabilization or functionalization [2].

The speciality of nanomaterials derives from their small size and large surface area-to-volume ratio, contributing to their quite different chemical [3], electronic [4], magnetic [5], and optical [6] properties from molecular and bulk counterparts. The application of nanomaterials has extended into broad fields, including medicine [7], biological sensor [8], antimicrobial agents [9], energy conservation [10], and catalysts [11]. For instance, semiconductor nanoparticles named as quantum dots (QDs) with a size of 2-10 nm have been used as fluorescent labels because of their bright tuneable emission spectra [12]. Gold nanoparticles (AuNPs) have been studied for disease diagnoses, drug delivery and thermal therapy due to their chemical stability, pronounced absorption of visual spectra and capability of efficiently converting light into heat [13]. Iron oxide nanoparticles have been explored as contrast agents in magnetic resonance imaging and

drug delivery because of their magnetic properties, biocompatibility and biodegradability [5]. Metal oxides (ZnO, CuO, CeO, TiO_2 and Al_2O_3), cationic antimicrobial peptides and some polymers in the nanoform have shown promising application in antimicrobial therapies, which can be used to modify medical devices, preventing clinical device-related infection and killing multidrug resistance pathogens [14]. Organic nanomaterials, such as liposomes, dendrimers, micelle and polymers, can be used as drug carriers for cancer treatments owing to their enhanced permeability and retention in tumour tissue and the ability to specifically target cellular surfaces [15]. Significant progress has been achieved in the synthesis and application of nanomaterials during the last two decades; but nanoscience is challenged by large-scale production for commercialization, precise control of size and shape, characterization *in vivo*, and their impacts on environment and human health.

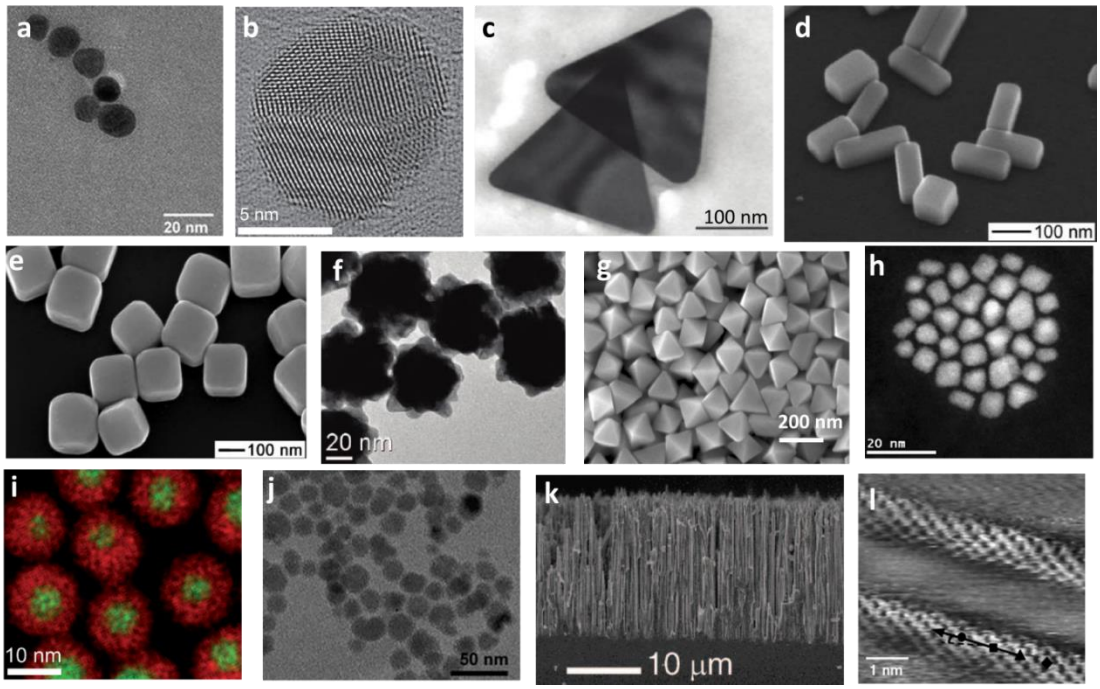

Figure 1.1 Morphologies of different nanomaterials
(a) Uncoated silver nanoparticles by transmission electron microscopy (TEM) [16]. **(b)** High resolution TEM image of uncoated silver nanoparticles [17]. **(c)** Citrate-capped silver nanopaltes (TEM) [18]. **(d)** Cetyltrimethylammonium bromide capped silver nanobars by scanning electron microscopy (SEM) [19]. **(e)** SEM image of silver nanocubes coated by poly(vinyl pyrrolidone) (PVP) [20]. **(f)** Flower-like gold nanoparticles coated by 2-[4-(2-hydroxyethyl)-1-piperazinyl]ethanesulfonic acid (HEPES) (TEM) [21]. **(g)** Cetylpyridinium chloride-capped gold nanocrystals (SEM) [22]. **(h)** High resolution TEM images of CdSe/ZnS core-shell quantum dots (QDs) [23]. **(i)** Core-shell structure of gold-palladium nanoparticles that are produced by depositing Pd atoms to the surface of Au nanoparticle seeds (Scanning TEM coupled with energy dispersive X-ray spectroscopy). Green colour refers to gold, and red colour refers to palladium [24]. **(j)** Polyvinylpyrrolidone-coated iron oxide nanoparticles [25]. **(k)** Cross-sectional SEM of vertically aligned silicon nanowire [26]. **(l)** Atomic structure of single-walled carbon nanotubes by scanning tunnelling microscopy [27].

1.1.2 Silver nanoparticles

Silver (Ag) is toxic to microorganisms. Silver sulfadiazine, traditionally, has been used as an antibacterial agent for a long time [28]. In the early antimicrobial applications, Ag was used for the treatment of eye infection and wound [28, 29]. Accompanying prolonged silver treatment, however, the deposition of silver in skin or tissue can cause

mucous membranes and darkness of skin that are referred to as argyria. Silver ions (Ag^{+}) can damage cell membranes, interact with ribosomes to inhibit protein production, and affect respiratory chains [30-32]. With the emergence of nanotechnology, silver nanoparticles (AgNPs) are one of the widely studied metal nanomaterials [9, 33]. Silver atoms gather together forming nanosize particles with different sizes, shape and surface coatings [34, 35]. Silver nanoparticles promote the application of Ag owing to their capability of delivering Ag to targets and high surface reactivity.

Silver nanoparticles have been used as antimicrobial agents in water treatment, cloth manufacture, burn and wound dressing, food packaging, medicine and medical instrument coating [9, 36-38]. Modifying the surface of medical devices and fabrics (e.g. heart valves, catheters and wound dressings) with antimicrobial components is believed to be an effective way to prevent healthcare-related infections and to improve healing performance in clinical practice [7]. According to a systematic comparison of antibiotic-impregnated, silver-impregnated and plain external ventricular drainage catheters for the prevention of catheter-related infections, the catheters with silver and antibiotics have similarly strong effectiveness for infection control [39]. In a clinical study, however, the catheters that are coated with chlorhexidine and silver sulfadiazine have less efficiency than minocycline and rifampin impregnated catheters in surgical intensive care units [40, 41]. The AgNP-modified catheters have also shown no significant difference in reducing catheter-related bloodstream infections from nonimpregnated catheters [42]. It is found that silver-impregnated external ventricular drain catheters may have a preferential reduction in Gram-positive bacteria in a meta-

analysis of several clinic trails [43]. The toxic effect of AgNPs depends on the characteristics of AgNPs and surrounding environment. The complexity of clinical setting complicates the action of AgNPs, hindering consistent conclusion from different studies.

Although there is no consensus on the effectiveness of impregnating silver onto a surface to prevent bacterial colonization and infection, AgNPs are still considered as a new generation of product for biomedical applications [9]. Acticoat, an approved AgNPs-coated wound dressing, has shortened healing time in a clinical study compared to silver sulfadiazine [37]. Treating wounds with AgNPs-contained dressings can raise serum silver levels but these decrease to baseline after stopping the treatment [44]. Laboratory-based studies have demonstrated the benefits of AgNPs, which can prevent bacterial growth and biofilm formation on the surface of medical devices [45]. Depositing AgNPs on a layer of pentafluorophenyl methacrylate that is coated on the surface of tracheal prosthesis gives rise to complete bacteria death on the surrounding surface and can reduce biofilm fouling [46]. The cover slips that are coated with mercaptosuccinic-AgNPs can kill both Gram-positive and Gram-negative pathogens and have significant antibiofilm activities without showing any negative effects on the function and viability of primary fibroblast cells and innate immune cells [47]. Silver nanoparticles undergo different transformations on contact with biological fluids, especially after prolonged exposure. One of the important changes is surface deactivation that inhibits Ag release, leading to less active Ag^{+} available for pathogen killing [48], which might explain the failure of some clinical trials.

Conventional methods may have limits in removing emerging and trace pollutants such as pharmaceuticals, personal care products and disinfection by-products to meet the increasingly stringent water quality standards. Nanosciences have obtained intensive interests in water treatment, water quality monitoring, recovery of contaminated environment, and water reuse [49]. Silver nanoparticles are promising candidates for water disinfection and membrane fouling control [50]. The AgNPs that are immobilized in alginate have reduced cell viability by five orders-of-magnitude after a contact as short as 1 min, demonstrating their great potential in killing pathogens in drinking water [38]. Sustainability and high efficacy are critical for large-scale commercialization of AgNP-based technologies. The AgNPs trapped in a stable metal oxyhydroxide-chitosan cage can slowly release Ag^{+} into water, deactivating bacteria and viruses while absorbing chemical contaminants [51]. Incorporating AgNPs into ultrafiltration membrane can reduce bacteria attachment and biofilm formation on membrane surfaces, which are used to control membrane fouling that usually causes deterioration of membrane water treatment plants [52]. The cost and performance stability should also be considered in the application of AgNPs in water treatment [53].

1.2 Environmental impact of AgNPs

One of the challenges of nanomaterials is the risk to ecosystem and human health, which is not well understood [54]. Silver nanomaterials are of especial concern due to their high toxicity towards living organisms, including bacteria [55], fungi [56], algae [57], plants [58] and animals [59, 60]. Silver cannot be destroyed or degraded after

being extracted. Except for those being recycled or within silver products, most silver will be disposed into the natural environment. It is estimated that more than 13 metric tons of Ag are globally emitted into the environment, most of which are discharged via landfill, in tailings of mining operations or by leaching during Ag separation and dissipation [61].

Jewellery, photography and industry contribute to 95% of total silver consumption [62], but the use of silver has changed during the past decade with increasing demand in textiles, plastics and medical industries [61]. With the advent of nanotechnology, the production of silver nanomaterials is also expected to grow. The annual production of silver nanoparticles was about 320 tons/year worldwide in 2012 and was estimated to reach 1120 tons/year in 2015 [63, 64]. Currently, AgNPs are mainly used in textiles, cosmetics, electronics and anti-microbial coatings [62, 63]. The majority of Ag is disposed as waste in municipal solid, electrical and electronic equipment, hazardous chemicals, sewage and sewage sludge estimated by a life cycle assessment [61]. For instance, the Ag in biocidal products that comprise more than 15% of total silver has flowed into wastewater, and is treated in wastewater treatment plants and deposited in sewage sludge [65]. Silver nanoparticles in fabrics can be released during washing, and disposed through landfill together with the fabrics [66]. Once AgNPs enter the sewage collection system, more than 90% of the Ag will be transformed into Ag_2S accumulated in the sludge of wastewater treatment plants (WWTP) and 10% of silver will be disposed into natural surface water [65, 67, 68]. Silver sulphide is extremely insoluble in water and is much less toxic towards microorganisms. To fully understand the

environmental fate of AgNPs, it is necessary to investigate the changes of silver sulphide complexes when the sewage sludge is transferred for landfilling, agricultural land or incineration [69]. The solid-waste incinerator can remove engineered nanoparticles from emitted gas but shifts most of them into slag and fly ash, since they remain stable after incineration, which still carry risk when disposing of the slag and fly ash residuals [70]. The increased AgNP levels in the receiving river is reported to be correlated with high concentrations of Ag in effluent from WWTP, but will be diluted to a few ng/L with water flow [71]. The impact of this low concentration of AgNPs on the environment is unknown.

Silver content in natural water is very low (Figure 1.2), but the bioaccumulation in organisms may promote Ag concentrations to a toxic level, which brings the concern about their environmental risk owing to the increasing use of silver products. The concentration of Ag in the open North Pacific Ocean ranges from 0 to 1.3 ng/L [72]. Dissolved Ag in the Bothnian sea is 0.26 ± 0.1 ng/L on average, which is comparable to the level in open ocean [73]. Silver-chloride complexes ($AgCl_x^{(x-1)-}$) are the dominate Ag species in sea water [74]. As a result of anthropogenic input, Ag contents in estuarine water and coastal regions are higher, in the range of 0.5-35 ng/L [74, 75]. It is predicted by life-cycle simulation that the upper level concentration of nanosilver in air, water and soil is 4.4 ng/m^3, 80 ng/L and 100 ng/kg, respectively [62]. The predicted concentration of Ag nanomaterials in Swiss rivers ranges from 0 to 6.7 ng/L [76]. It has been reported that the average concentration of Ag in typical soil in Japan is 0.17 ± 0.08 mg/kg [77]. A study reveals that the Ag content in sewage-treated soil in Berlin is 16.6

mg/kg, which is high compared with 0.62 mg/kg in forest soil [78]. Silver content in sewage (8-800 mg/kg) is much higher than the background level (0.1 mg/kg), suggesting that long-term use of activated sludge as a soil conditioner poses the risk of Ag enrichment [67].

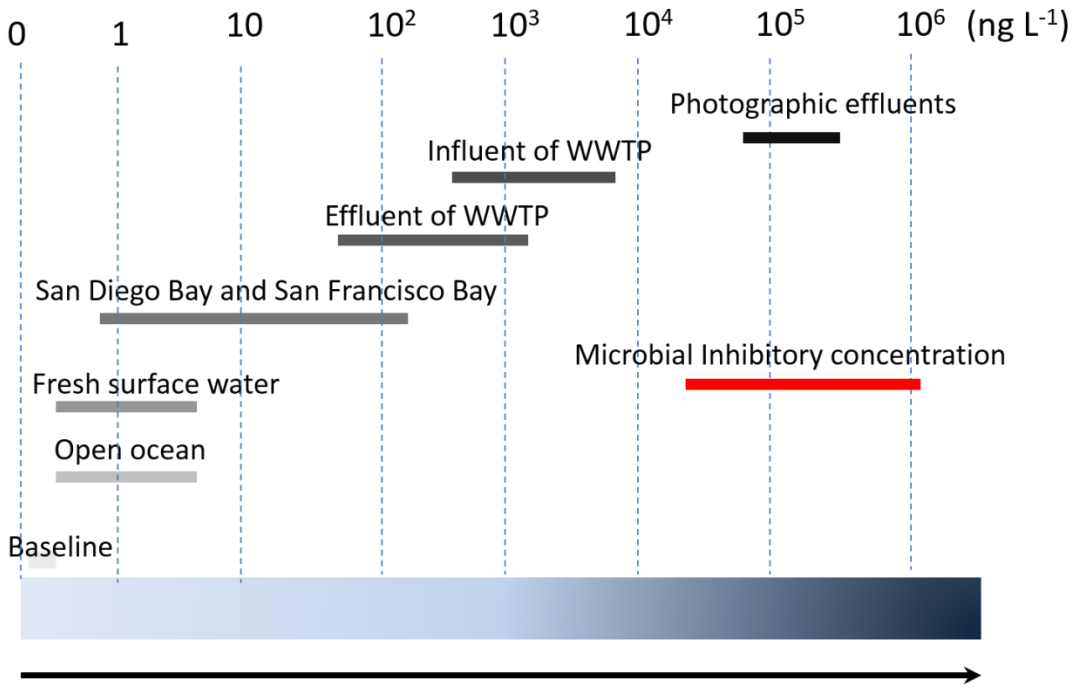

Figure 1.2 Concentration of Ag in environment

The arrow indicates an increasing Ag concentration. In open ocean and fresh surface water compartments, Ag concentration is lower than 10 ng/L. Silver contents in estuarine water and coastal regions (San Francisco Bay) are in the range of 0.5-35 ng/L owing to anthropogenic activities. The Ag content in sewage influent is 1.8-100 μg/L since many silver-containing products are discharged into wastewater collection systems. Wastewater treatment plants have a removal efficiency of >95% for immobilization of Ag into sewage sludge. The photographic industry emit large amount of Ag-containing waste, the contribution of which is diminishing as digital photographs become dominant. The microbial inhibitory concentration of Ag^+ ranges from 0.05 to 2 mg/L, which is much larger than the concentrations in the natural environment.

1.3 Synthesis of AgNPs

There are three steps in nanocrystal formation [16, 79] (Figure 1.3). First step is the rapid reduction of silver precursor forming a silver nucleus. The burst nucleation forms

monomers that are the basic building units of nanocrystals. They diffuse and precipitate on the surface of the nucleus to form large particles. Meanwhile, small nanoparticles have a tendency to dissolve owing to their high surface energy. The formation process of nanoparticles is thermodynamically controlled by the competition between growth and dissolution.

Burst nucleation induces high concentrations of monomers. If the growth process is diffusion controlled, it can be described as

$$dr/dt = V_m D(C_b - C_s)/r \quad (1.1)$$

where C_b is the monomer concentration in bulk. C_s is the monomer concentration on particle surfaces. r is the size of particles. Smaller particles have higher chemical potential and need to overcome higher energy barriers for growth:

$$S_r = S_b \exp(2\sigma V_m/rRT) \quad (1.2)$$

Where S_r and S_b are the solubility of nanocrystals and bulk solid, respectively. σ is the specific surface energy. V_m is the molar volume of the material. R is the gas constant. T is the temperature. A critical size, r^*, exists. Dissolution dominates for the nanocrystals that have a size below r^* and the nanocrystals that have a size larger than r^* will form mature nanoparticles. The growth rate is described as:

$$\frac{dr}{dt} = K(1/r + 1/\delta)(1/r^* - 1/r) \quad (1.3)$$

Where K is a constant that is proportional to the diffusion constant of the monomer. δ is the thickness of the diffusion layer. r^* is the critical size.

Another process called Ostward ripening also controls nanoparticle's growth [79]. The critical size will increase after monomers are depleted. Larger particles are more likely

to grow by receiving monomers from dissolving particles and smaller particles shrink or even disappear, resulting in the restriction of size to certain regions. During the formation of AgNPs, the concentration of monomers is changing. Therefore, the critical size, growth rate and final stable size distribution, which are dependent on monomer concentrations, change accordingly. In addition, nanoparticles with the same crystallographic orientation can directly combine together to form large particles, which is known as coalescence and aggregative growth [80, 81]. Some capping agents and ions preferably interact with certain nanoparticle's surfaces and can direct nanoparticles to grow into different sizes and shapes [35].

Frequently, AgNPs are produced by reducing Ag^+ into metallic Ag in solution [35, 82]. Silver nanostructures in the forms of particles, rods, plates and cubes can be achieved by adjusting temperature, precursor concentration, reducing agent, capping agent and reaction kinetics [20, 35]. The comparison of standard reduction potential of Ag^+/Ag with different chemicals is listed in Table 1.1 [83]. Silver ions have a high potential of being reduced to metallic Ag due to their strong capability as an electron acceptor. Reducing agents such as ethylene glycol [20], citrate [84], sodium borohydride ($NaBH_4$) [16], poly(vinyl pyrrolidone) (PVP) [82] and oleylamine [85] have been used to react with Ag^+ forming AgNPs. Green synthesis of AgNPs can be obtained by using environment-friendly reductants such as starch [86], peptides [87] and leaf extract [88]. Peptides that contain silver-binding amino acid moieties can selectively provide deposit sites for Ag^+ and a reducing environment to direct the growth of AgNPs [89]. Given the relatively reducing environment and rich content of proteins in bacterial cells, it is not

surprising that *Pseudomonas stutzeri* are capable of reducing Ag^+ to different sizes and shapes of Ag nanocrystals that are mostly accumulated in the periplasm [90]. Demonstrated by darkfield microscopy and hyperspectra, *Chlamydomonas reinhardtii* take up Ag^+ and reduce them into AgNPs in cells [91]. Silver nanoparticles have been found in natural environment where Ag^+ react with natural organic substances to form Ag nanocrystals and the generation rate is accelerated under elevated temperatures or with intensive light exposure [92]. It is postulated that phenolic natural organic matter (DOM) in rivers react with dissolved oxygen under sunshine to produce superoxide free radicals that reduce Ag^+ to form AgNPs [93].

Table 1.1 Standard reduction potential of different chemicals (pH = 7)

Half-cell reaction	Potential (mV)
$CO_2 + 4H^+ + 4e^- \rightarrow [CH_2O]glucose + H_2O$	-430
$2H^+ + 2e^- \rightarrow H_2$	-420
$NAD^+ + 2H^+ + 2e^- \rightarrow NADH + H^+$	-320
$FAD + 2H^+ + 2e^- \rightarrow FADH_2$	-220
$FMN + 2H^+ + 2e^- \rightarrow FMNH_2$	-190
$NO_3^- + 6H^+ + 5e^- \rightarrow 1/2N_2 + 3H_2O$	+740
$Fe^{3+} + e^- \rightarrow Fe^{2+}$	+770
$Ag^+ + e^- \rightarrow Ag$	+799
$1/2O_2 + 2H^+ + 2e^- \rightarrow H_2O$	+820

To reduce the surface energy, nanomaterial cores have the tendency to absorb or react with molecules such as inorganic [94] or organic ions [84] and polymers [20, 95]. The surface coating provides an identity for nanoparticles which can be specifically functionalized for different purposes, such as molecule sensing and drug delivery [96].

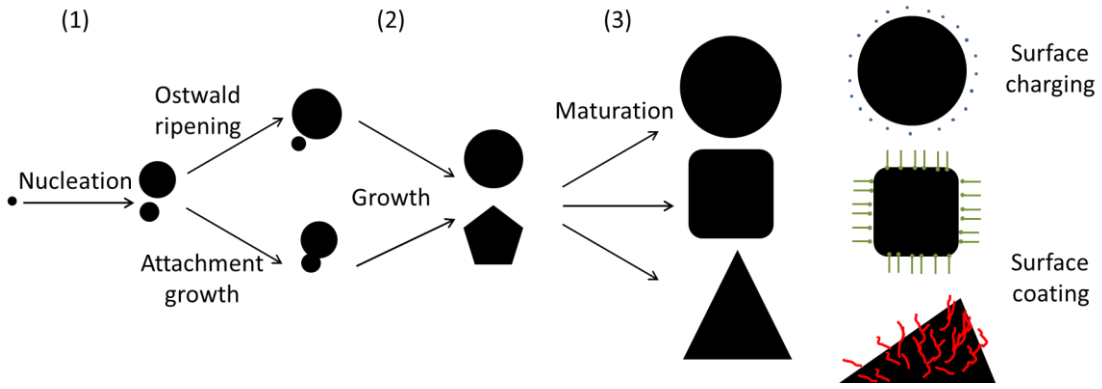

Figure 1.3 Schematic diagram of the formation of AgNPs
(1) Silver ions are reduced to form metallic Ag as nuclei in different sizes (nucleation). (2) The nuclei will grow into relatively large AgNPs, this is controlled by Ostward ripening and attachment growth. These Ag nanocrystals may have different morphologies with a relatively narrow size distribution. (3) If there are more Ag^+ reduced to atomic Ag, the AgNPs will grow further to generate mature nanoparticles in various shapes under the control of capping agents. Finally, ions (for charging) and large molecules (for coating) are attached to nanoparticle's surface for stabilization.

1.4 Characterization of nanomaterials

It is important to characterize nanomaterial physical and chemical properties, including elemental composition, morphology and surface chemistry, which have fundamental roles in nanomaterial interactions with surrounding environments. Energy dispersive X-ray spectroscopy, electron energy loss spectroscopy and X-ray powder diffraction can be used to detect the elemental compositions of nanomaterials and have been used to examine the oxidation [97], sulfidation [98] and dissolution [99] of AgNPs, detect AgNPs in organisms [100], and investigate the formation of AgNPs in cells [90]. The arrangement of atoms into nanoparticles has been revealed at atomic resolution using high-angle annual dark field scanning transmission electron microscopy [101]. It is difficult to characterize the surface chemistry of nanoparticles by conventional techniques. By investigating p-mercaptobenzonic acid-protected gold nanoparticles

through X-ray crystal structure at single atom resolution, it was found that the surface ligands not only bind with the surface atoms of nanoparticles but also interact with each other through phenyl-phenyl and phenyl-sulphur interactions forming a rigid shell layer on the surface [102].

It is critical to characterize the size [59, 103] and shape [6, 104] of nanomaterials. Due to the resolution limits of light microscope, electron microscopy, including transmission electron microscope (TEM) and scanning electron microscope (SEM), is applied to observe nanomaterials. But they usually measure the nanomaterial core and need tedious sample preparation and image capture. Atomic force microscopy (AFM) can be used to measure size and number distribution of nanoparticles [105] as well as the change of size [106]. By utilizing the high light reflectivity of metal nanoparticles, dark field microscope can detect AgNPs distribution around and inside cells [91, 107]. Dynamic light scattering (DLS) is the most common technique for measuring the hydrodynamic size of nanomaterials. It calculates nanoparticle size based on the pattern of scattered light for different size of nanoparticles, which is induced by the Brownian motion of nanoparticles. Asymmetric flow field-flow fraction (AF4) and differential centrifugal sedimentation (DCS) are based on the movement of nanoparticles under the force of liquid flow and centrifugation, which also measure hydrodynamic size that is always larger than nanoparticle's core size. Single particle inductively coupled plasma mass spectrometry (spICP-MS) is an emerging nanoparticle size characterization technique and can measure the environmentally relevant concentration of nanoparticles and their aggregates in complex matrix but needs complicate initial parameter setting

to measure large size nanoparticles (> 20 nm) [108]. Different size characterization techniques have their advantages and limitations as listed in Table 1.2. Electron microscopy and AFM analyse the sizes of nanoparticle cores. DLS, FFF, DCS and NTA measure the hydrodynamic sizes of nanoparticles that include the core, surface coating and surrounding solvated ions, which are larger than the diameter of cores.

Table 1.2 Comparison of different techniques for characterizing the size of nanomaterials

Technique	Advantages	Disadvantages
TEM	• Observe the structure at atomic level • Directly measure size and shape with high accuracy • Visualize interactions between nanomaterials and various objects • Small amount of samples	• Require large number of counts from image analysis • Potential artefacts, especially aggregates during drying and sample fixation • Cannot measure nanoparticles in solution
SEM	• Directly observe three-dimensional structure at nanometre resolution • Measure size and shape of large nanoparticles with high accuracy	• Long time for sample preparation and image capture • Potential artefacts • Cannot measure small nanoparticles
AFM	• Roughly measure the size distribution at nanometre level • Can measure the sample in complex environments	• Cannot observe the detailed structure • Need to fix sample on substrate which may produce artefacts
DLS	• Measure the sample with a broad ranges of sizes from nm to μm in solution • Convenient and quick operation	• Only measure the hydrodynamic size • Need monodispersed samples • Cannot measure very diluted samples • Large error for small nanoparticles
FFF	• Measure hydrodynamic size of samples in complex environment with good accuracy • Can measure poly-dispersed samples in liquid	• Need standards for calibration • Time consuming and complex to optimize operation
DCS	• Measure hydrodynamic size of sample in liquid with high accuracy • Probably able to measure the thickness of surface coating but will need good experiment design	• Sample should be larger than 3 nm • Need standards for calibration • Limited to concentrated samples for high accuracy • Long operation time to measure small nanoparticles
NTA	• Measure the samples with large size in complex environment • Can give estimate of particle number concentration	• Can only measure large nanoparticles (> 10 nm) with very high refractive index with accuracy • Low accuracy for poly-dispersed samples • Needs dilute samples
spICP-MS	• Detect low concentration of samples in the μg/L range • Can measure the number and size distribution at the same time • Can measure polydispersed samples with high precision • Require low sample volumes	• Have the size limitation of 20 nm • Complicated parameter setting • Need validation with standards • Lack of selectivity to detect different nanoparticles with different elemental compositions

AFM: atomic force microscopy; NTA: nanoparticle tracking analysis; FFF: field-flow fraction; spICP-MS: single particle inductively coupled plasma mass spectrometry.

Metal nanomaterials support localized surface plasmon resonances (LSPR). The

oscillation of electron conduction bands in metal nanoparticles interacts with the light electromagnetic field, enabling strong optical absorption and scattering in the visual spectrum, which is associated with nanoparticle's size [17, 109], shape [6], composition, surface chemistry [110] and surrounding environment [6]. Therefore, LSPR has been explored to characterize a nanoparticle's size and concentration [111], aggregation state [112] and reaction with molecules [113]. Surface enhanced Raman spectroscopy, which is based on LSPR, has been developed for sensitive and selective molecular sensing with nanomaterials [114]. Currently, there is a lack of approaches to directly measure surface ligands and attached ions.

1.5 Physical and chemical transformations of AgNPs

1.5.1 Dissolution

Silver nanoparticles undergo various physicochemical transformations in different environments. Dissolution is one of the important changes which plays a central role in the antimicrobial activities of AgNPs. Release of Ag^+ from AgNPs is thermodynamically favourable at room temperature (ΔG_{298}^{Θ} = -11.25 kJ/mol). Silver will be oxidized when oxygen is available, followed by a reaction with H_2O to release free Ag^+ (Equation 1.4-1.7) [115]. The dissolution of AgNPs is affected by the concentration of dissolved oxygen, temperature, pH, particle size, surface coating and anion/organic composition in the dispersion media.

$$2Ag\ (s) + 1/2O_2 \leftrightarrow Ag_2O\ (s) \qquad \Delta G^{\Theta}(298\ K) = -11.25\ kJ/mol \qquad (1.4)$$

$$1/2Ag_2O\ (s) + 1/2H_2O \leftrightarrow Ag^{+} + OH^{-} \qquad \log K_s\ (298K) = -7.71 \pm 0.03 \qquad (1.5)$$

$$1/2Ag_2O\ (s) + 1/2H_2O \leftrightarrow AgOH \qquad \log K_s\ (298K) = -5.75 \pm 0.25 \qquad (1.6)$$

$$1/2Ag_2O\ (s) + 1/2H_2O + OH^{-} \leftrightarrow Ag(OH)_2^{-} \qquad \log K_s\ (298K) = -3.72 \pm 0.03 \qquad (1.7)$$

Oxygen is a prerequisite for dissolution of AgNPs [97], which is inhibited in anaerobic conditions [116]. The presence of H_2O_2 promotes oxidation and thereby dissolution [117]. The reduction of the outer layer of Ag_2O by H_2 reduces the dissolution [97]. It is observed that the outer layer of AgNPs is steadily oxidized into a Ag_2O shell upon prolonged illumination by UV-blue light in an oxic environment [118]. The oxidation rate is thermodynamically enhanced in small nanoparticles according to the change of Gibbs free energy

$$\Delta G^{\Theta}(298\ K) = -11.25 - 57.5/r\ kJ/mol \qquad (1.8)$$

where r is the radius of nanoparticle [119]. The adsorption energy of oxygen to the nanoclusters surface decreases with decreasing particle size [120]. Consequently, smaller nanoparticles are more likely to be oxidized than larger ones. Additionally, the mass faction of Ag_2O increases as particle size decreases [97]. One or two layers of Ag_2O may be formed in AgNP suspension [97], but it also reported that oxygen can penetrate into the interior of nanoparticles, resulting in the oxidation of 89% of total AgNPs that are deposited on nickel TEM grids in 9.3 h under the enhanced illumination by white lamp, according to the red-shift and damping of LSPR [118]. Theoretical study has confirmed a red-shift of maximum extinction surface plasmon resonance wavelength and a decrease of extinction peak intensity upon increasing oxidation of

AgNPs [121].

A model based on the Arrhenius Equation suggests that primary size of AgNPs is an important factor determining dissolution kinetics of nanoparticles [122]. The relative surface area of nanoparticles exponentially increases with a decrease in particle size, inducing the accelerated release of Ag^+ from small AgNPs [103, 123]. Besides, smaller AgNPs have higher solubility in H_2O (equation 1.2) [123]. Silver nanoparticle aggregates show declined dissolution rate [124]. Decreasing pH accelerates Ag^+ release (Equation 1.4 and 1.5). Liu *et al.* have observed that the concentration of dissolved Ag^+ released from AgNPs is much higher at pH 4 than that at pH 9 in air saturated water [117]. In alkaline condition, dissolved Ag may exist in the forms of AgOH and $Ag(OH)_2^-$ (Equation 1.6 and 1.7). The dissolution rate increases with rising temperature since this process is thermodynamically favourable [125].

Complete dissolution of citrate-AgNPs (4.8 ± 1.6 nm) in air-saturated deionized (DI) H_2O (pH = 5.68) was observed at room temperature [117]. Partial dissolution of AgNPs (50 ± 20 nm) was also obtained and the dissolution rate depends on surface coating and temperature [125]. It has also reported that citrate-coated AgNPs with a concentration of 10.8 mg/L were relatively stable for 104 d when they were stored in dark [126]. It is difficult to compare dissolution rates from different studies because nanoparticle's properties and environmental conditions, which are always unique, combine to affect dissolution kinetics and equilibrium.

1.5.2 Surface chemistry

Surface ligands will interfere with various transformations of nanoparticles. Citrate has been demonstrated to inhibit the dissolution of AgNPs since increasing citrate/AgNPs concentration ratio promotes the stability of AgNPs in H_2O [126, 127]. Coating agents such as cysteine, glutathione and oxidized glutathione can strongly reduce the Ag^+ release rate due to their potential activities of surface passivation, reversibly binding with surface atoms or inducing the formation of insoluble films on the surfaces [127]. The inhibition ability of surface ligands might be associated with their affinities for the nanoparticle's surface atoms. For example, cysteine, which is able to strongly bind with Ag, can substantially decrease the dissolution of citrate-AgNPs [116].

Silver nanoparticles can react with environmental chemicals on their surfaces. In a chloride-rich environment such as seawater, Cl^- can drive the dissolution of AgNPs forming AgCl precipitates in the environment [128], on the other hand the formation of AgCl (s) on surface hinders Ag^+ release, which has been demonstrated by a slower dissolution rate of PVP-AgNPs in NaCl solution than that in H_2O [129]. Meanwhile, increasing Cl^- concentration supports the transformation of AgCl (s) into soluble $AgCl_x^{(x-1)-}$ complexes, which in turn promotes the dissolution of AgNPs [129]. Accelerated shrinking of AgNPs that are immobilized on glass substrates was observed by AFM upon exposure to increased NaCl concentrations, providing direct evidence to support the conclusion that Cl^- ions catalyse the dissolution of AgNPs [106].

In a reducing environment, silver tends to react with sulphide forming Ag_2S that might

precipitate on the surface of AgNPs [130]. By competing with coating agents for the surface reaction the sulfidation of AgNPs might influence desorption of capping agents, surface charge, aggregation state and dissolution [130]. Oxidation is likely to be a prerequisite for sulfidation of AgNPs since the formation of Ag_2S is significantly inhibited in an argon atmosphere [98]. In addition, sulfidation preferentially occurs on the surface of AgNPs [131]. Under high sulphur concentrations (0.1-1 mM) (e.g. wastewater treatment plant), silver directly reacts with sulphur forming Ag_2S. In low sulphur conditions (e.g. natural water), AgNPs slowly dissolve into Ag^+ as the intermediate species that reacts with sulphur [98]. Sulfidation of AgNPs leads to decreased dissolution [130] since the solubility constant (K_{sp}) of Ag_2S is quite small (5.92×10^{-51}) compared to other Ag compounds e.g. AgCl (1.77×10^{-10}) and Ag_2CO_3 (8.46×10^{-12}) [119]. There is a strong negative correlation between sulfidation and toxicity of AgNPs because the sulfidation transforms Ag into non-soluble Ag_2S that is much less toxic to microorganisms and thus inhibits Ag^+ release and reduces surface active area [132].

1.5.3 Aggregation

Nanoparticles are easy to aggregate owing to their high surface energy. The aggregation states of AgNPs affect their mobility [133], bioavailability [134] and toxicity [135]. The aggregation can be explained by classic Derjaguin-Landau-Verwey-Overbeek (DLVO) theory. There are mainly two forces controlling the nanoparticle's stability: van der Waals attractive force and electrostatic repulsive force [136]. Hydration effect, steric

effect, coverage and configuration of surface coating also contribute to the interactions between nanoparticles [137]. When the distance between nanoparticles decreases to a few nanometres, ion-specific effects, ion solvation and polarization of the nanoparticle core should be considered, adding to the complexity of a nanoparticle's interaction at the nanoscale [3].

Aggregation originates from attachment of individual nanoparticles to form large nanoparticle clusters. Silver nanoparticles should have high enough kinetic energy to overcome an energy barrier to achieve efficient attachment and many efforts need to be made to prevent them from aggregating [138]. Ions are absorbed onto the nanoparticle's surface enabling the charging of AgNPs and large molecules covering the surface have steric effects. Both increase the energy barrier. On the other hand, counterions and many functional molecules can modify nanoparticle's surface chemistry, which might reduce the energy barrier to trigger aggregation. Silver nanoparticles have a strong tendency to aggregate in electrolyte solution as a result of neutralization of surface charge that leads to the dominancy of attractive force when AgNPs move close. Decreasing pH can reduce the surface potential of negatively-charged AgNPs, accelerating the aggregation in NaCl solution [139]. High concentrations of counterions with large valences always promote aggregation [140]. In comparison, increasing surface potential with same-charged chemicals enhances nanoparticle stability. Increased resistance to aggregation for citrate-AgNPs (negatively charged) was observed after humic acid (negatively-charged) was added [140]. Positively-charged polymer (poly(3-(6-(negative1-methylimidazolium-3-yl)hexyl)thiophene-2,5-diyl bromide, PMHT) induced the

aggregation of BO_3^--AgNPs by neutralizing the surface charge [141]. Interestingly, their surface charge changed from negative to positive when more PMHT were added, which restabilized the nanoparticles [141]. Surface capping with polymers can reduce the susceptibility of AgNPs to aggregate in an electrolytic environment. PVP and BPEI coated AgNPs can maintain their stability in 1 M $Ca(NO_3)_2$ solution, but H_2-AgNPs and citrate-AgNPs completely aggregated in 5 mM $Ca(NO_3)_2$ solution [142]. Coexistence of high concentration of Ca^{2+} with humic acid induced intermolecular bridging, leading to enhanced growth of nanoparticle aggregates [143].

1.6 Toxicity of Ag^+ and AgNPs to microorganisms

1.6.1 Toxicity of Ag^+

Many metals are crucial for cellular metabolism and are essential components of biomolecules [144]. Bacteria require different orders-of-magnitude of metals for cellular process [145], but excessive levels of even essential metals in bacterial cells have lethal effects. Some transition metals such as silver (Ag) are not essential for microorganisms, and can influence cellular physiology and even kill bacteria at low concentration [29, 146]. The toxicity of heavy metals has been reported to be linked to their standard redox potential and affinity with sulphide [147]. Metals with high reduction potential and low solubility of metal-sulphide complexes have stronger bactericidal effects.

Silver and its compounds have a long history of use as antimicrobial agents [28]. There are several mechanisms by which Ag is toxic to bacteria (Figure 1.4). Silver can

promote intracellular reactive oxygen species (ROS) stress. The ROS, including superoxide (O_2^-), hydrogen peroxide (H_2O_2) and hydroxyl radical (HO·), are primarily produced by accidental autoxidation in aerobic conditions [148]. Silver might disrupt Fe-containing proteins, inducing Fenton-type ROS stress. It has been reported that copper displaces the iron atom of iron-sulphur clusters diminishing enzyme activities [149]. Similarly, Ag is able to disturb cellular iron homeostasis, releasing Fe^{2+} that can drive a Fenton reaction in cells [148, 150]. Silver might attack antioxidants (e.g. glutathione) and ROS-scavenging enzymes, especially those containing thiol groups, leaving cells vulnerable to ROS. Silver has high affinity for thiol residuals (e.g. the stability constant for Ag-cysteine is 7.9×10^{11}) [28, 119]. It is reported that Ag^+ disturbs the electron transport chain, which imposes superoxide radical stress on bacteria [150, 151]. For instance, the Ag^+ released from Ag-coated titanium substrates attacked thiol groups of respiration chain and TCA cycle enzymes, inducing rapid accumulation of hydroxyl radicals in *Staphylococcus epidermidis* [152].

Silver can kill Gram-negative and positive bacteria in anaerobic conditions where ROS stress is absent [151, 153], suggesting that ROS alone cannot explain the bactericidal actions of Ag. Silver can directly attack a variety of proteins [154, 155]. Silver is capable of non-specifically binding to proteins, leading to increased membrane permeability [150] and damage [156]. Silver can abolish the activities of Fe-S-dependent dehydratases and mononuclear iron proteins [148]. Silver ions might modify membrane protein, leading to the H^+ leakage in *Vibrio cholera* [157]. Small concentrations of $AgNO_3$ (≤10 μM) can interfere with the activities of respiratory chain

enzymes causing bacterial cell death, or directly interact with cell membrane leading to bacterial deformation [30]. Silver ions can also interact with ribosomes inside cells to interfere in protein expression and ATP production without attaching to the cell membrane [31], demonstrating their direct attack on bacterial compartments. DNA bases could be the target of Ag; but there is a lack of evidence of mutations directly caused by Ag [158, 159]. Genotoxicity of Ag might be associated with the oxygen radicals produced via other Ag-biomolecule interactions. In summary, the high affinity of Ag with a variety of biomolecules causes a broad spectrum of bacteria to be extremely susceptible to a toxic dose of Ag.

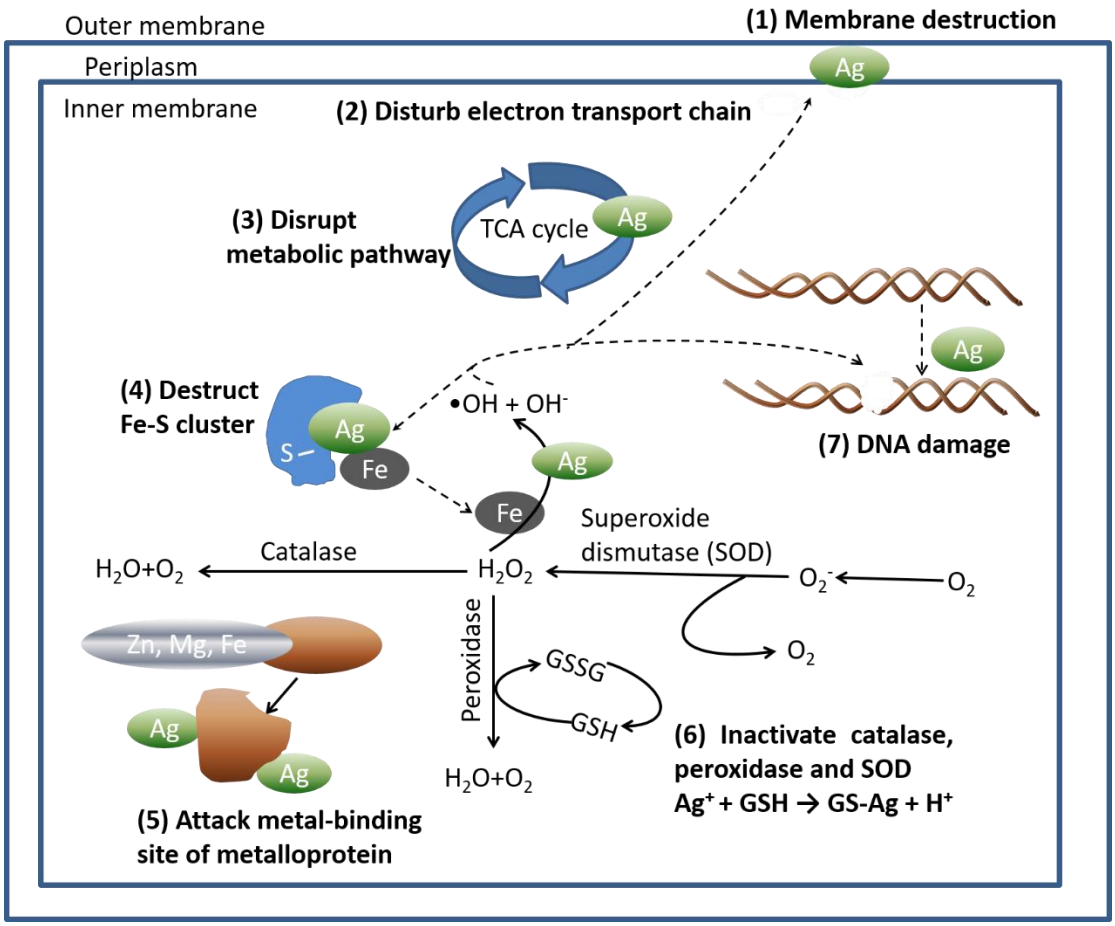

Figure 1.4 Antibacterial activities of Ag (Gram-negative bacterium as the model) (1) Membrane destruction or damage caused by ROS or through directly binding with membrane molecules. (2) Disturb electron transport chain (ETC) via impairing the activities of ETC enzymes. (3) Disrupt metabolic pathways such as the TCA cycle. (4) Disrupt cellular Fe-containing proteins, releasing free iron that can enhance the Fenton reaction and increase ROS stress. (5) Attack metal-binding sites of metalloproteins, disabling their function or damaging the protein structure. (6) React with cellular thiol, including catalase and superoxide dismutase (SOD), causing dysfunction of antioxidants. (7) Damage DNA by Ag or ROS.

1.6.2 Bacterial resistance to Ag

Antibiotic resistance is marked as a global crisis owing to the emerging of antibiotic-resistant pathogens and a lack of novel drugs to treat these bacteria [160, 161]. Given the non-selective binding of Ag with various biomolecules, it is generally accepted that strong resistance towards Ag in bacteria is not as common as for antibiotics, but it can

occur by frequent sublethal exposure of bacteria to Ag (Figure 1.5). Silver resistance was firstly reported in *Salmonella* in a hospital in the 1970s, and was transferable among different bacterial species [162]. Later, it was found that the plasmid pMG101 in the strain was responsible for the Ag resistance [163]. Plasmid pMG101 contains *silE* gene that encodes a periplasmic-specific binding protein, the *silRS* gene that is closely related to a sensor/responder pair and homologous to *proRS* in copper resistance plasmid, the *silCBA* gene that encodes a three-polypeptide membrane cation/proton antiporter efflux pump, and the *silP* that is deduced to be a member of the P-type ATPase heavy metal efflux family [163, 164]. Apart from this plasmid-mediated Ag resistance, the active efflux machines associated with chromosomal genes *copA* and *cus* that are responsible for bacterial Cu resistance also contribute to Ag resistance [165, 166]. The P-type ATPase transporter, CopA that transports Cu from the cytoplasm into the periplasm, has a role in exporting Ag [165]. The RND-type transporter CusCBA complex that has the function of pumping Cu^{+} from cytoplasm or periplasm into extracellular space [167] might play an active role in Ag efflux. The *E. coli* mutants selected under Ag^{+} treatment show strong Ag resistance as a result of a decline in the outer membrane permeability and reduced intracellular Ag accumulation [168]. A mutant that is deficient in porins (β-barrel proteins that cross cellular membranes) has shown comparable Ag susceptibility to the parent strain, suggesting that active Ag efflux might also contribute to the Ag resistance [168]. Probably, the active efflux and reducing Ag permeability combine to determine bacterial defence against Ag. Because a double mutation of *ompR* that regulates the expression of porin OmpC and OmpF and

the gene *cus* that is responsible for the expression of CusCBA, is required for strong Ag resistance [166].

Given the reducing environment in bacterial cells, it is not a surprise that Ag^+ can be reduced to metallic Ag in bacterial cells, which contributes to the Ag detoxification. A *Pseudomonas* strain isolated from a silver mine is capable of transforming Ag^+ into particulate Ag accumulated in the periplasm [90]. The engineered *E. coli* HS2019 that expresses high Ag-affinity periplasm protein (MBP-AgBP2p) by a plasmid exhibits strong tolerance to Ag^+ [169]. This Ag-binding peptide protects cells by reducing Ag^+ to Ag. Small AgNPs have been found evenly distributing in *E. coli* cells treated with Ag^+, indicating that Ag^+ can be also reduced in the cytoplasm [170]. Microbial extracellular substances are capable of protecting bacteria by transforming Ag^+ to AgNPs and immobilizing the AgNPs outside cells [171].

Biofilm, which represents the dominant life form of bacteria in the natural environment is an important strategy to tackle environmental stress [172]. A bacterial biofilm is the assemblage of cells that are embedded in self-produced extracellular polymeric substances (EPS) [173, 174]. A concentration gradient of nutrients, signalling compounds and bacterial waste is generated within the biofilm due to chemical diffusion along with microbial metabolism [173]. Biofilms can have up to 100-fold strengthened tolerance to ampicillin, chloramphenicol and other antibiotics [175]. The bacteria in biofilms are also less susceptible to heavy metals than their planktonic counterparts [147]. *Pseudomonas aeruginosa* can tolerate up to 25 folds of the concentration of metal cations (Cu^{2+}, Ni^{2+}, Co^{2+}, Zn^{2+}, Al^{3+}, and Pb^{2+}) in a biofilm than

those in planktonic culture [176]. Several mechanisms are involved in the enhanced metal resistance of cells in a biofilm. Extracellular polysaccharides and proteins provide a strong and enduring yet flexible physical support structure, acting as a filter that protects cells from external chemical assault while allowing diffusion of nutrients [177]. Both bacteria and cellular metabolites can bind with Ag^+ to reduce the bioavailability of free Ag, which will encourage bacterial regrowth and surface colonization in an Ag-diluted environment [178]. Dead cells and EPS have sorption, complexation or precipitation sites that capture and fix Ag in biofilms [147]. Furthermore, the cells in a biofilm undergo complex and adaptive physiology changes in response to Ag stress, allowing phenotypic diversification to withstand toxic metals [147, 176].

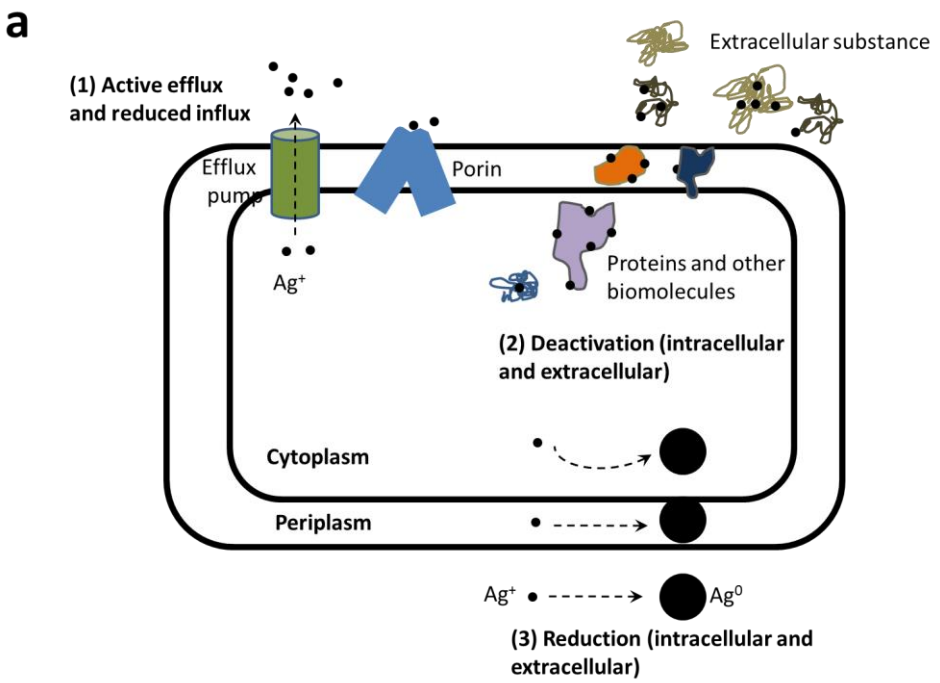
a
Extracellular substance
(1) Active efflux
and reduced influx
Efflux
pump
Porin
Ag+
Proteins and other
biomolecules
(2) Deactivation (intracellular
and extracellular)
Cytoplasm
Periplasm
Ag+
Ag0
(3) Reduction (intracellular and
extracellular)

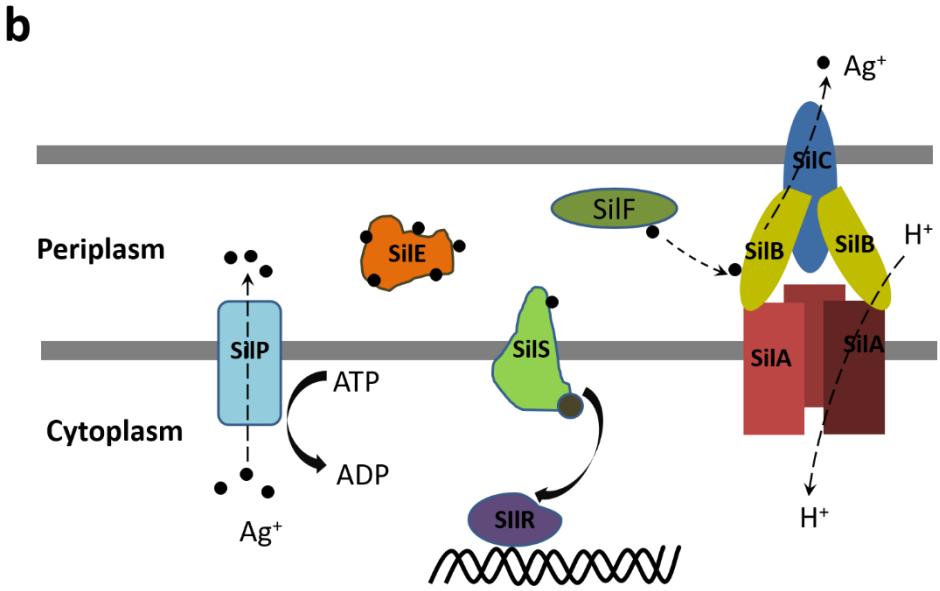
b
Ag+
SilC
SilF
Periplasm
SilE
SilB
SilB
H+
SilP
SilS
SilA
SilA
ATP
Cytoplasm
ADP
Ag+
SilR
H+

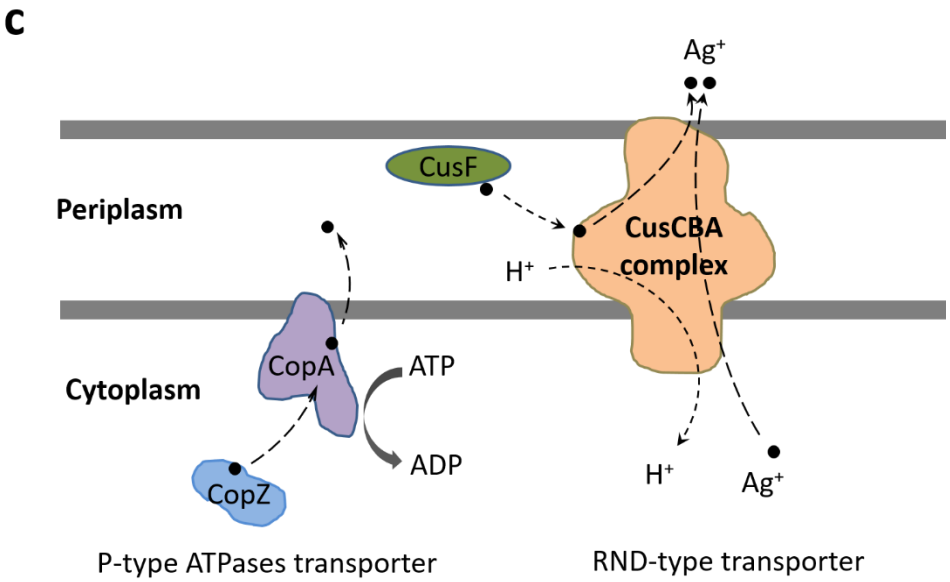

Figure 1.5 Bacterial resistance to Ag

(a) The mechanisms of bacterial defence against Ag. Bacteria translocate Ag from the cytoplasm to extracellular spaces by efflux pumps, or control the expression of membrane proteins (porins) to reduce the influx of Ag (1). Silver ions can be deactivated through binding with various biomolecules inside cells or extracellular substances outside cells (2). Bacteria are capable of reducing Ag^+ to metallic Ag or AgNPs in different cellular compartments or outside cells (3). **(b)** Efflux-mediated Ag resistance of the *sil* system in the plasmid pMG 101 in *Salmonella enterica* serovar Typhimurium [179]. The sensor SilS detects Ag in the periplasm and phosphorylates SilR that regulates the transcription of *silCBA*, *silP* and *silE*. The SilCBA complex is an RND-type transporter that uses proton motive force to drive the efflux of Ag. It consists of SilA that spans the inner membrane, SilB that is a membrane fusion protein and SilC that is an outer membrane protein. Silver binds to SilB, which triggers the SilCBA complex to pump Ag out of cells. SilP is a P-type ATPase efflux pump. SilE is a periplasmic protein that binds Ag. **(c)** Silver resistance related to Cu resistance chromosomal genes [167]. The *copA* and *cus* system that encodes P-type ATPase transporter (CopA) and RND-type transporter (CusCBA), respectively. The CopZ in cytoplasm and CusF in periplasm deliver Ag to CopA and CusCBA complex that export Ag into extracellular space.

1.6.3 Toxicity of AgNPs

Morphology (size and shape) and surface chemistry of nanomaterials play major roles in the toxicity [180, 181]. A meta-analysis of cellular toxicity for quantum dots (QD) by mining 1741 cell viability data samples has revealed that surface properties, size and

nanoparticle concentration have the most influence on their toxicity towards eukaryotes [182]. Size, surface chemistry and aggregation state of nanomaterials determine the initial deposition of nanomaterials on cell surfaces and subsequent internalization. Surface coating also affects nanomaterial behaviours in biological media and transformation in the cell cytoplasm. Enhanced membrane attachment and internalization of mercaptoundecanoic acid-capped and dodecylamine-modified poly(isobutylene-alt-maleic anhydride)-coated AgNPs have been reported causing membrane damage, autophagy and cytoskeletal deformation of human cells, but the AuNPs coated with poly(ethylene glycol) have limited uptake by cells and thereby weak toxicity [183]. AuNPs capped bysurface ligands with same chemical composition but different structure have shown different pathways to penetrate into cells [184]. The nanoparticles that can penetrate through a cell membrane should be in a critical size range, which depends on the surface properties and internalization pathway [185]. For instance, only the antibody-coated AuNPs with diameter of 40 and 50 nm that have high binding affinity towards the membrane receptors on cellular surfaces can be internalized through endocytosis by human breast cancer cells, but the AuNPs with too large or small diameters are excluded [186].

Starch-capped AgNPs (6-20 nm) can penetrate the cytoplasm of human lung fibroblast cells and glioblastoma cells, disrupting the mitochondrial respiratory chain, inducing ROS production and interrupting ATP synthesis, and causing DNA damage [187]. Oxidative stress is an important mechanism involved in the toxicity of nanomaterials [180]. To trigger ROS stress, nanomaterials are able to directly catalyse ROS formation

(Fenton reaction and photo activation) (TiO_2, Fe_2O_3), release metal ions to induce ROS stress (ZnO, CuO and Ag, etc.), and interact with metabolic processes such as electron transport chains and antioxidant defences (TiO_2, Fe_2O_3, ZnO, CuO and Ag, etc.) [188]. The silver nanoparticles without surface coating (9-21 nm) have been shown to induce elevated levels of intracellular ROS to kill nitrifying bacteria [189]. Citrate-AgNPs (9.3 ± 2.8 nm) can also cause accumulation of envelope proteins precursors, collapse of cytoplasmic membrane potential, loss of intracellular potassium and depletion of cellular ATP in *E. coli* [190]. Several studies have demonstrated the disintegration of cell membrane induced by AgNPs [191, 192], but it is difficult to distinguish if the membrane damage was caused by ROS or through direct attack from AgNPs. Graphite nanosheet (0.31-6.87 ηm in average)have been reported to deposit on bacterial membranes, inducing membrane and oxidation stress via disrupting the activities of glutathione without the detection of superoxide species [193], suggesting that direct interaction between nanomaterials with membrane biomolecules plays a role in membrane destruction.

Silver nanoparticles with different sizes and various coatings have been shown to be toxic to different organisms, including bacteria [29], yeast [194, 195], algae [57], invertebrate [196, 197], plants [58], fish [59] and human cells [187]. For eukaryotic cells, nanomaterials can be internalized via endocytosis or diffusion [198]. Antibacterial mechanisms of nanomaterials should be different from the toxicity in eukaryotes. There is a natural barrier of a cytoplasm membrane and lack of endocytosis in bacteria. Currently, there is a lack of evidence that AgNPs can penetrate the bacterial

cytoplasm and enter cells. Electron microscopy images have shown AgNPs attached to or transported into bacterial cells [192], but the intracellular AgNPs might be the result of the reduction of Ag^+ [170].

The toxicity of AgNPs in bacteria is mainly mediated by the release of dissolved Ag^+. It is unclear whether the antibacterial activities of AgNPs are solely due to the dissolved Ag^+ or ionic and nanoparticulate Ag combined effects. It is difficult to differentiate Ag^+ from AgNP effects since Ag^+ always coexist with AgNPs [199, 200]. Under anaerobic conditions where release of Ag^+ is inhibited, the lethal concentration of AgNPs to *E. coli* is reported to be several thousand higher and dissolved Ag^+ are responsible for the toxicity [201]. In contrast, nano-specific effects have been reported for ZnO nanoparticles where their toxicity is inversely proportional to particle size in the absence of large amount of free Zn^{2+} [202].

Because AgNPs cannot enter bacterial cells, they might attach to the cell surface, release toxic Ag^+, interfere with the function of membrane proteins, and damage the membrane. Nanoparticle-cell membrane interactions are very complicated. The factors not only include the physiochemical forces such as electrostatic force, steric repulsive force, van de Waals force and solvation effects but are also affected by cell physiology [48]. Positively-charged BPEI-AgNPs have shown stronger toxic effects on *Bacillus* species than negatively charged citrate-AgNPs, H_2-AgNPs and PVP-AgNPs [203]. Positively-charged AuNPs also show higher toxicity and larger cellular uptake rate in 3T3 fibroblast cells in comparison to negatively-charged ones [204].

It is unclear that AgNPs have a direct role in the toxicity. Different pathways may be

involved in the bacterial response to treatments of Ag^+ and AgNPs. A single-gene knockout library of *Escherichia coli* mutants present different sensitivity profiles towards Ag^+ and AgNPs [205], suggesting that the toxicity mechanism of nanoparticulate Ag could be different from ionic Ag. A transcriptomic study demonstrates that exposure of *E. coli* to Ag^+ or AgNPs induces different gene regulation and expression that are linked with protein production, iron metabolism and transport and redox stress [206]. Direct toxic effects from AgNPs may be not strong but cannot be excluded. Silver nanoparticles might mostly act as Ag reservoir that deliver Ag close to cells creating a local environment with high concentration of dissolved Ag^+ to kill bacteria [207, 208].

1.7 Overview of the thesis

This thesis investigated the toxicity mechanisms of AgNPs in an environmental model bacterium *Pseudomonas putida*. Firstly, a new method to separate dissolved Ag from AgNPs was developed. This new approach was used to measure the concentrations of dissolved Ag^+ in AgNP-treated bacterial cell culture. To understand the toxicity mechanism of AgNPs in bacteria, real-time toxicity kinetics tests, which combined the dynamic transformations of AgNPs in microbial media and their bacteria-killing actions, were carried out. An evolution experiment was carried out to explore the different toxicity models of Ag^+ and AgNPs in *P. putida* at genetic level.

(1) A convenient and reliable method was developed to quantify dissolved Ag in Ag^+/AgNP mixtures by combining aggregation with centrifugation. The aggregation of

AgNPs in different concentrations of $Ca(NO_3)_2$ solutions was investigated to examine how the aggregation mediated by Ca^{2+} facilitated the sedimentation of AgNPs during centrifugation. By comparing with ultrafiltration this new method provided a simple, fast and effective way to monitor dissolved Ag in AgNP suspensions.

(2) The toxicity of AgNPs in a bacterium *P. putida* was investigated by monitoring the transformations of AgNPs and bacterial response over time under as well defined conditions as possible. A citrate minimal medium was used to minimize potential changes of AgNPs during exposure to test media. Uncoated AgNPs, stored under N_2 to reduce oxidation, were used to avoid interferences from surface ligands and ensure the consistency of primary AgNP dispersions. The aggregation and dissolution of AgNPs in Davis minimal medium was measured. The effect of AgNP concentration and bacterial cell density on the minimum inhibitory concentration (MIC) was investigated. Lower doses of AgNPs which are typical in the environment were used for toxicity kinetics studies. The dissolution of AgNPs and corresponding death or growth of bacterial populations were examined to investigate how the release of Ag^+ governs the bactericidal effects of AgNPs over time. Furthermore, dose-response studies of high time resolution were carried out to quantify the antibacterial activities of ionic and nanoparticulate Ag.

(3) An evolution experiment was used to investigate the nano-specific toxicity of AgNPs in bacteria. It was hypothesised that bacteria will evolve differently in the presence of Ag^+ and AgNPs if they have different antibacterial activities. Because the ancestral *P. putida* population had not previously evolved in the same environment in

the absence of Ag, a pre-evolution experiment was carried out. Five parallel *P. putida* cultures that were from the same strain firstly evolved without Ag stress for 70 d before splitting the fittest culture for main evolution. Each independently evolved in the presence of Ag^+, well defined AgNPs or Ag free controls for 75 d in five replicates. The pre-evolved *P. putida* populations made the adaptions upon the challenges of sublethal concentrations of Ag^+ or AgNPs. Whole genome sequencing was used to identify genetic changes in the evolved populations during the evolution experiment. Different mutation patterns in these evolved populations treated by Ag^+ or AgNPs were identified.

2 Chapter Two

New, Rapid Method to Measure Dissolved Silver Concentration in Silver Nanoparticle Suspensions by Aggregation Combined with Centrifugation

Feng Dong, Eugenia Valsami-Jones, Jan-Ulrich Kreft (2016) New, rapid method to measure dissolved silver concentration in silver nanoparticle suspensions by aggregation combined with centrifugation. Journal of Nanoparticle Research 18(9): 1-12.

2.1 Introduction

Nanomaterials (NM) have received increasing attention due to their distinctive physicochemical properties at nanosize [10, 53, 209], especially for their medical application potential, as multi-drug resistant pathogens become ever more frequent [150, 161, 210, 211]. Silver nanoparticles (AgNPs) are widely used nanomaterials due to their toxic effects on microorganisms [9, 150, 212]. However, the mechanisms involved in their toxicity to microorganisms are still unclear. The antibacterial activities of AgNPs are generally thought to be indirectly mediated by the release of silver ions (Ag^+) [201, 213, 214], but some studies have suggested nanoparticles themselves can play a direct role in toxicity to bacteria [205, 206] because of their potential to directly interact with microbial components [212] and their large proportion of reactive surface sites compared to bulk materials [215]. It is therefore essential to differentiate ionic and nano Ag and measure the concentrations of different Ag species to understand their bactericidal effects.

Silver nanoparticles become oxidized, releasing Ag^+ in aquatic environments, when oxygen is available [103, 117, 122]. The dissolved Ag usually coexists with nanoparticles during storage [116]. Quantifying Ag species in AgNP dispersions, however, is quite challenging due to the difficulty of separating dissolved Ag^+ from AgNPs. Ultracentrifugation and ultrafiltration are the methods used routinely. Both have their limits. In ultracentrifugation, precipitating the tiny nanoparticles requires large centrifugal forces and long running times [216], which might be problematic when

AgNPs continuously release Ag^+ in an oxic environment. Sorption of Ag^+ to membranes may occur when ultrafiltration [214, 217] or dialysis is used. Ion-selective electrodes (ISE) can be used to measure free Ag^+ concentration in bulk liquid but not the total dissolved Ag^+ that include free Ag^+ and any dissolved Ag^+ complexed with the chemicals in the bulk liquid and attached to the surfaces of AgNPs [213]. Emerging techniques such as single particle inductively coupled plasma mass spectrometry (SP-ICP-MS) and asymmetrical flow field-flow fractionation coupled with inductively coupled plasma mass spectrometry (AF4-ICP-MS) are complex to operate and standardize but allow small errors in detection of nanoparticles and free ions [108, 218]. In this study, a convenient and reliable method was developed to quantify dissolved Ag in Ag^+/AgNPs mixtures by combining aggregation with centrifugation. Silver nanoparticles aggregate in $Ca(NO_3)_2$ [140]. Two mM Ca^{2+} is sufficient to rapidly aggregate various concentrations of uncoated AgNPs (10-40 nm) for removal of the aggregates by centrifugation. This approach only requires small sample volumes and low-speed bench-top centrifuges. This new method can provide a simple, fast and effective way to monitor dissolved Ag in AgNP suspensions.

2.2 Materials and methods

2.2.1 Synthesis of uncoated AgNPs

Uncoated AgNPs were produced by the solution-phase method [16, 219]. Silver nitrate ($AgNO_3$, Sigma-Aldrich) was used as the precursor and reduced by sodium borohydride ($NaBH_4$, Sigma-Aldrich) to form AgNPs at room temperature (19 ± 4 °C). All the glassware for AgNPs synthesis was soaked in 10% HNO_3 overnight and rinsed with copious amounts of deionized (DI) water (18.2 mΩ, Millipore), followed by drying in an ambient environment. The $AgNO_3$ solution (100 mL, 0.12 mM) was poured into the $NaBH_4$ solution (100 mL, 3 mM) in a 500 mL beaker. The $NaBH_4$ concentration was in 25-fold excess. The mixture was homogenized by magnetic stirring (1200 rpm). The $NaBH_4$ solution was freshly prepared to reduce the degradation resulting from its reaction with water to produce H_2 and BO_4^-. The solution turned to grey within a few seconds after mixing and changed to light yellow after a few minutes. As the reaction continued, the colour slowly changed to dark yellow at ~25 min and then back to yellow. After 1 h, the stirring was stopped, and the solution was stored for 24 h in the dark at room temperature. Finally, the stirring bar was removed and the AgNP suspension was transferred into glass bottles (250 mL, Duran) and stored at 4 °C in the dark.

2.2.2 Characterization of uncoated AgNPs

The localized surface plasmon resonance (LSPR) of uncoated AgNP suspensions was measured by UV-Vis spectrometry (UV-Vis 6800, Jenway, Staffordshire, UK). The relationship between LSPR signal and AgNP concentration was obtained by measuring

the absorption spectra of a dilution series of AgNP suspensions.

The size distribution of AgNPs was measured by dynamic light scattering (DLS) (Zetasizer Nano, Malvern Instruments, Malvern, UK) and differential centrifugal sedimentation (DCS) (DC24000, CPS Instruments Europe, Oosterhout, Netherlands).

The dissolved Ag fraction in AgNP suspensions was obtained by filtering the suspensions through a 3 kDa membrane filter (Amicon Ultra-15 Centrifugal Filter Unit, Millipore (U.K.) Limited, Hertfordshire, UK) at a centrifugal force of 4000 g for 20 min at 4 °C. The filtrate was collected and stored at 4 °C for future analysis. Total Ag concentration was measured by acidifying 1 mL AgNP suspension with 9 mL 70% HNO_3 (w/w) overnight at room temperature. The digested suspension was diluted with DI H_2O (18.2 mΩ, Millipore) to a final HNO_3 concentration of 0.2% (w/v). The silver content was measured by graphite furnace atomic absorption spectrometry (GFAAS) (AAnalyst 600, PerkinElmer Instruments, Massachusetts, USA). A silver concentration series (0-25 μg/L) was obtained by diluting a standard $AgNO_3$ solution (1000 μg/mL Ag, PerkinElmer Life and Analytical Sciences, Shelton, USA) with 0.2% HNO_3 concentration (w/v). Those standards were measured together with samples to obtain a calibration curve for calculating sample concentrations.

The morphology of AgNPs was imaged by transmission electron microscopy (TEM, JEOL 1200EX, Tokyo, Japan). About 20 μL AgNP suspension was loaded onto TEM grids (CF300-Cu Grids, Electron Microscopy Sciences, Pennsylvania, USA), followed by drying at room temperature. In order to reduce aggregation of AgNPs after loading the grids, grids were coated with 20 μL 100 mg/L polylysine, which carries many

positive charges while the AgNPs have a negative surface charge. After one hour, the grids were rinsed with DI water followed by drying. The morphology of AgNPs in $Ca(NO_3)_2$ solution was analysed by adding 100 mg/L bovine serum albumin (BSA) to stabilize the aggregates before loading the sample on a TEM grid without polylysine. BSA can be used to preserve the nanoparticle state in electrolyte solutions to avoid artefacts of drying [220].

2.2.3 Determining aggregation kinetics of AgNPs in $Ca(NO_3)_2$ solutions

The long-term aggregation of AgNPs in $Ca(NO_3)_2$ solution was followed for 96 h after mixing 20 mL of a AgNP suspension with the same volume of a 2 mM $Ca(NO_3)_2$ solution by vortexing (~20 s) in screw-cap glass vials (Bijou, capacity 46 mL) and allowing the mixture to settle on a lab bench at room temperature (17 ± 1 °C). The liquid from the top layer (5 mL) was taken for recording UV-Vis absorption spectra after 0, 1, 6, 24, 48 and 96 h.

The short-term aggregation kinetics was monitored for 0.5-2 h after mixing AgNP and $Ca(NO_3)_2$ solutions by recording the hydrodynamic size of aggregates by DLS in real-time. The AgNP suspension (0.5 mL, total Ag 5012 ± 75 μg/L, dissolved Ag 28 ± 0.5 μg/L at time zero) was mixed with 0.5 mL of different concentrations of $Ca(NO_3)_2$ in a disposable plastic cuvette and immediately placed in the Zetasizer Nano to record the Z-average diameter. Temperature was controlled at 25 °C.

2.2.4 Centrifugation of AgNPs in $Ca(NO_3)_2$

The sedimentation speeds of AgNPs with or without Ca^{2+} mediated aggregation were

compared at the same centrifugal force. AgNPs were aggregated by mixing 10 mL AgNP suspension with 10 mL $Ca(NO_3)_2$ solution (2 mM). After 10 min, the AgNPs/$Ca(NO_3)_2$ mixture was aliquoted into several centrifuge tubes (1 ml for each tube). Diluting 10 mL of the same AgNP suspension in 10 mL DI H_2O was used as control. Centrifugation was undertaken to sediment aggregates or individual AgNPs at a centrifugal force of 20,100 g (Centrifuge 5417 C, Eppendorf, Engelsdorf, Germany). To investigate the extent to which pre-aggregation can reduce centrifugation time, one tube from each treatment was taken to measure the Ag content in the supernatant (0.4-0.5 mL) at 0, 0.5, 1, 1.5, 2, 2.5, 3 and 4 h. The supernatants were acidified to 1% HNO_3 (w/v) overnight (more than 12 h) at 80 °C, and further diluted to a final HNO_3 concentration of 0.2% (w/v) for Ag concentration measurement by GFAAS.

2.2.5 Measurement of AgNP content in supernatant after centrifugation of AgNPs in $Ca(NO_3)_2$

Suspensions of AgNPs (0.5 mL) were mixed with $Ca(NO_3)_2$ (0.5 mL) in 1.5 mL microcentrifuge tubes (safe-lock microcentrifuge tubes, Eppendorf, Germany) to form large aggregates. After reacting for 10 min, aggregates were centrifuged at 20,100 g for 30 min. Ten aliquots were processed in parallel. The amount of AgNPs in the supernatant was measured by UV-Vis absorption spectroscopy. The supernatants (0.5 mL) from those ten aliquots were pooled into one tube since 4 mL was the minimum volume required for a UV-Vis absorption measurement with a 10 cm path length quartz cuvette. Although the UV-Vis absorption of nanoparticles depends on their size, shape,

surface coating, aggregation states and surrounding environmental conditions, it can still be used for concentration measurement as long as the particles and surrounding environmental conditions are similar [221]. A low concentration of AgNPs (< 10 μg/L) can be detected by UV-Vis spectrometry using a 10 cm path length quartz cuvette. The peak absorbance, typically between 390 and 400 nm, was used to quantify the AgNPs, and the absorbance at longer wavelengths (500-700 nm) was used to monitor the aggregates [126].

2.2.6 Measuring dissolved Ag in AgNPs suspension with aggregation-centrifugation or ultrafiltration

Different concentrations of AgNPs were prepared by diluting the AgNP stock with DI H_2O. The total Ag concentration of the AgNP stock was 5012 ± 75 μg/L, and it contained around 10% dissolved Ag. Those diluted AgNP suspensions were aggregated in 2 mM $Ca(NO_3)$ for 10 min and then centrifuged (20,100 g, 30 min). The supernatant (0.4-0.5 mL) was collected carefully and stored at -20 °C for dissolved Ag analysis. Each concentration was assayed in duplicate. Ultrafiltration was carried out by filtering the same AgNP suspensions through 3 kDa membrane filters (Amicon Ultra-15 Centrifugal Filter Unit, Millipore (U.K.) Limited, Hertfordshire, UK). The filtrates were stored at -20 °C. The dissolved Ag concentrations were always analysed by GFAAS.

2.3 Results

2.3.1 Synthesis of uncoated AgNPs

Three batches of AgNP suspensions were synthesized by the same procedure and characterised (Table 2.1, Figure 2.1). They were reasonably monodispersed in H_2O and had a spherical shape (Figure 2.1a). The size distributions of the three batches were similar. Measured by DCS, they showed the same peak diameter of 13 ± 1 nm (Figure 2.1b). Measured by TEM, the diameters of more than 83% of the counted AgNPs ranged between 10 and 40 nm (Figure 2.1c). The three batches also had similar UV-Vis absorption spectra and the same peak-absorbance wavelength (390 ± 1 nm) (Figure 2.1d).

Table 2.1 Characteristics of AgNPs
All data are shown as mean ± standard deviation of three batches produced with the same procedure. Diameters were measured by TEM, DLS (peak size based on intensity distribution) and DCS (peak size based on relative weight distribution).

pH	Diameter (nm)			Zeta potential in DI water (mV)
	TEM	DLS	DCS	
9.6 ± 0.3	17 ± 4.5	27 ± 4.2	13 ± 0.5	-40 ± 17

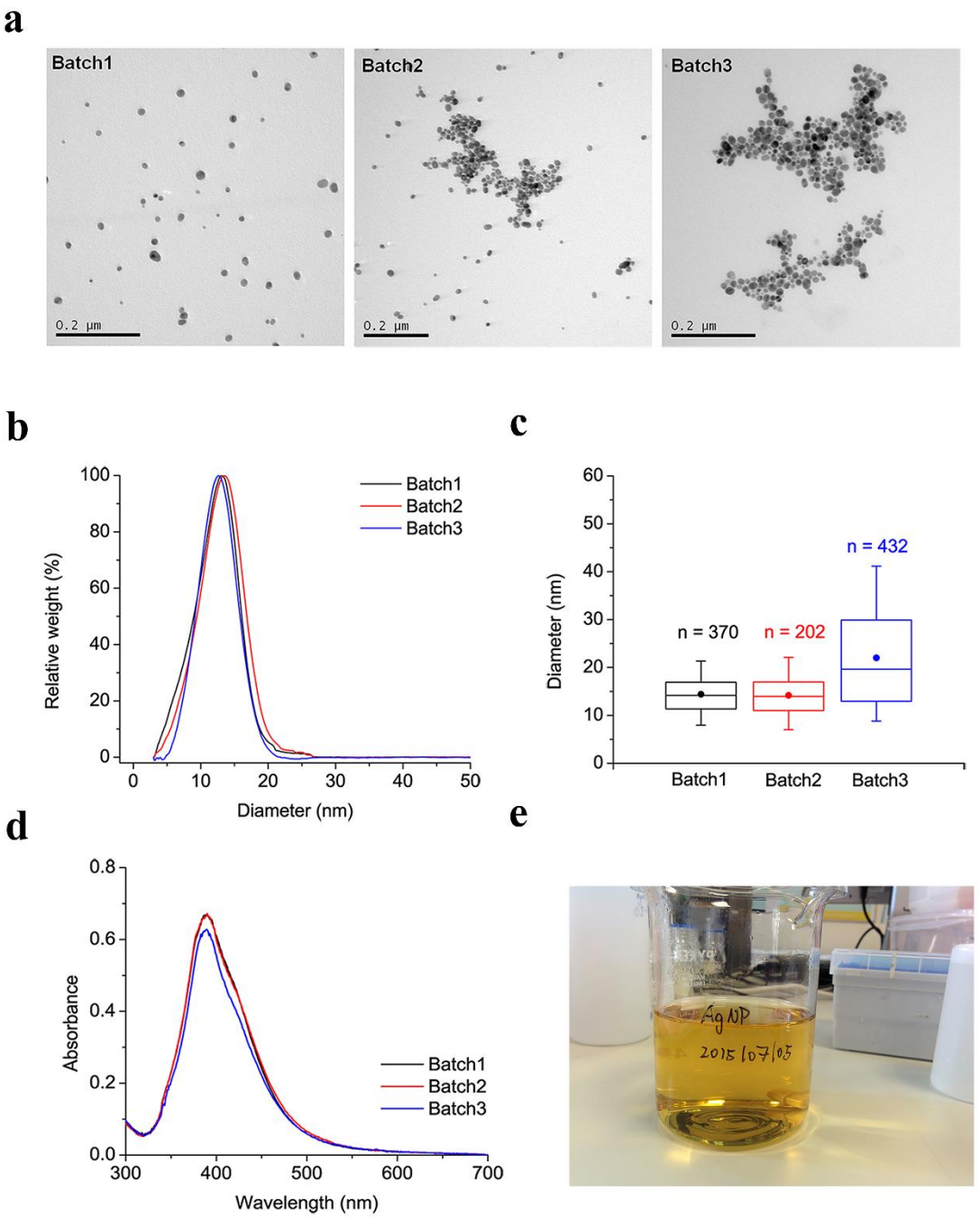

Figure 2.1 Characterisation of uncoated AgNPs and reproducibility of synthesis
Three batches of uncoated AgNPs were produced by the same procedure. **(a)** Morphology by TEM. **(b)** Comparison of size distributions measured by DCS. **(c)** Size distributions analysed by ImageJ [222] based on the TEM images. The boxes represent interquartiles, and the whiskers represent 5% and 95% percentiles. The points in the box are the means, and the bars represent the median. **(d)** UV-Vis absorption spectra one day after synthesis. **(e)** Photograph of AgNP suspension.

2.3.2 AgNPs aggregate in $Ca(NO_3)_2$ solutions

The small particle size made complete separation of AgNPs from ionic Ag difficult. Therefore, we investigated whether the particles would aggregate quickly in the presence of $Ca(NO_3)_2$ and could thus be separated by precipitation (Figure 2.2). Individual AgNPs were stable in H_2O as the UV-Vis absorption spectra did not change significantly during 96 h, indicating lack of aggregation (Figure 2.2a). The absorbance of AgNPs (at the wavelength of maximal absorbance) was proportional to the concentration of AgNPs and can therefore be used to measure the concentration of AgNPs (Figure 2.3). In $Ca(NO_3)_2$ solution, the red shift of the peak absorbance wavelength from 600 to 650 nm accompanied by the decreasing absorbance at 400 nm suggested that the aggregation took place during the first 6 h. The declining absorbance at both 400 and 650 nm from 6 to 96 h indicated the sedimentation of the aggregates. After 96 h, the absorbance in the range of 350-700 nm declined to less than 0.09, suggesting that most of the AgNPs and aggregates had sedimented. This aggregation and precipitation of AgNPs in $Ca(NO)_3$ solution was also confirmed by the colour transformations from yellow to pink and then blue of the AgNP suspension from 0 to 6 h (Figure 2.2b). Due to the formation of a dark precipitate at the bottom, the liquid phase became colourless at 96 h.

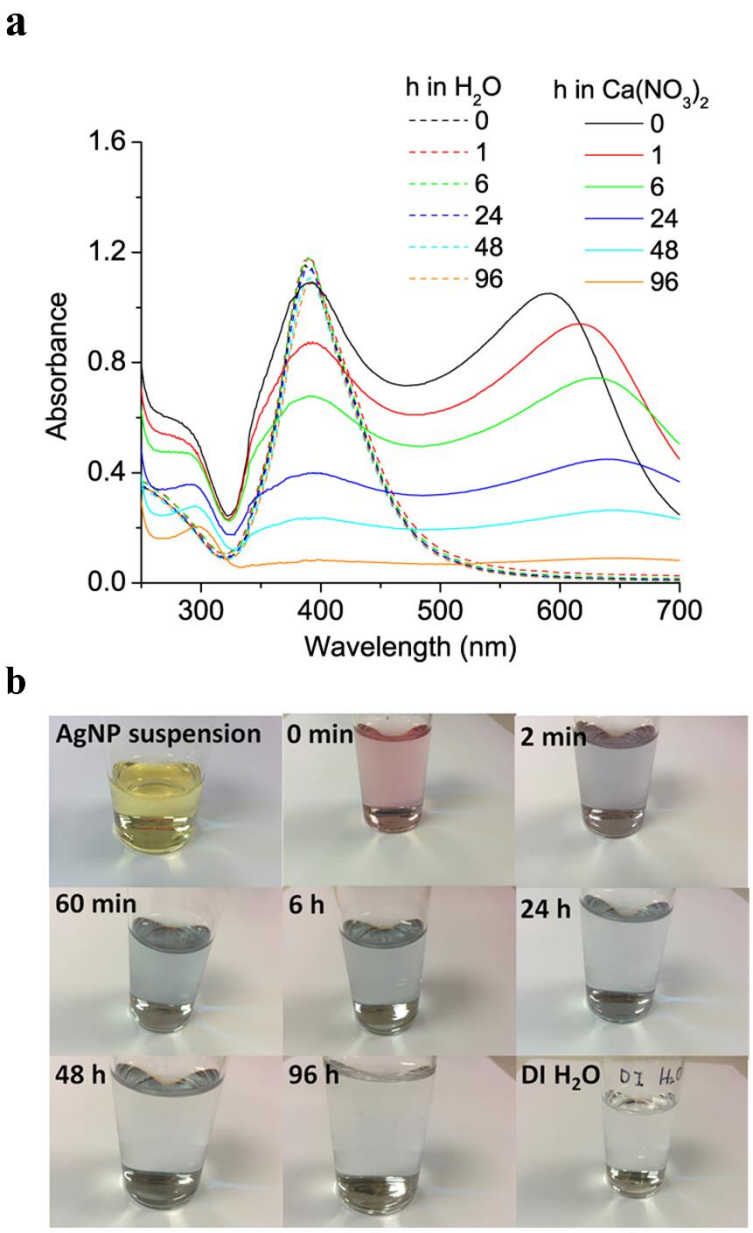

Figure 2.2 Aggregation of AgNPs in 2 mM $Ca(NO_3)_2$ solution
(a) UV-Vis absorption spectra of AgNP suspensions in H_2O or 2 mM $Ca(NO_3)_2$ as a function of time, from 0 to 96 h. The AgNP suspension was quite stable in H_2O but aggregated quickly in the $Ca(NO_3)_2$ solution. The top layers of the two mixtures were sampled for UV-Vis absorbance measurements. **(b)** Photographs of the AgNP dispersion in 2 mM $Ca(NO_3)_2$ taken over time. The colour of the AgNP suspension changed from yellow to pink in a few seconds (referred to as 0 min) after mixing the AgNP suspension with $Ca(NO_3)_2$ solution, followed by light blue during the first hour. Afterwards, the colour strength declined slowly, and the dispersion was as colourless as DI H_2O at 96 h while a dark precipitate had formed at the bottom.

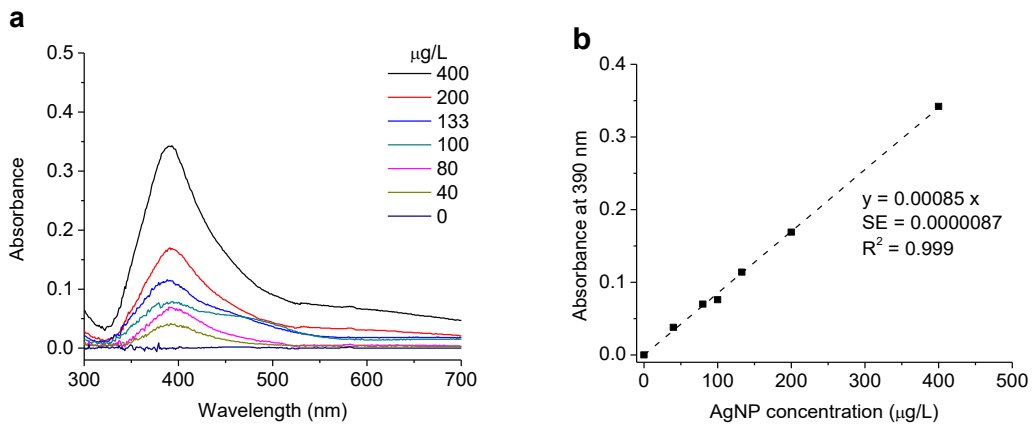

Figure 2.3 Calibration of UV-Vis absorption against concentration for AgNPs
(a) UV-Vis absorption spectra of different concentrations of AgNPs. The shapes of the absorption spectra were the same, and all had the peak absorbance at 390 ± 1 nm. **(b)** Linear regression of the absorbance at 390 nm versus AgNP concentration. SE represents the standard error of the slope.

2.3.3 Concentration dependence of aggregation of AgNPs in $Ca(NO_3)_2$

We investigated the $Ca(NO_3)_2$ concentration dependence of AgNP aggregation. The aggregation rate of AgNPs markedly increased from close to zero to 11 nm/min at the initial aggregation phase when the $Ca(NO_3)_2$ concentration increased from 0.1 to 0.2 mM (Figure 2.4a). It did not increase further once the $Ca(NO_3)_2$ concentration was higher than 0.5 mM (Figure 2.4b). Hence, 2 mM $Ca(NO_3)_2$ ensured sufficient aggregation to allow separation. Following this, we investigated the AgNP concentration dependence of aggregation in 2 and 20 mM $Ca(NO_3)_2$. Higher concentrations of AgNPs aggregated more quickly, both in 2 and 20 mM $Ca(NO_3)_2$ (Figure 2.4c). When the AgNP concentration increased from 250 to 5012 μg/L, the aggregation rate increased from 5 to 24 nm/min. Linear regression was carried out to assess the relationship between aggregation rate and AgNP concentration (Figure 2.4d). The regression slopes ± SE in nm/min were 17.7 ± 1.6 (p-value = 3.62×10^{-4}) and 20.1

± 1.7 (p-value = 3.25×10^{-4}) in 2 and 20 mM $Ca(NO_3)_2$, respectively. Increasing the $Ca(NO_3)_2$ concentration from 2 to 20 mM increased the aggregation rate only slightly. This suggested that a concentration of 2 mM $Ca(NO_3)_2$ was sufficient to trigger AgNP aggregation, even when the concentration of AgNPs in suspension was quite low. Aggregation of AgNPs in $Ca(NO_3)_2$ containing media led to formation of large clusters (Figure 2.5a, b, c) compared to singly scattering AgNPs in H_2O (Figure 2.5d, e, f).

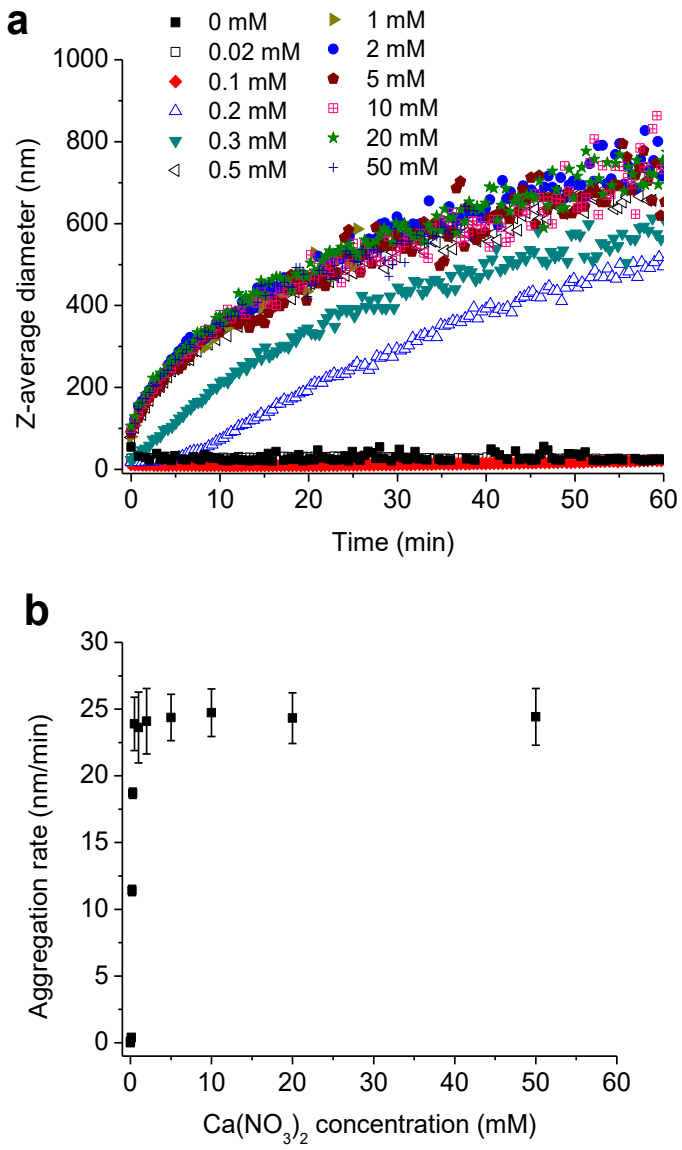

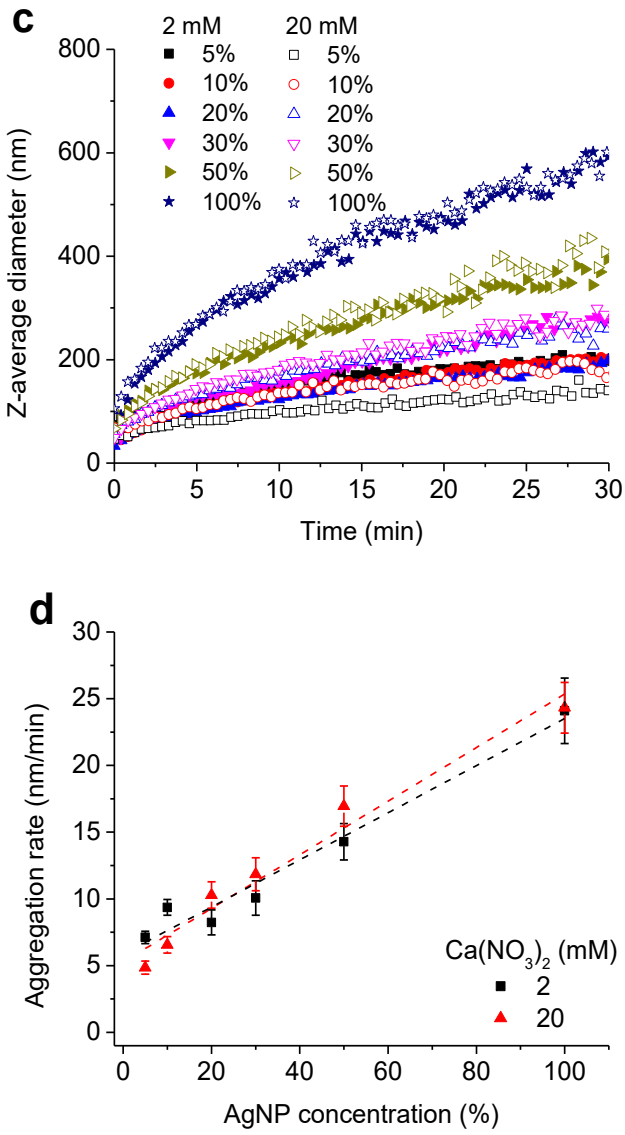

Figure 2.4 Aggregation kinetics of AgNPs in $Ca(NO_3)_2$ solution

The total and dissolved Ag concentration (mean ± SD) of the AgNP stock was 5012 ± 75 and 28 ± 0.5 µg/L, respectively. **(a)** Dependence of AgNP aggregation kinetics on $Ca(NO_3)_2$ concentration. The AgNP stock (0.5 mL) was mixed with 0.5 mL $Ca(NO_3)_2$ solution. The hydrodynamic size was measured by DLS. The aggregation process appears to be divided into two phases, the faster initial aggregation phase presumably corresponds to aggregation of individual AgNPs or small clusters and the second, slower aggregation phase corresponds to aggregation of larger aggregates. **(b)** Aggregation rates calculated by linear regression of the first aggregation phase shown in panel a. Error bars indicate 95% confidence intervals. **(c)** Aggregation kinetics of different concentrations of AgNPs in 2 and 20 mM $Ca(NO_3)_2$. The AgNP stock was diluted by DI H_2O to obtain different concentrations of AgNPs. Higher AgNP concentrations favoured aggregation, and larger aggregates were formed. **(d)** Aggregation rates calculated by linear regression of the first aggregation phase in 2 and 20 mM $Ca(NO_3)_2$ shown in panel c. Error bars indicate 95% confidence intervals.

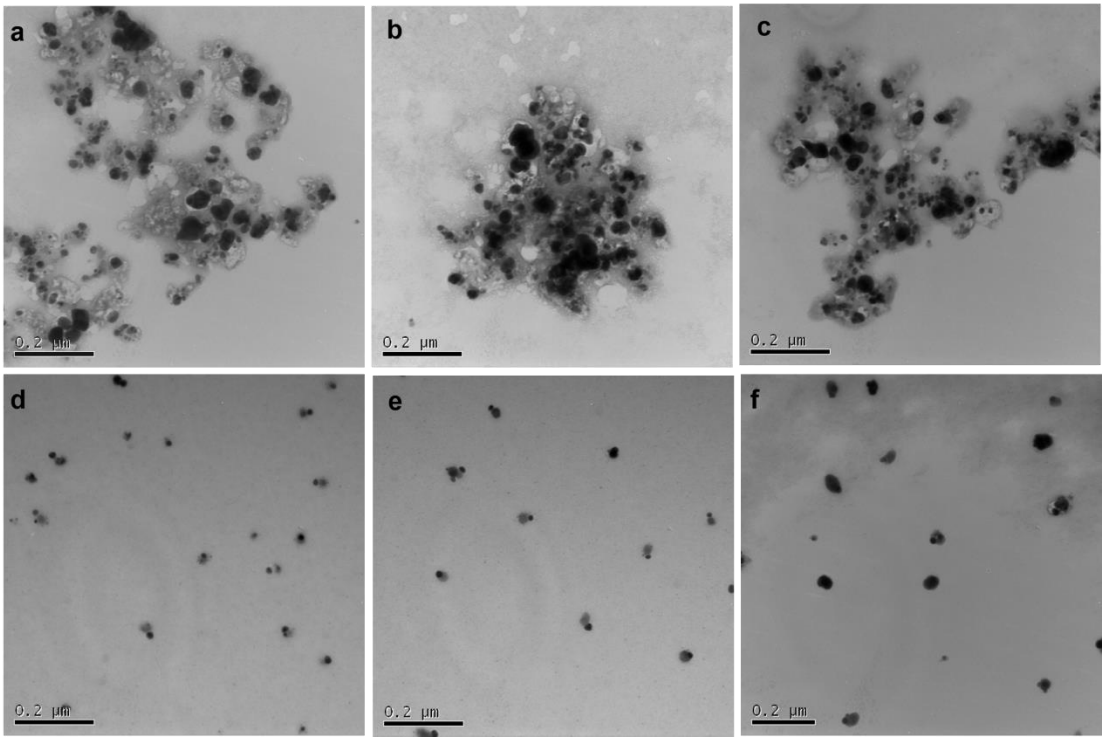

Figure 2.5 TEM images of AgNPs aggregates
TEM images of AgNPs in 2 mM $Ca(NO_3)_2$ **(a - c)** or H_2O **(d - f)**. Individual AgNPs formed aggregates in $Ca(NO_3)_2$. The AgNP suspension (0.7 mL) was mixed with 0.7 mL 2 mM $Ca(NO_3)_2$ and incubated for 10 min, and the mixture was stabilized by adding 100 mg/L bovine serum albumin (BSA) to preserve the aggregation state of the AgNPs before loading them on TEM grids. The AgNPs in H_2O were directly loaded on TEM grids.

2.3.4 Time required to sediment AgNPs after aggregation

The change of Ag content in the top layer of AgNP/$Ca(NO_3)_2$ and AgNP/H_2O mixtures during centrifugation was measured. After 30 min of centrifugation, 66% of the AgNPs had sedimented towards the bottom in H_2O. A slower decrease of Ag content in the supernatant was observed after this steeper initial decline (Figure 2.6). At least four hours of centrifugation were required to sediment all AgNPs in H_2O. When AgNPs were aggregated by $Ca(NO_3)_2$, all the AgNPs sedimented to the bottom of the vessel in 30 min of centrifugation. Prolonged centrifugation did not further decrease the Ag content in the supernatant (Figure 2.6). Hence, 30 min were sufficient to precipitate virtually

all AgNPs in 2 mM $Ca(NO_3)_2$ solutions.

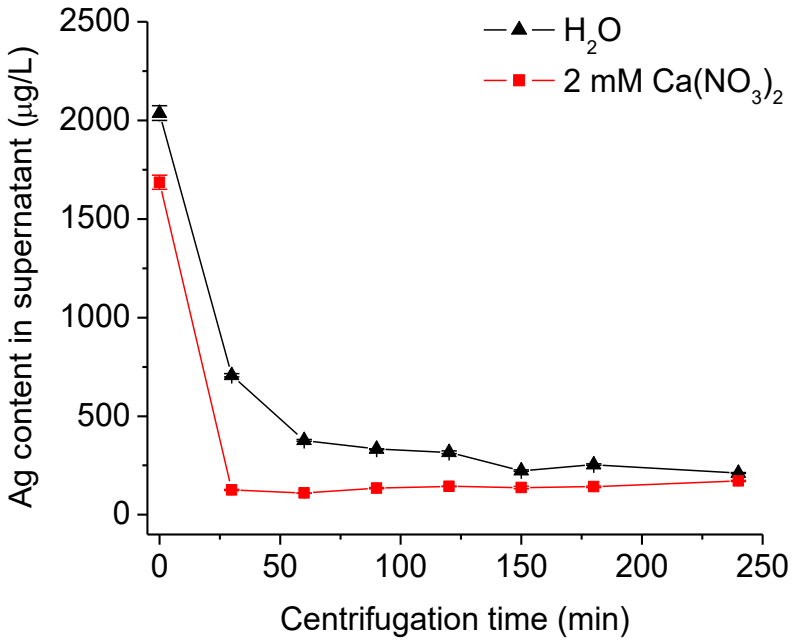

Figure 2.6 The time required to sediment AgNPs
The Ag content in supernatants after centrifuging AgNPs in 2 mM $Ca(NO_3)_2$ or H_2O. Supernatants were sampled at 0, 30, 60, 90, 120, 150, 180 and 240 min after start of centrifugation. Error bars represent the standard deviations of three measurements of the sample by GFAAS.

2.3.5 Sedimentation of Ca^{2+}-aggregated AgNPs is complete

To investigate the effects of aggregation on nanoparticle sedimentation, AgNPs were aggregated in different concentrations of $Ca(NO_3)_2$ before centrifugation. The absorption spectra of the supernatants had the same shape as absorption spectra of monodispersed AgNP suspensions, suggesting that the absorption of supernatants was due to individual AgNPs in the supernatant (Figure 2.7a). Therefore, absorbance at the wavelength of maximal absorption can be used to quantify AgNPs. Increasing the $Ca(NO_3)_2$ concentrations from 0 to 0.5 mM progressively reduced the AgNP content in

the supernatant from 34% of initial AgNPs to below the detection level of the GFAAS. Concentrations of $Ca(NO_3)_2$ larger than 0.5 mM ensured that all AgNPs aggregated, leading to complete sedimentation as shown by negligible absorption in the long wavelength region (550-700 nm) (Figure 2.7a).

The efficiency of combining aggregation with centrifugation to precipitate different concentrations of AgNPs (total Ag, 100-5012 µg/L) was investigated. Supernatants did not show any absorption from 350 to 700 nm after aggregating those concentrations of AgNPs in 2 mM $Ca(NO_3)_2$. By contrast, 21-50% of AgNPs remained in the supernatant without Ca^{2+} (Figure 2.7b). Therefore, 2 mM $Ca(NO_3)_2$ was sufficient to aggregate even the very dilute AgNPs.

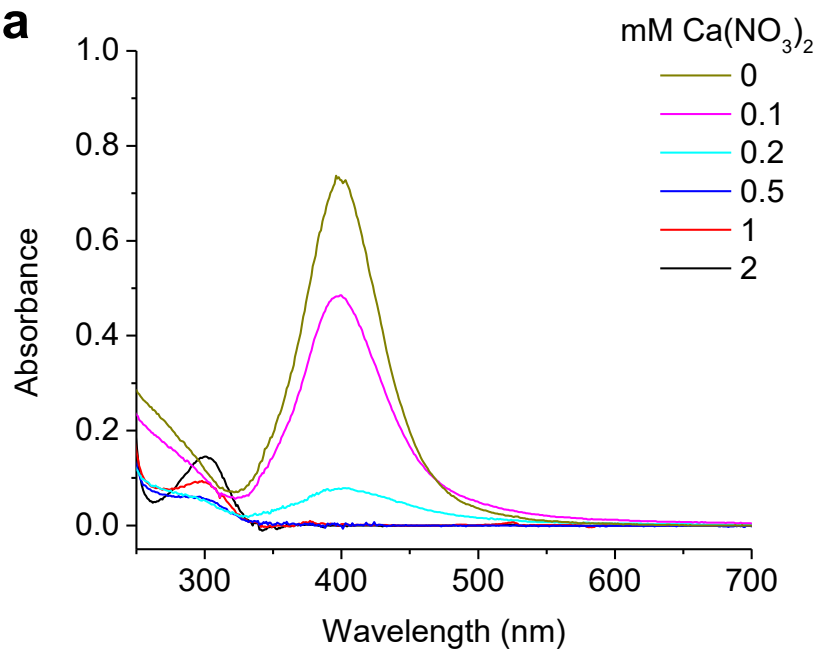

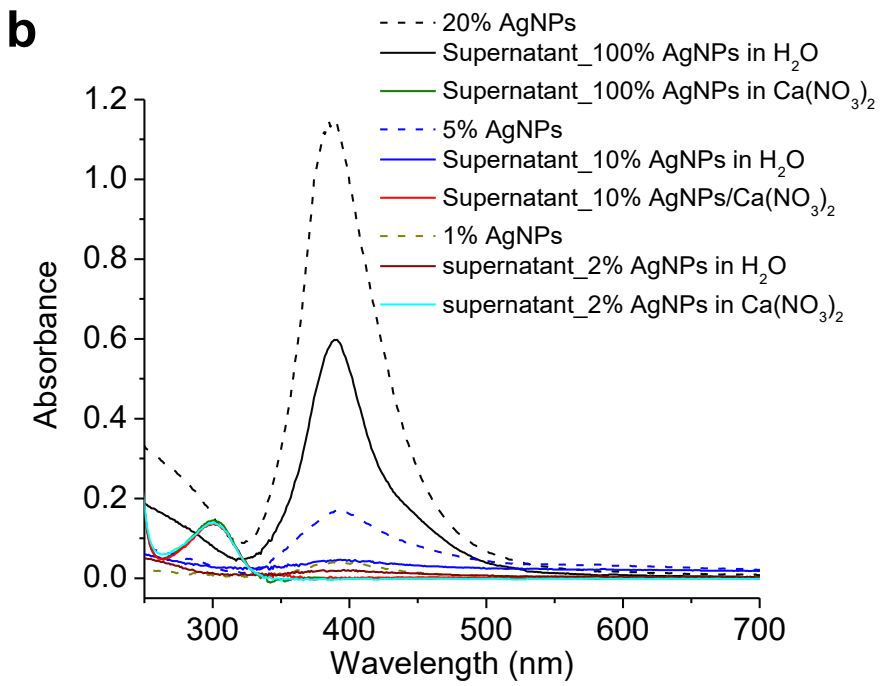

Figure 2.7 Sedimentation of AgNPs in $Ca(NO_3)_2$ by centrifugation
(a) UV-Vis absorption spectra of supernatant after centrifugation of AgNPs (100%) in various concentrations of $Ca(NO_3)_2$. **(b)** The same for various concentrations of AgNPs in 2 mM $Ca(NO_3)_2$ or H_2O. Three concentrations of AgNPs (100%, 10% and 2% AgNPs) were mixed with H_2O or $Ca(NO_3)_2$. The percentages refer to the dilutions of the AgNP stock (100%) with DI H_2O. Since the concentration of the AgNP stock (total Ag 5012 ± 75 µg/L; dissolved Ag 283 ± 13 µg/L) was too high for recording the spectrum, it was diluted to 20%.

2.3.6 Measuring dissolved Ag in AgNP suspensions by aggregation or ultrafiltration

Silver nanoparticle samples containing various concentrations of dissolved Ag were obtained by diluting the AgNP stock with H_2O. The dissolved Ag concentrations in these samples should therefore be proportional to the AgNP concentration. This was confirmed by linear regression as the adjusted R^2 were high in each case (0.974 for aggregation-centrifugation and 0.977 for ultrafiltration) (Figure 2.8). However, the slope of the regression line for aggregation-centrifugation was 1101 ± 54, i.e. 6.4 times larger than the slope for ultrafiltration (173 ± 8). This means that 6.4-fold more

dissolved Ag was detected by aggregation-centrifugation. A partial explanation for this difference was the loss of Ag during ultrafiltration (Figure 2.9). The amount of Ag lost was proportional to the initial Ag^+ concentration before filtration. Although Ag recovery gradually improved over five cycles of filtration of the same $AgNO_3$ solution, there was still a loss of 39-44% of Ag in the last cycle (Figure 2.9).

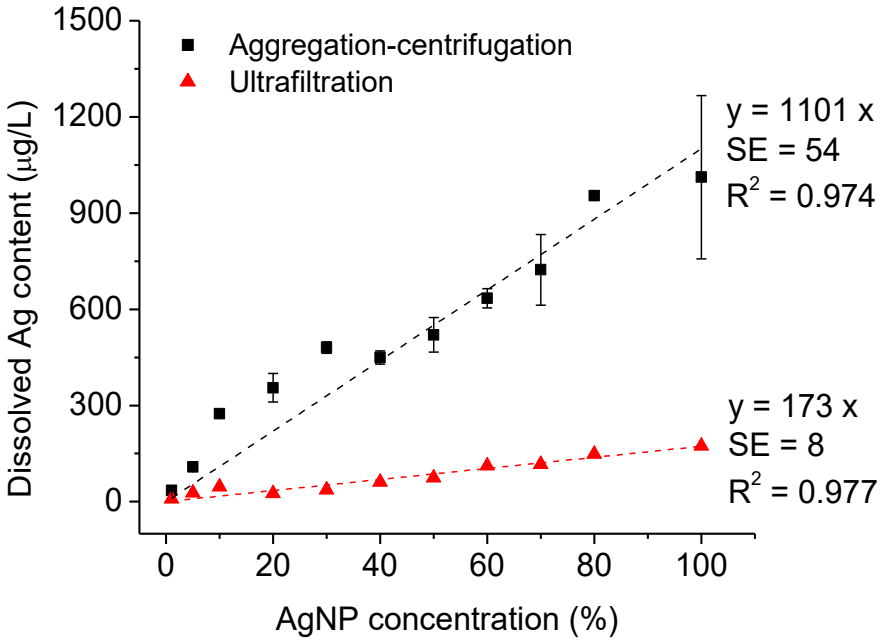

Figure 2.8 Comparison of aggregation-centrifugation with ultrafiltration
Dissolved Ag content measured by aggregation-centrifugation or ultrafiltration is proportional to the concentration of AgNPs. The AgNP suspensions with different concentrations of dissolved Ag were obtained by diluting the AgNP stock (100%) with DI H_2O. Therefore, the dissolved Ag content should be proportional to the AgNP concentration. AgNPs were aggregated by 2 mM $Ca(NO_3)_2$, followed by centrifugation before measuring the dissolved Ag concentration in the supernatants. Error bars indicate standard deviation (n = 2). The dissolved Ag content was also measured by ultrafiltration. Linear regression of dissolved Ag concentration versus AgNP concentration confirmed the proportionality. SE indicates standard error of the slopes (the intercept was set to 0). The relative SEs were similar for both methods (0.049 for aggregation-centrifugation, 0.046 for ultrafiltration) while the dissolved Ag concentration was 6.4-fold higher measured by aggregation-centrifugation than by ultrafiltration.

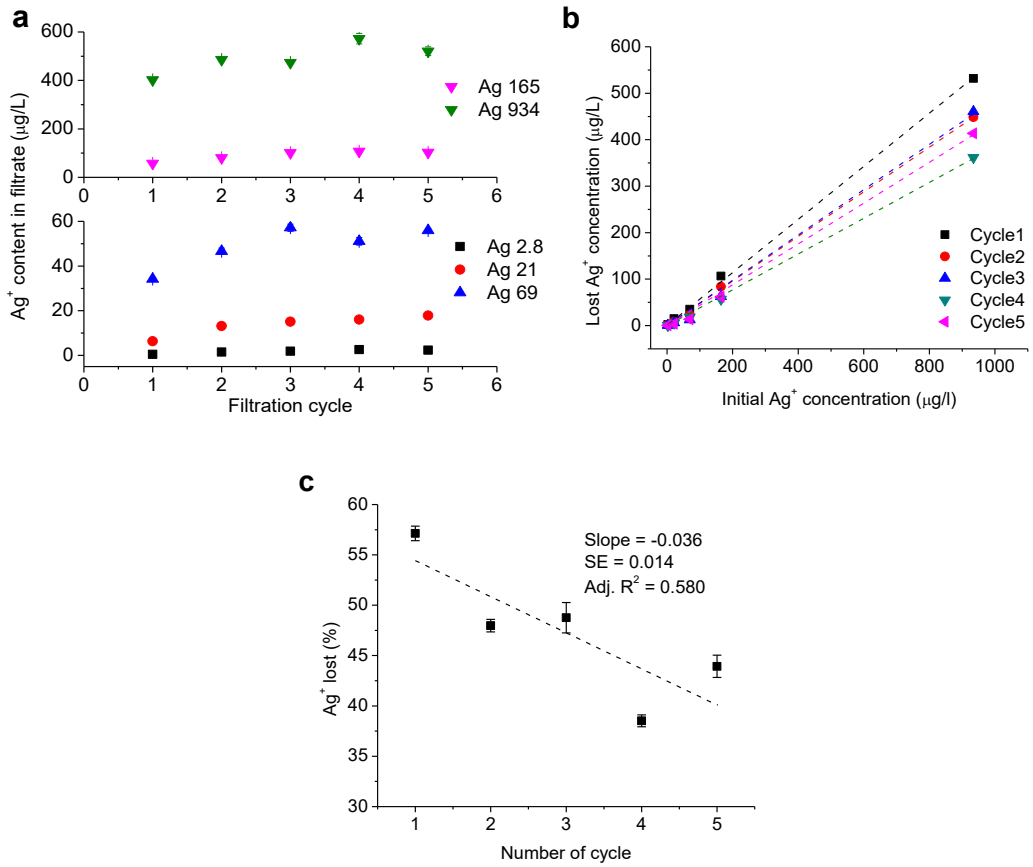

Figure 2.9 Adsorption of Ag^+ to ultrafiltration units during ultrafiltration
(a) Ag^+ concentrations in filtrates during five cycles of filtration by centrifugation (4 °C, 4000 g, 20 min) with one of five different concentrations of $AgNO_3$ (2.8, 21, 69, 165 and 934 µg/L Ag^+). After each filtration step, filtrates were collected and the Ag^+ concentration in the filtrates measured by GFAAS. Error bars indicate the standard deviations of three measurements of the sample by GFAAS. **(b)** Linear regression of Ag^+ loss versus initial Ag^+ concentration for each cycle of filtration. The intercept was set to zero. **(c)** Linear regression of the slopes of the linear regressions in panel b versus filtration cycle. The negative slope of this regression line indicates that the fraction of Ag^+ lost decreased somewhat with each cycle. The error bars represent standard errors of the slopes.

2.4 Discussion

2.4.1 Formation of stable, uncapped AgNPs

This study demonstrated the successful synthesis of monodispersed uncoated AgNPs (Figure 2.1). The formation of uncoated AgNPs is controlled by the aggregative growth of small AgNPs [16, 223], but aggregation of the NPs can lead to the failure of synthesis [94]. Frequently, the electrolyte with highest ionic strength contributes most to the aggregation [140, 224]. As expected, by decreasing initial $AgNO_3$ and $NaBH_4$ concentrations to reduce the ionic strength and increasing the $NaBH_4/AgNO_3$ concentration ratio so more BH_4^- is available to stabilize uncoated AgNPs [219], stable uncoated AgNPs were produced. The process was reproducible, and the three batches of AgNPs produced in this manner did not differ significantly in their aggregation in $Ca(NO_3)_2$ or sedimentation by centrifugation.

2.4.2 Aggregation of AgNPs in $Ca(NO_3)_2$ solution

According to classic colloidal theory, interactions between nanoparticles are determined by van der Waals forces, electrostatic repulsive forces, and steric effects due to surface stabilizers and solvation effects [48]. For uncoated AgNPs, negatively charged ions such as BH_4^- adsorb onto the nanoparticles with counter ions enriched near the surface [94, 225]. Positively charged Ca^{2+} ions screen the negative surface charge of AgNPs, thus decreasing surface energy and repulsion between nanoparticles. Aggregation of AgNPs occurs when the kinetic energy of Brownian motion overcomes the nanoparticle-nanoparticle energy barrier, which is reduced in $Ca(NO_3)_2$ solution i.e.

as nanoparticles become essentially neutral [138]. The structure of aggregates formed, such as configuration and monomer numbers, depends on nanoparticle concentration, size distribution, surface coating, and conditions in the surrounding liquid [139, 226]. The gap between clustered nanoparticles can be as narrow as a few nanometres [3]. Under normal gravitational force, gold nanoparticles (40-100 nm) take days or weeks to settle a few millimetres [227]. In contrast, the AgNPs completely sedimented to the bottom in 2 mM $Ca(NO_3)_2$ solution within 4 d (Figure 2.2), suggesting that aggregation facilitates sedimentation of AgNPs.

The aggregation rate of AgNPs increased markedly when the $Ca(NO_3)_2$ concentration was increased from 0.1 to 0.2 mM, reaching a maximum rate at 0.5 mM (Figure 2.4). This suggests that ~0.2 mM was the concentration separating the slow and fast aggregation regimes, which is known as the critical coagulation concentration (CCC). The aggregation rate was proportional to AgNP concentration in both 2 and 20 mM $Ca(NO_3)_2$ solutions (Figure 2.4). Increasing AgNP concentration will increase the number of AgNPs with high enough kinetic energy to overcome the energy barrier upon collision and thereby increase the aggregation rate. Notably, 2 and 20 mM $Ca(NO_3)_2$ aggregated equivalent concentrations of AgNPs equally fast, suggesting that any concentration above the CCC is sufficient to ensure optimum aggregation of AgNPs.

2.4.3 Efficiency of AgNP sedimentation in $Ca(NO_3)_2$ solution by centrifugation

It is predicable that centrifugation will shorten the sedimentation time of AgNP aggregates. As the sedimentation velocity is proportional to the square of nanoparticle

diameter, the distance settled declines dramatically with decreasing nanoparticle size (Figure 2.10) [228]. Consequently, it takes exceedingly long to sediment small AgNPs (<10 nm) completely. Centrifugation of AgNPs in H_2O will especially increase the sedimentation of the larger AgNPs, leading to a steep initial decrease of Ag content in the upper layer of the suspension and a slowdown afterwards. In $Ca(NO_3)_2$ solutions, complete sedimentation was achieved in half an hour (Figure 2.6). As TEM graphs showed (Figure 2.5), individual AgNPs assembled into compact clusters that sedimented much faster due to their larger sizes.

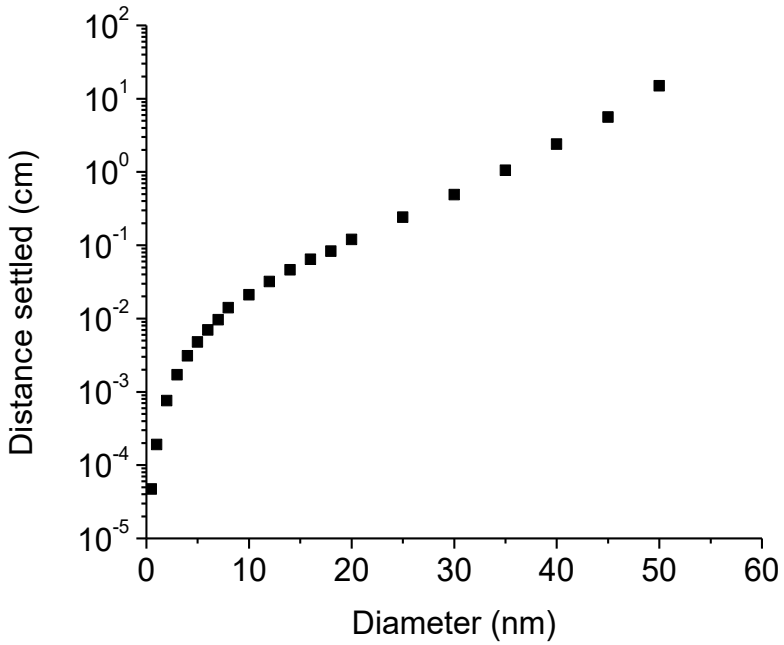

Figure 2.10 Simulation of sedimentation of AgNPs by centrifugation
Simulation of sedimentation of AgNPs by centrifugation according to [228] assuming spherical particles. The distance settled after 30 min was plotted against the diameter of AgNPs. The parameters for simulation were set as follows: density of AgNPs 10.49 g/cm^3, density of medium 1 g/cm^3, liquid viscosity 1 mPa·s, angular velocity of centrifugation 14,000 rpm and rotor radius 9.2 cm.

Judging from the similar shapes of UV-Vis absorption spectra of supernatant and

monodispersed AgNP suspensions, coupled with negligible absorption in the long wavelength region that is characteristic for aggregates (Figure 2.7), the aggregates but not all individual AgNPs were sedimented by centrifugation. Increasing $Ca(NO_3)_2$ concentrations enhanced the aggregation rate and therefore the sedimentation rate of AgNPs. When the $Ca(NO_3)_2$ concentration was larger than the CCC, the fast aggregation regime was obtained and virtually all AgNPs precipitated, making this pre-aggregation approach applicable to a broad range of AgNPs concentrations.

2.4.4 Comparing the aggregation-centrifugation method with ultrafiltration

Both the aggregation-centrifugation method and ultrafiltration enabled measurement of the dissolved Ag concentration in AgNP suspensions. Larger dissolved Ag concentrations were obtained by aggregation-centrifugation than by ultrafiltration (Figure 2.8). This suggests that some of the dissolved Ag is not effectively separated from the AgNPs by ultrafiltration or is lost to the apparatus, either as ions or nanoparticles. The various Ag species in AgNP suspensions include nanoparticulate Ag, free Ag^+ in the bulk liquid [217], Ag bound to ions or organic groups in the bulk liquid [127, 129, 229], and Ag^+ attached to the nanoparticle surface [225]. During ultrafiltration, nano Ag together with any attached Ag^+ would presumably be retained by the membrane. Silver loss also occurs due to the adsorption of Ag^+ to the filter units during ultrafiltration (Figure 2.9). Silver ion adsorption by the same brand of ultrafiltration units has been reported in several studies [213, 214, 217]. In the aggregation-centrifugation method, Ag loss by adsorption is minimized. Presumably,

all free Ag^+ except that attached to nanoparticle surface in the bulk liquid will remain in the supernatant. Once individual AgNPs aggregate into compact clusters by Ca^{2+} bridging, the dissolved Ag^+ ions that acted as counter ions to balance the negative charges on AgNP surfaces might become released from the AgNP. Additionally, Ca^{2+} could replace the surface-attached Ag^+ in the diffuse and Stern layer, releasing Ag^+ into the bulk liquid. Therefore, more dissolved Ag can be collected by centrifugation after aggregation. Since both of these pools of Ag^+ species contribute to the toxicity of AgNPs, it is advantageous to include their concentration in measurements of dissolved Ag in AgNP suspensions.

2.5 Conclusions

In this study, a new method to measure dissolved Ag in AgNP (10-40 nm) suspensions was developed. By combining aggregation with centrifugation, only half an hour was required to separate dissolved Ag from AgNPs. Uncoated AgNPs were aggregated by $Ca(NO_3)_2$ and a concentration of 2 mM was sufficient to induce the formation of large AgNPs clusters. This pre-aggregation facilitated the sedimentation of a wide range of AgNP concentrations by centrifugation. The combined aggregation-centrifugation method avoided the loss of Ag in ultrafiltration. That more dissolved Ag was obtained by the new method has significant implications for the study of AgNPs toxicity. Since the combined aggregation-centrifugation method significantly reduces centrifugation time to separate nanoparticles from ions, it will be especially helpful for real-time toxicity assays where speed and the convenience of table top centrifugation represent a major methodological improvement compared to conventional ultracentrifugation and ultrafiltration. The method may also be applicable for separating ions from nanoparticles with coatings (electrostatically and sterically stabilized) in the complex environment such as toxicity test media.

3 Chapter Three

A Real-time Toxicity Study Reveals the Dynamic Interactions between Uncoated Silver Nanoparticles and Bacteria

Feng Dong, Eugenia Valsami-Jones, Jan-Ulrich Kreft. A real-time toxicity study reveals the dynamic interactions between uncoated silver nanoparticles and bacteria. Submitted to Nanotoxicology, 2016.

3.1 Introduction

Silver (Ag) is not known to be required for any metabolic process, rather, it disturbs cellular metabolism and kills bacteria at low concentrations [29, 146]. Hence, silver and its compounds have been used as antimicrobial agents since ancient times [28]. Several mechanisms are responsible for the toxicity of Ag for bacteria such as generating reactive oxygen species (ROS) [148], abolishing protein activity [30], collapsing membrane proton motive force [157], and disturbing gene regulation [206]. Owing to the high antimicrobial activity of Ag, AgNPs are heavily used nanomaterials [209, 230]. The large surface to volume ratio leads to the high activities of nanomaterials including surface reaction and chemical modification [96, 118], dissolution [123] and aggregation in electrolyte solutions [140]. It is generally believed that the antibacterial activities of AgNPs are entirely due to the released Ag^+ [201, 231]. However, it is unclear whether nano Ag also has direct toxic effects on bacteria due to the difficulties of disentangling Ag^+ from nano Ag effects.

The dissolution of AgNPs is affected by nanoparticle properties such as surface coating [232] and particle size [103, 123] as well as environmental conditions such as ionic strength [117, 128], light [126], oxygen concentration [116, 125], temperature [117] and pH [233] and additionally chemical reactions at the nanoparticle surface including silver-chloride complexation [129], oxidation [97], sulfidation [127] and modification by organic substances [229, 234]. Silver nanoparticles undergo aggregation upon exposure to electrolyte solution [139], toxicity test medium [235] and natural water

[236]. The extent of aggregation influences sedimentation rates [133, 237], particle accessibility to cells [238] and dissolution kinetics [124]. All these transformations combine to control the toxicity of AgNPs towards cells. Therefore, it is critical to combine nanoparticle characterization with toxicity assays in real-time to understand the toxicity mechanisms. Moreover, any differences in AgNP synthesis, storage and toxicity test media compositions can give rise to differences in results, hampering comparability of studies [239].

In this study, AgNPs were systematically characterized and their toxicity to the environmental model bacterium *Pseudomonas putida* was investigated in real-time, which also helps understand the environmental risk of AgNPs. To minimize nanoparticle changes during exposure to test media, a citrate minimal medium was used. Moreover, uncoated AgNPs, stored under N_2 to reduce oxidation, were used to avoid interferences from surface ligands, in order to investigate the dynamic interactions between AgNPs and bacteria under as well defined conditions as possible. It was found that the concentration of Ag^+ or AgNPs to kill a bacteria population was highly corrected with initial population density. Dissolved Ag^+ mainly contributed to the toxicity of AgNPs that can continuously release Ag^+ to inhibit bacterial growth.

3.2 Materials and methods

3.2.1 Synthesis of uncoated AgNPs

Uncoated AgNPs were synthesized by reducing silver nitrate ($AgNO_3$, Sigma-Aldrich) with sodium borohydride ($NaBH_4$, Sigma-Aldrich) at room temperature (19 ± 4 °C) according to [16]. All glassware for AgNPs synthesis and storage was soaked in 10% HNO_3, rinsed with DI water and dried under ambient environment. The procedures for synthesis of AgNPs are described in section 2.2.1.

3.2.2 Characterization of AgNPs

The LSPR of uncoated AgNP suspensions was measured by UV-Vis absorption spectrometry (UV-Vis 6800, Janway). The hydrodynamic size of AgNPs was measured by DLS (Zetasizer Nano, Malvern Instruments) and DCS (DC24000, CPS Instruments). Zeta potential was measured by Malvern Zetasizer Nano. The morphology of AgNPs was examined by TEM (JEOL 1200EX). The sample preparation for TEM is described in section 2.2.2.

3.2.3 Storage of AgNPs

The stability of AgNPs under ambient air or nitrogen atmosphere at 4 °C in the dark was compared by measuring the dissolved Ag concentration in these two atmospheres over 4 months by ultrafiltration (Amicon Ultra-15 Centrifugal Filter Unit 3 kDa, Merck Millipore) at the centrifugal force of 4,000 g for 30 min at 4 °C (Centrifuge 5804R, Eppendorf). For incubation under N_2, the bottle (100 or 250 mL, Duran) was flushed

with large amounts of nitrogen gas for at least 5 min to minimize O_2 in the liquid and gas phase. The AgNP-N_2 stock was flushed again with N_2 and sealed as quickly as possible after every sample collection. To determine the total Ag concentration of AgNP stocks, the AgNP suspensions were digested by 70% HNO_3 (1 mL AgNP suspensions added into 9 mL HNO_3) overnight at room temperature. The mixture was then diluted to a final HNO_3 concentration of 0.2% for GFAAS (AAnalyst 600, PerkinElmer Instruments). UV-Vis absorption spectra and TEM morphology of these two AgNP stocks were monitored during the long-term storage.

3.2.4 Aggregation of AgNPs in defined medium

The aggregation kinetics of AgNPs in a minimal medium was determined by real-time DLS and time-resolved UV-Vis absorption spectrometry. The hydrodynamic size changes of AgNPs in Davis minimal medium salts solution (DMM without the carbon source citrate) were measured over two hours. The AgNP suspensions (0.5 mL, total Ag 100, 200 and 400 μg/L) were mixed with the same volume of DMM salts solution (pH, 7.1) in disposable plastic (polystyrene) cuvettes, followed by immediate sample analysis. Thus, the final concentrations of AgNPs and DMM salts solution were halved. Temperature was controlled at 25 °C. The AgNP suspensions were obtained by diluting the stock (total Ag 2470 ± 183 μg/L, dissolved Ag 304 ± 10 μg/L) with DI H_2O. The composition of DMM is as follows (per litre) (pH, 7.2): 7.0 g K_2HPO_4, 2.0 g KH_2PO_4, 1.0 g $(NH_4)_2SO_4$, 0.1 g $MgSO_4$, 1.530 g sodium citrate dihydrate and 1 mL SL10 trace elements solution. The SL10 trace elements stock solution contains per litre: 1500 mg

$FeCl_2 \cdot 4H_2O$, 190 mg $CoCl_2 \cdot 6H_2O$, 100 mg $MnCl_2 \cdot 4H_2O$, 70 mg $ZnCl_2$, 6 mg H_3BO_3, 36 mg $Na_2MoO_4 \cdot 2H_2O$, 24 mg $NiCl_2 \cdot 6H_2O$ and 2 mg $CuCl_2 \cdot 2H_2O$. Precipitation of silver as chloride and sulfate salts in DMM can be neglected according to solubility calculations carried out with Visual MINTEQ that is used for chemical equilibrium calculations (Version 3.0, The Royal Institute of Technology, Sweden), e.g. Ag^+ is completely dissolved and 96% of the Ag is free Ag^+ for 500 μg/L Ag^+ in DMM.

3.2.5 Dissolution of AgNPs

The dissolution of AgNPs in DMM salts solution and H_2O was examined at 30 °C, the same temperature used for the toxicity tests. AgNP suspensions (20 mL with 134, 328 or 730 μg/L) were mixed with the same volume of DMM salts solutions in 100 mL glass flasks, resulting in final Ag concentrations of 67, 164 and 365 μg/L, respectively. The glass flasks were cleaned in the following way: soaked in disinfectant (Virkon, Rely+On, DuPont) for 1 h, rinsed with tap water, washed with detergent, washed with Lanceracid (containing 20-50% acetic acid) (Lancer UK Ltd, Cambridge, UK), rinsed with distilled water, dried and sterilized at 160 °C for 2 h. To prevent settling of AgNPs, the flasks were shaken at the speed of 120 rpm. The change of concentration of dissolved Ag was quantified by the method described in Chapter Two. In brief, 0.5 mL AgNPs were aggregated by addition of the same volume of 2 mM $Ca(NO_3)_2$ (1 mM final concentration after mixing) for 10 min and then centrifuged at 20,100 g for 30 min at room temperature (Centrifuge 5417 C, Eppendorf). Supernatants (0.5 mL) were carefully collected and stored at -20 °C for future analysis. Before the GFAAS

measurement, the supernatants were digested by adding the same volume of 2% HNO_3 at 80 °C for at least 12 h.

Adsorption of Ag^+ to the glass flasks under the same conditions was also examined. Silver ions solution (20 mL, 62 or 126 μg/L) was mixed with same volume of DMM salts solution or DI H_2O in 100 mL glass flasks with shaking at 120 rpm at 30 °C. Samples (1 mL) were collected from 0 to 96 h and frozen at -20 °C. The Ag content in these samples was measured by GFAAS.

3.2.6 Bacterial strain and culture conditions

The environmental model bacterium *Pseudomonas putida* was chosen in this study. The green fluorescent protein (GFP) tagged derivative JB279 of *P. putida* KT2442 was generously donated by Prof. Søren Molin (Technical University of Denmark). A stable GFP is expressed from the strong LacI repressible promoter $P_{A1/04/03}$ that is part of the mini-Tn5-Km-T_1-T_0-gfpmut3*-$P_{A1/04/03}$ randomly inserted into the bacterial chromosome [240]. Davis minimal medium (containing SL10 trace elements as described in section 3.2.4) supported growth at 30 °C. The low concentrations of borate (< 1.5 mM) introduced with the AgNP suspensions have negligible effects on the growth of bacteria [241, 242].

3.2.7 Measurement of growth rate

Pseudomonas putida KT2442 was grown in LB overnight. The overnight culture was transferred into 50 mL DMM that contained 50 μg/L kanamycin. The culture was aerated at a shaking speed of 200 rpm in a water bath shaker at 30 °C. OD was measured

at 600 nm for 10 h using a UV-Vis spectrophotometer (Bioware DNA Life Spectrophotometer, WPA).

A flow-cell was used to monitor the growth of individual cells and biofilm formation. A glass cover slip was placed on the top of flow-cell chamber and fixed with glue. *P. putida* can attach to the surface of the cover slip. DMM was pumped through the chamber to support bacterial growth. A time-lapse fluorescent microscope was used to monitor the bacterial growth at room temperature (18-25 °C), as shown in Figure 3.1.In the flow-cell AgNPs can be immobilized on the surfaces of cover slip, which might release Ag^{+} into the main channels of flow-cell. As DMM is continuously pumped through the channels the dissolved Ag^{+} in the channels are expected to be washed away by the flow, solely exposing the attached AgNPs to bacterial cells and separating nanoparticle from ion effects, which will allow to directly observe the nanoparticle-cell interactions. Additionally, the formation of biofilm on the surfaces can also be monitored by confocal microscopy. The cells attached to the surfaces of cover slip were focused by an oil objective (100.0 × 1.40). An area of 75 μm × 75 μm was scanned with 8.26 μm in depth for z-stacks at the interval of 2 min for 4 h. After three days, formation of biofilm was observed.

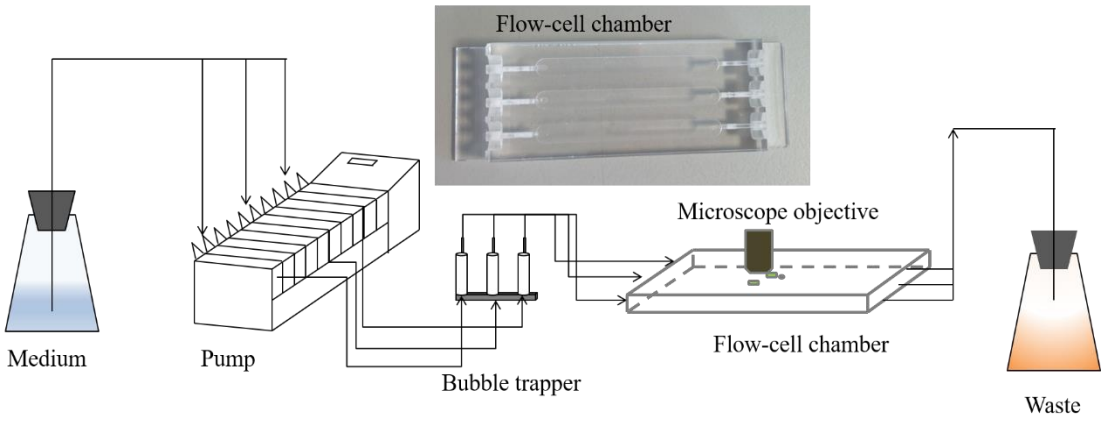

Figure 3.1 Flow-cell system
Schematic diagram of flow-cell. The medium (DMM) was supplied by pump into the flow-cell chamber. A bubble trapper was used to release sir bubbles. The flow rate was controlled by the pump. Waste was collected. A cover slip was placed on the top of flow-cell chamber. *P. putida* cells attach to the surface of cover slip and use the substrate in the chamber for growth. The division of individual cells and biofilm formation were captured at a resolution of 2 min by a confocal laser scanning microscope (Leica SP2 Upright Confocal).

3.2.8 Determination of MICs

The minimum inhibitory concentrations (MICs) of AgNPs and Ag^+ were determined according to a standard protocol [243]. The protocol was modified to study the influence of cell density on MICs by varying the initial cell numbers. Four or five *P. putida* KT2442 colonies on LB plates were picked and inoculated into DMM (containing 50 μg/L kanamycin) for overnight growth at 30 °C. The overnight culture was transferred into 50 mL fresh DMM (containing 50 μg/L kanamycin) and grown for 4-6 h to reach the mid-exponential phase. After the density of the culture reached around 1.5×10^8 CFU/mL, the culture was diluted with fresh DMM to obtain different densities (10^4, 10^5, 10^6, 10^7 and 10^8 CFU/mL). Within 30 min, 100 μL of the diluted culture was mixed with 100 μL different concentrations of AgNP suspensions or Ag^+ solution in a 96-microwell plate. Each treatment was conducted in triplicate. The plates were

covered with lids and incubated at 30 °C for 16-24 h. Optical density (OD) was monitored to determine the MICs as the lowest concentrations that prevented growth (OD remaining < 0.05).

3.2.9 AgNP and Ag^+ kill kinetics

Kill kinetics were determined by monitoring cell viability over 5 h at different concentrations of AgNPs or Ag^+. Low initial bacterial cell densities were chosen to avoid titration of AgNPs or Ag^+ by the biomass. Overnight cultures were diluted with fresh DMM and grown to mid-exponential phase as above, followed by dilution with DMM salts (no carbon source) to obtain final densities around 10,000 CFU/mL. These diluted cultures (20 mL) were mixed with the same volumes of AgNP suspensions (0-100 μg/L) or Ag^+ solutions (0-50 μg/L) in 100 mL glass flasks. To prevent sedimentation of AgNPs, the cultures were shaken at 120 rpm at 30 °C. Plates were immediately set up with taking samples and spreading cell cultures on LB plates for viable counts at the interval of 0.5 or 1 h. Dissolved Ag contents in the culture treated by AgNPs were determined as described in Chapter Two. The Ag contents in the supernatant were measured by GFAAS. For Ag^+-treated cultures, 1 mL cell culture was centrifuged (20100 g, 30 min), and 0.5 mL supernatants were collected and stored at -20 °C.

Dose-response curves were measured as above but with higher time resolution in order to obtain the killing rates by linear regression of viable count versus time. The order of these treatments was randomized. Viable counts were examined by spreading 100 μL

culture on LB plates at time 0, 10, 20, 30, 45 and 60 min.

3.3 Results

3.3.1 Synthesis and characterization of uncoated AgNPs

Because the sorption of BH_4^- on the surface of AgNP cores is responsible for the stabilization of uncoated AgNPs [94, 219, 244], a high $NaBH_4/AgNO_3$ ratio was chosen to synthesize AgNPs without surface ligands. Stable, uncoated AgNPs with spherical shape were obtained (Figure 3.2a). The characteristics of AgNP suspensions are listed in Table 3.1. Nearly 90% of Ag^+ was reduced to AgNPs. Most of the AgNPs were in the size range between 10 and 40 nm (Figure 3.2b). No aggregates were observed in the AgNP suspension with clear light yellow colour. The absorbance peak of the AgNP suspension was 394 ± 1 nm (Figure 3.2c), which is in agreement with their surface plasmon resonance [17, 109].

Table 3.1 Characteristics of uncoated AgNP suspensions
Zeta potential and pH are shown as mean ± SD of three batches of uncoated AgNPs produced in the same way. The diameter (mean ± SD) was based on TEM images of the AgNPs used for this study, analysed with ImageJ (n = 438) [222]. The diameters from DCS and DLS were the peak diameters of size distribution curves in Figure 3.2. The concentrations of total Ag and dissolved Ag^+ in the AgNP stock for this study (mean ± SD) were measured by GFAAS.

pH	Diameter (nm)			Zeta potential in DI water (mV)	Ag species (μg/L)	
	TEM	DCS	DLS		Total Ag	Ag^+
9.6 ± 0.3	21 ± 11	13	24	-40 ± 17	2,470 ± 184	272 ± 22

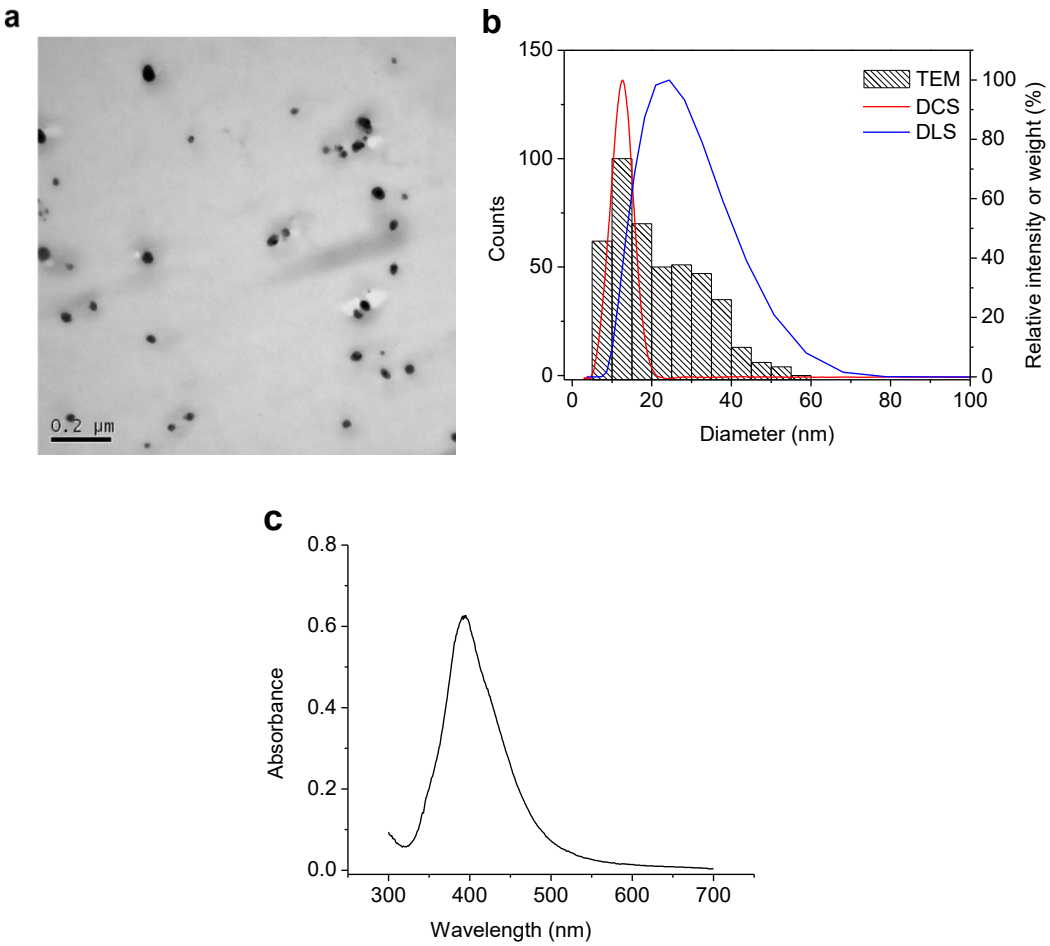

Figure 3.2 Characteristics of uncoated AgNPs
(a) Morphology of uncoated AgNPs by TEM. **(b)** Size distributions of the AgNP stock. The histogram of size distribution (n = 438) was obtained from TEM images analysed with ImageJ [222]. The size distributions measured by DLS and DCS show intensity and relative weight against diameter, respectively. **(c)** UV-Vis absorption spectrum of an uncoated AgNP stock, peak at 394 ± 1 nm (2 d after the synthesis).

3.3.2 Stability of AgNPs during long-term storage

Uncapped AgNP suspensions stored under ambient air slowly released Ag^+. The dissolved Ag concentration increased from 74 to 627 µg/L in 3 months. Under nitrogen atmosphere, in comparison, the dissolved Ag content in AgNP suspensions did not change significantly (Figure 3.3a), confirmed by the lack of change of the UV-Vis absorption spectra (Figure 3.3b). The morphology of AgNPs under N_2 changed little

over 100 d (Figure 3.4a-c). The dissolution of AgNPs under air should decrease particle size, but instead they tended to fuse into larger particles, even nanobars (Figure 3.4d and e). They also transformed from a spherical to a triangular shape (Figure 3.4f).

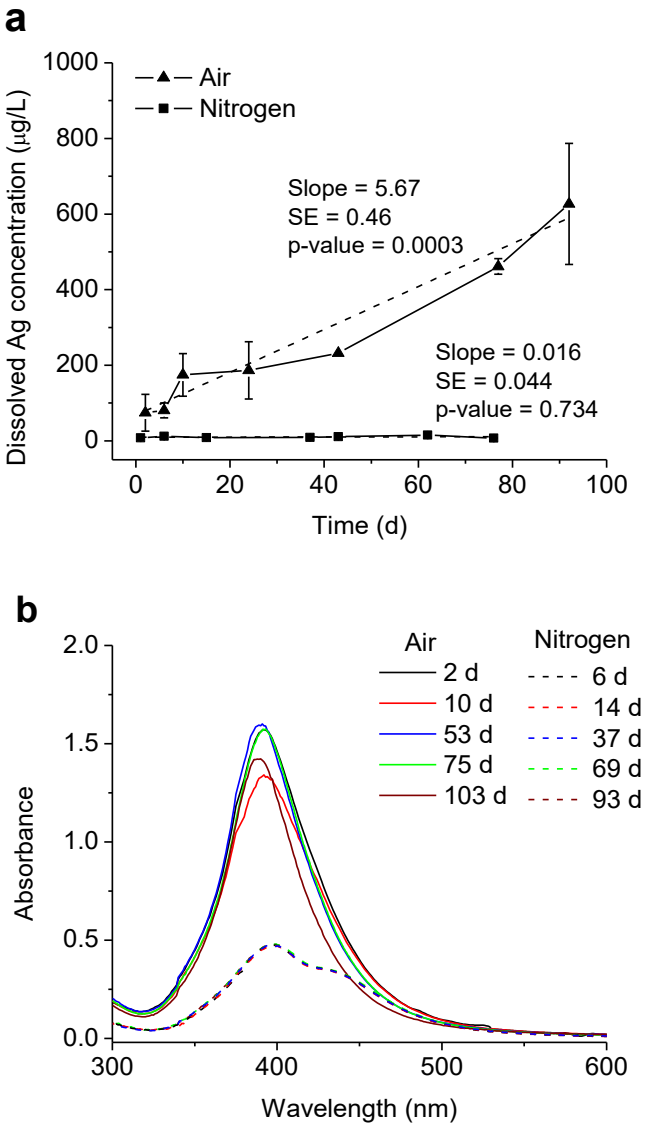

Figure 3.3 Stability of uncoated AgNPs stored in ambient air or under nitrogen Silver nanoparticles were stored in ambient air or under nitrogen atmosphere at 4 °C in the dark. The two AgNP stocks were synthesized by the same procedure. **(a)** Dissolved Ag concentration in the two AgNP suspensions over time. The total Ag concentration of AgNPs under air and AgNPs under N_2 was 25 and 2.28 mg/L, respectively. Error bars indicate standard deviations of at least two measurements. Linear regression was carried out to test whether the slop is significantly different from zero. **(b)** UV-Vis absorption spectra of AgNPs under air or nitrogen.

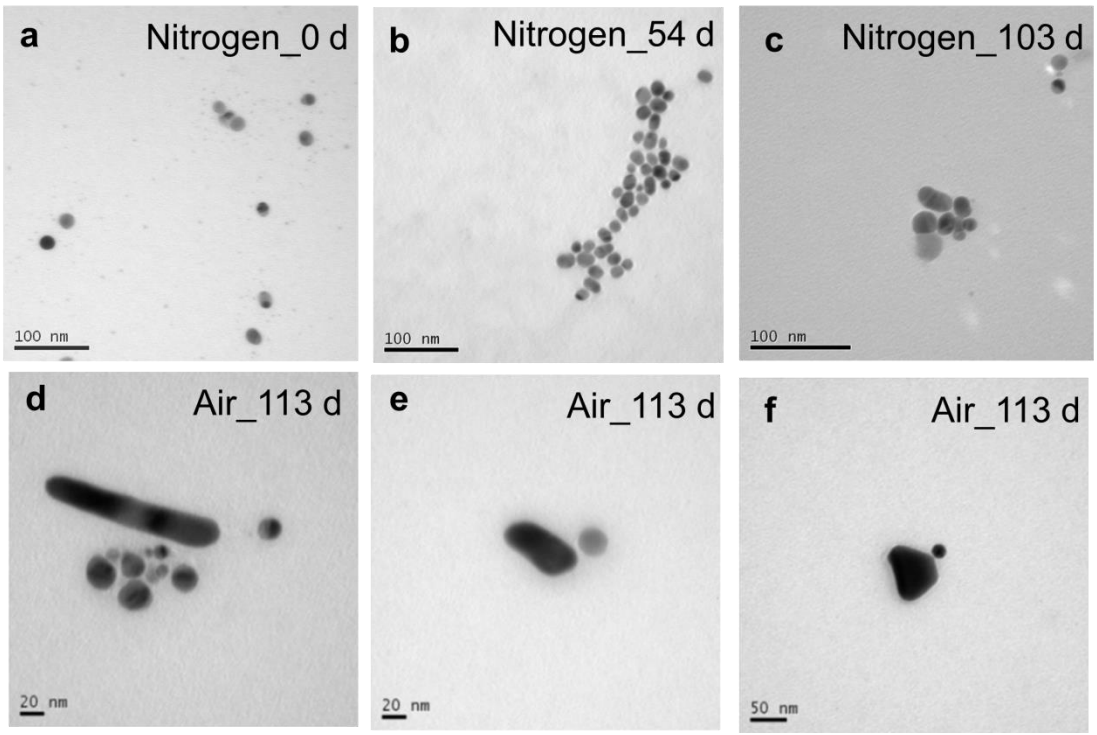

Figure 3.4 TEM images of AgNPs stored under nitrogen or in ambient air over time
(**a**, **b**, and **c**) Under nitrogen; (**d**, **e** and **f**) In ambient air (numbers indicate days).

3.3.3 Aggregation of AgNPs in a mineral medium

The hydrodynamic diameter and UV-Vis absorption spectra of AgNPs in DMM, a defined mineral medium for microbial growth, were measured over time to examine their potential for aggregation during toxicity testing. Uncoated AgNPs underwent different degrees of aggregation in DMM (Figure 3.5). Quicker aggregation leading to larger AgNP clusters was observed for higher concentrations of AgNPs in DMM salts solution (Figure 3.5a). The hydrodynamic sizes of 200 µg/L AgNPs increased strongly compared with the slight rise for 50 µg/L AgNPs. The transformations of UV-Vis absorption spectra also demonstrated faster and more extensive aggregation of the AgNPs at the highest concentration by the quicker decrease of peak absorption, the larger red-shift of the LSPR band and the broadening of the UV-Vis absorption spectra

(Figure 3.5b, c and d). These changes are in agreement with the changes of hydrodynamic size.

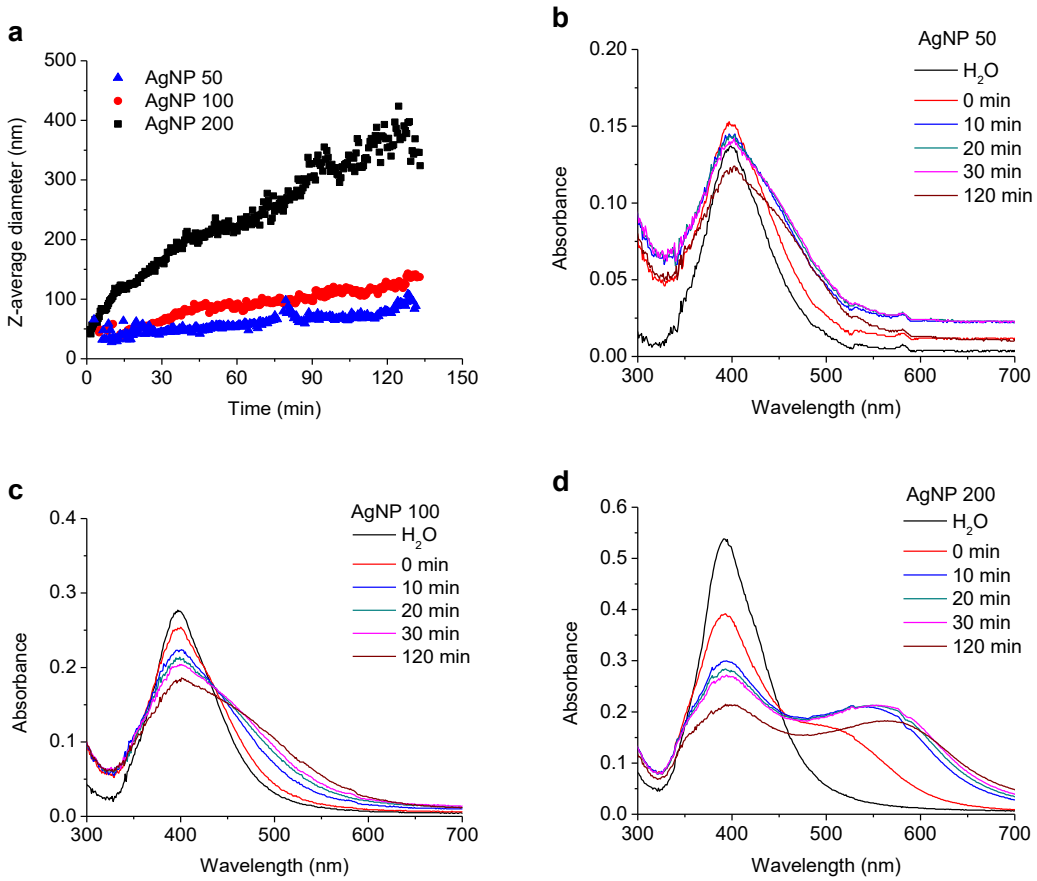

Figure 3.5 Aggregation kinetics of AgNPs in DMM salts solution
(a) The hydrodynamic size (Z-average size) of AgNPs (50, 100 and 200 µg/L) in DMM salts solution was measured by real-time DLS. (**b**, **c** and **d**) Time-resolved UV-Vis absorption spectra of (b) 200, (c) 100 and (d) 50 µg/L AgNPs in DMM salts solution.

3.3.4 Dissolution of AgNPs in a mineral medium

Dissolved Ag plays a central role in the toxicity of AgNPs. Silver nanoparticles release Ag^{+} into solution in oxic conditions. The dissolution kinetics of uncoated AgNPs in DMM salts solution and H_2O were recorded over 7 d (Figure 3.6). Silver nanoparticles dissolved faster in H_2O than in DMM salts (Figure 3.6a). In H_2O, half of the nano Ag dissolved in one day, followed by a slow Ag release over the next several days. A first-

order dissolution kinetics model (p-value = 2.8×10^{-7}) revealed that the equilibrium dissolved Ag concentration was 232 ± 16 μg/L. It was calculated that 69% and 13% of the AgNPs were dissolved for 365 μg/L AgNPs in H_2O and DMM salts solution in 7 d, respectively. The salts in media might reduce Ag dissolution but cannot prevent Ag^+ adsorption (Figure 3.6b). The dissolution rates are listed in Table 3.2. The dissolution rates of AgNPs in DMM salts solution were nearly 40-fold smaller than that in H_2O.

Table 3.2 Dissolution rates of AgNPs in DMM salts solution and H_2O
Linear regression was carried out based on the data within the range of 24-154 h in DMM salts solution and 0-3 h in H_2O, respectively. The dissolution rate was defined as slop of regression/initial concentration of AgNPs.

Concentration of total Ag in AgNP suspension (μg/L)	Solution	Dissolution rate (m ± SE) ($\times 10^{-3}$ μg Ag/(μg AgNP·h))	p-value
67	DMM salts	1.9 ± 0.4	0.0130
164		1.7 ± 0.04	2.27×10^{-6}
365		0.85 ± 0.04	2.25×10^{-4}
365	H_2O	80 ± 19	0.0238

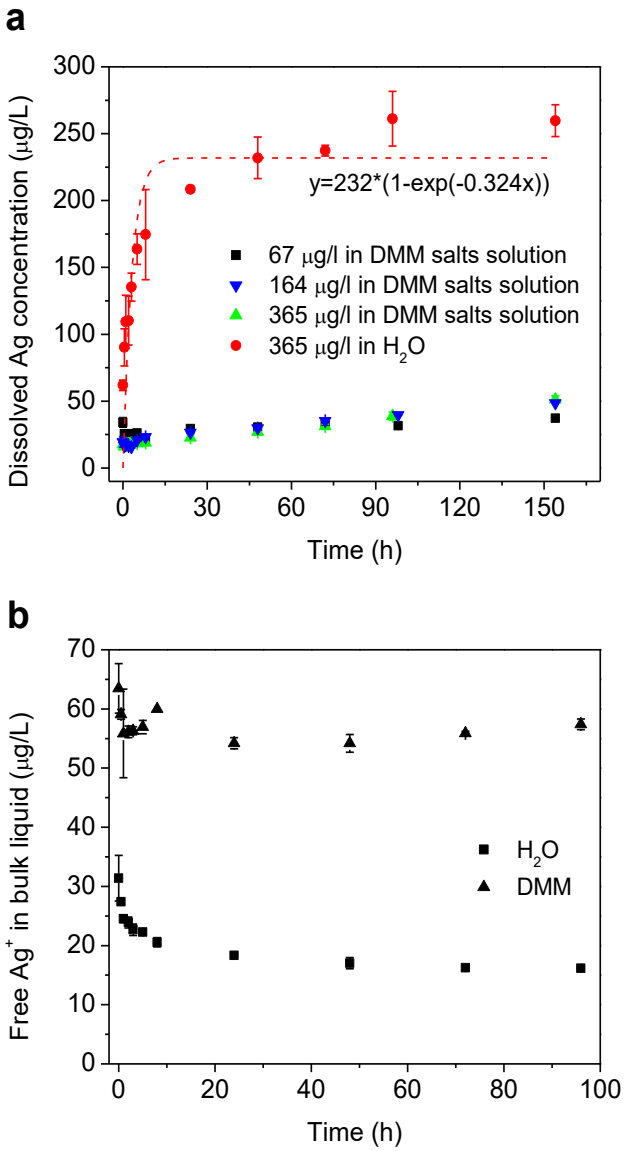

Figure 3.6 Dissolution or adsorption kinetics of AgNPs in H_2O or DMM salts solution

Dissolution or adsorption kinetics of AgNPs in H_2O or DMM salts solution at 30 °C. The volume loss due to evaporation at this temperature was calibrated to be 0.322 mL/d. Error bars indicate the standard errors of triplicates. **(a)** The concentrations of dissolved Ag in H_2O or DMM salts solution. The AgNP stock (total Ag 2,470 ± 184 µg/L, dissolved Ag 272 ± 22 µg/L) was diluted with DI H_2O to obtain different concentrations of AgNPs (67, 164 and 365 µg/L). **(b)** Adsorption kinetics of Ag^+ to a glass flask in H_2O (31 µg/L Ag^+) or in DMM salts solution (63 µg/L Ag^+). The type of glass flasks, washing procedures for glass flasks, volume of liquid and temperature were the same as for the dissolution kinetics experiment. The silver samples in the DMM solution or H_2O were taken from 0 to 96 h and stored at -20 °C. Each sample was measured in triplicate by GFAAS.

3.3.5 Growth rates of *P. putida*

Flow cell was used to observe individual cells. Several cells attached to the surfaces of the cover slip (Figure 3.7a). Production of GFP by the strain allows a direct observation of growth and division of individual cells by microscopy (Figure 3.7a). After the division, some daughter cells stayed on the surface (Figure 3.7a) and form large cell clusters in 3 d (Figure 3.7b). The average time between cellular divisions was 75 ± 13 min (m ± SD) based on the pedigree tree (Figure 3.7c). This generation time was slightly larger than 55 ± 5 min calculated from the growth curves (Figure 3.7d). The reason could be a lower temperature for cells in the flow-cell.

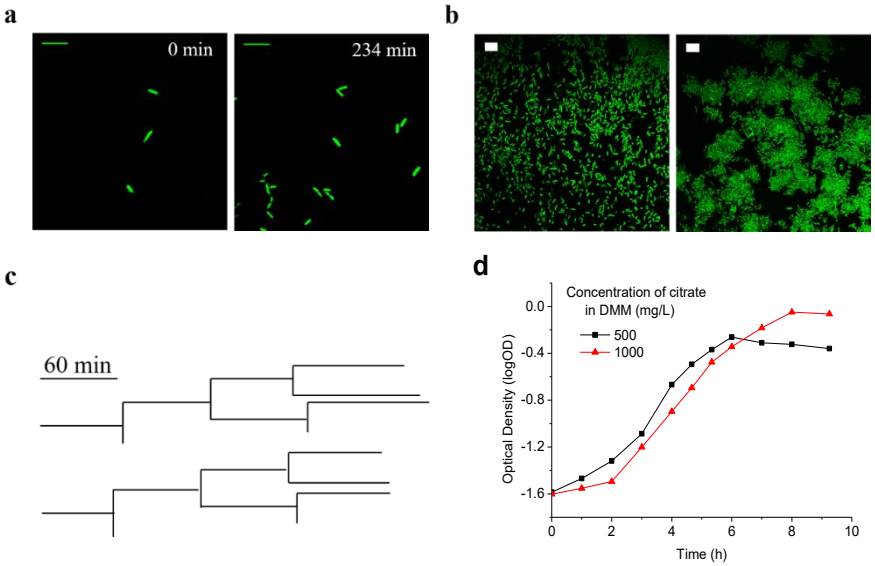

Figure 3.7 Growth rate of *P. putida* KT2442
(a) Attachment of individual cells on the surface (0 min) and their division in 234 min (scar bar = 10 µm). The green colour indicates a production of GFP. **(b)** Formation of cell clusters on the surface in 3 d (scar bar = 10 µm). **(c)** Pedigree tree of two *P. putida* cells based on the images from time-lapse microscopy. The length of branch represents the generation times of cells. The nodes refer to cell division events. A lack of branch indicates detachment of daughter cells from the surface. **(d)** Growth curves of *P. putida* in DMM containing 500 or 1000 mg/L citrate at 30 °C.

3.3.6 Effect of cell density on inhibition

In the standard protocol for determination of MICs, cell cultures are grown into the exponential phase to reach a cell density of 5×10^5 CFU/mL [243]. In this study, MICs of AgNPs and Ag^+ were examined at various initial bacterial densities. Both MICs increased by about one order-of-magnitude when the initial cell density increased by three orders-of-magnitude, from 10^4 to 10^7 CFU/mL (Figure 3.8). *P. putida* was more susceptible to Ag^+ than to AgNPs by more than one order-of-magnitude (Figure 3.8). For instance, 30 μg/L Ag^+ versus 500 μg/L AgNPs were required to completely inhibit bacterial replication at the cell density of 6.4×10^5 CFU/mL. The dissolution of AgNPs can occur during incubation of the cells, resulting in additional Ag^+ release into the culture. As it was not feasible to measure dissolved Ag concentrations over time in the small assay volumes of 96-well plates during the MICs tests, flasks with larger culture volumes were used for determining toxicity kinetics.

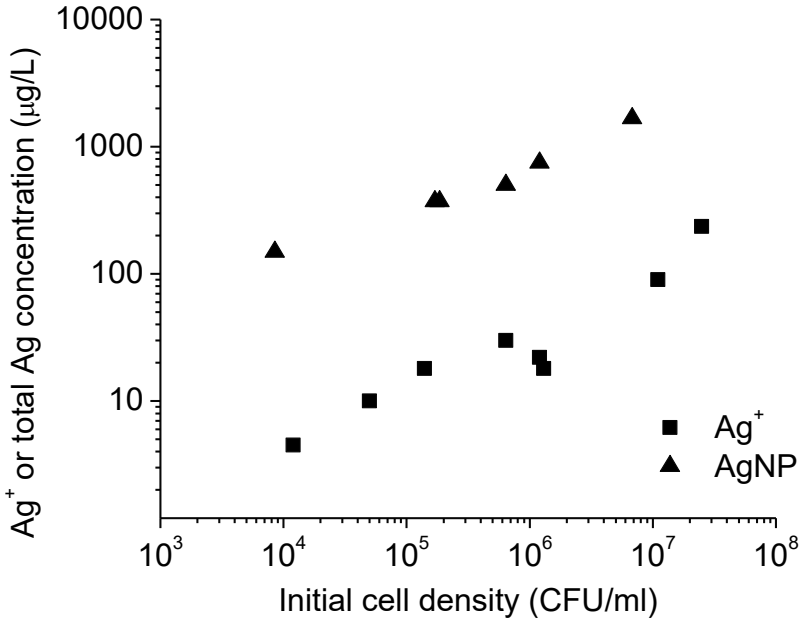

Figure 3.8 MICs of Ag^+ and AgNPs increase with initial cell densities
Mid-exponential cultures were diluted to obtain different cell densities which were treated with different concentrations of Ag^+ or AgNPs. The MICs of AgNPs are shown as the total Ag concentration of AgNP suspensions.

3.3.7 Growth rate depends on Ag^+ or AgNP concentration

As with MICs, specific growth rates decreased more strongly with increasing Ag^+ and AgNP concentration at lower initial cell densities (Figure 3.9). These data show that effects are too dependent on initial cell densities to infer inhibition kinetics reliably, so further results were obtained with lower initial cell densities to avoid any density effects.

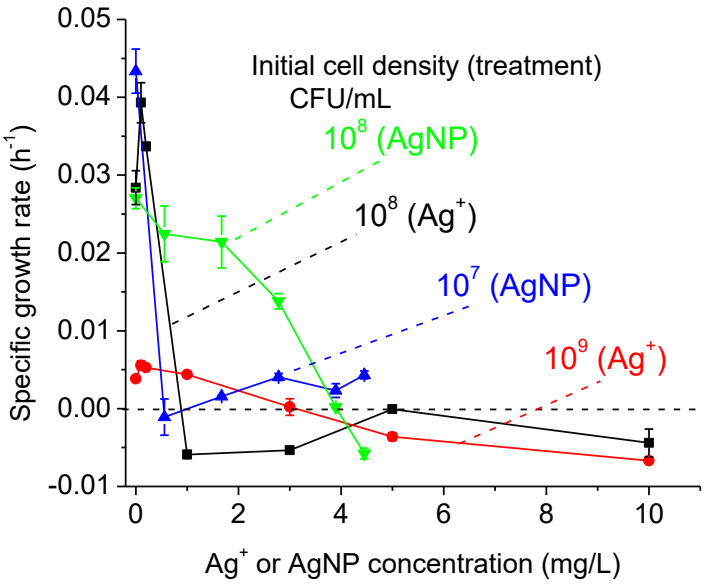

Figure 3.9 Effect of Ag^+ and AgNPs on specific growth rate
The effect of increasing concentrations of Ag^+ and AgNPs on specific growth rate of *P. putida* in DMM. The total Ag concentration of the AgNP stock was 2.1 ± 0.6 mg/L. The dissolved Ag in the AgNP stock was 0.01 ± 0.003 mg/L, measured by ultrafiltration. The AgNP stock was diluted or concentrated to obtain the desired concentrations. Different initial densities of cells (10^7, 10^8 and 10^9 CFU/mL) were treated with Ag^+ or AgNPs. The initial cell densities were calculated based on the relationship between OD and viable counts (7×10^8 CFM/(mL·OD)). The ODs were recorded for 5 h to calculate growth or death rates. A 'growth' rate below zero indicates the complete inhibition of growth. The error bars indicate standard deviations of duplicates.

3.3.8 Inhibition kinetics

Viable cell counts and dissolved Ag concentrations were monitored over time to determine the inhibition kinetics for Ag^+ or AgNPs. Figure 3.10a and b show that Ag^+ and AgNPs killed the cells during the first 1-2 h at this low initial cell density of about 5,000 CFU/mL. Treatment with 30 µg/L of Ag^+ killed all cells within one hour but most cells survived treatment with 5 and 10 µg/L of Ag^+ for 5 h (Figure 3.10a). Several hundred cells/mL survived 20 µg/L of Ag^+ for 5 h. Interestingly, the populations treated with 0, 5, 10, and 20 µg/L Ag^+ recovered during prolonged exposure (72 h), but not at

30 μg/L of Ag^+ (Table 3.3). The concentrations of dissolved Ag in the cell cultures declined during the initial 1-2 h.. Under the treatment with 5, 10, and 20 μg/L of Ag^+, the dissolved Ag concentration decreased to <1.2 μg/L within 2 h (Figure 3.10c) and to undetectable levels after 72 h (Table 3.3). In contrast, relatively high concentrations of residual Ag^+ (6.5-9 μg/L) remained in the culture treated with 30 μg/L of Ag^+, which killed all cells (Figure 3.10c, Table 3.3).

Toxicity of AgNPs was lower than that of Ag^+. At 10 μg/L growth was similar to the control (Figure 3.10b). At higher concentrations, the larger the AgNPs concentration was, the quicker viability declined. Around 50 cells/mL survived treatment with 20 μg/L AgNPs. All cells were eradicated by 50 and 100 μg/L AgNPs within 5 h. The concentrations of dissolved Ag in the cell cultures also decreased while the bacterial cells were killed. After 72 h, no regrowth occurred at 50 and 100 μg/L AgNPs but large populations were obtained at lower concentrations (Table 3.3). The initial dissolved Ag^+ concentration in the 50 μg/L AgNP treatment was 18 μg/L. Regrowth would be expected in 72 h at this concentration of dissolved Ag based on the Ag^+ inhibition kinetics (treatment with 20 μg/L Ag^+) (Table 3.3). But continuing dissolution of AgNPs released new Ag^+ into the culture. At low concentrations of AgNPs (10 and 20 μg/L), the amounts of Ag^+ released from AgNPs were too limited to kill the cells, allowing regrowth. At high concentrations of AgNPs (50 and 100 μg/L AgNP), sufficient Ag^+ was released to ensure complete killing of bacteria in the long term (Table 3.3).

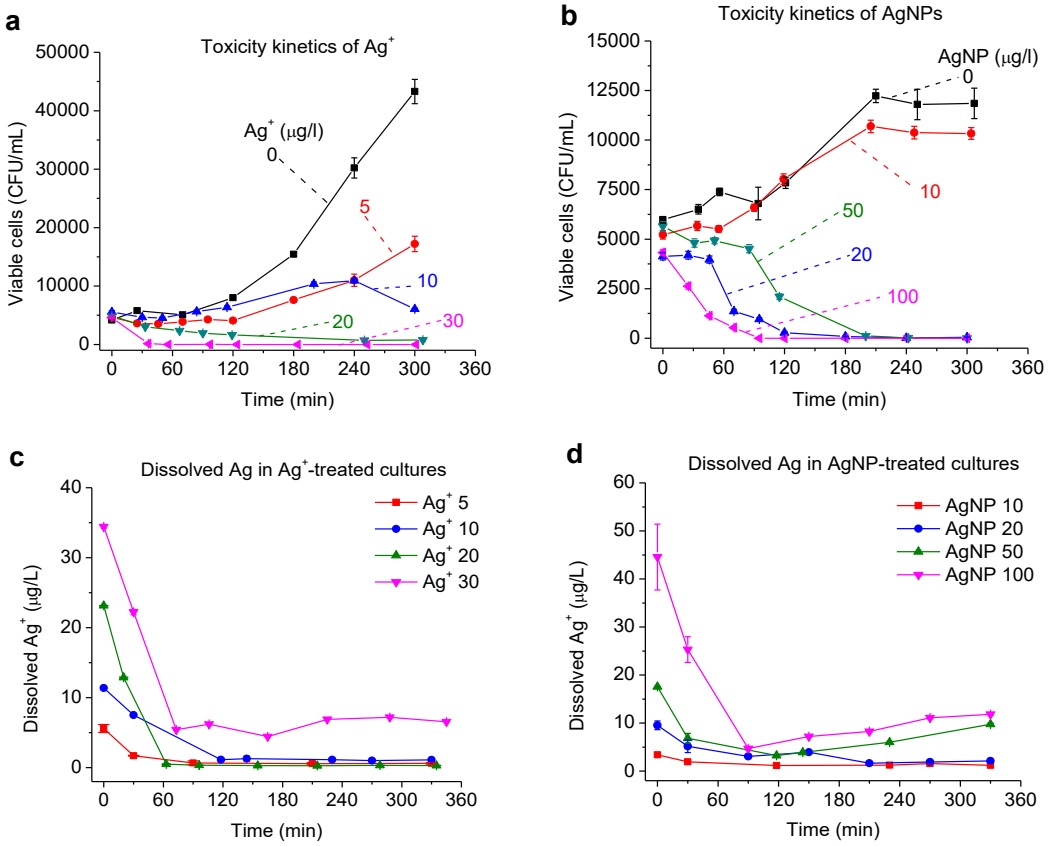

Figure 3.10 Toxicity kinetics of Ag^+ or AgNPs to *P. putida*

(**a** and **b**) Viable cell counts for (a) Ag^+ treatment (0, 5, 10, 20 and 30 μg/L) or (b) AgNP treatment (0, 10, 20, 50 and 100 μg/L). Error bars represent the SDs of viable counts. (**c** and **d**) Dissolved Ag concentrations in (c) Ag^+-treated cultures corresponding to panel (a) or (d) in AgNP-treated cultures corresponding to panel (b). The error bars indicate SDs of triplicate measurements of each sample by GFAAS.

Table 3.3 Cell viability and dissolved Ag concentration

Cell viability and dissolved Ag concentration (mean ± SD) after exposure to Ag^+ or AgNPs for 72 h

Ag^+			AgNPs		
Treatment (μg/L)	Viable count ($\times 10^6$ CFU/mL)	Dissolved Ag (μg/L)	Treatment (μg/L)	Viable count ($\times 10^6$ CFU/mL)	Dissolved Ag (μg/L)
0	22.7 ± 1.5	N/A	0	0.82 ± 0.03	N/A
5	4.9 ± 0.2	0.19 ± 0.01	10	11.5 ± 0.3	0.10 ± 0.10
10	4.8 ± 0.2	0.10 ± 0.02	20	4.8 ± 0.2	0.05 ± 0.06
20	8.0 ± 0.9	0.18 ± 0.06	50	0	14.8 ± 0.5
30	0	8.4 ± 0.3	100	0	17.8 ± 0.2

3.3.9 High-resolution inhibition kinetics

Since most of the change in viability happened very quickly (Figure 3.10), the inhibition kinetics with a higher time resolution were further performed (Figure 3.11). The number of cells at the start of the experiment varied somewhat, which may explain why fewer cells, 3 rather than 680 CFU/mL, survived at 10 than at 15 μg/L of Ag^+. Therefore, the toxicity in terms of death rate was quantified by linear regression of cell viability against time (Figure 3.12a). The death rates gradually increased from about 0 to 86 ± 17 CFU/(mL·min) when Ag^+ concentrations increased from 0 to 32 μg/L. A further increase to 40 μg/L did not significantly increase toxicity. Silver nanoparticles' highest death rate was somewhat lower, 64 ± 7 CFU/(mL·min), at the higher concentration of 80 μg/L. Assuming that the toxicity of AgNPs is solely due to dissolved Ag, the toxicity of AgNPs can be expressed in terms of dissolved Ag. As expected, the AgNP death rates in terms of dissolved Ag were closer to the death rates for Ag^+ (Figure 3.12a). There was no significant difference in the specific death rates for Ag^+ and dissolved Ag in AgNP suspension (Figure 3.12b, Table 3.4). This suggested that the toxicity of AgNPs was mainly due to dissolved Ag.

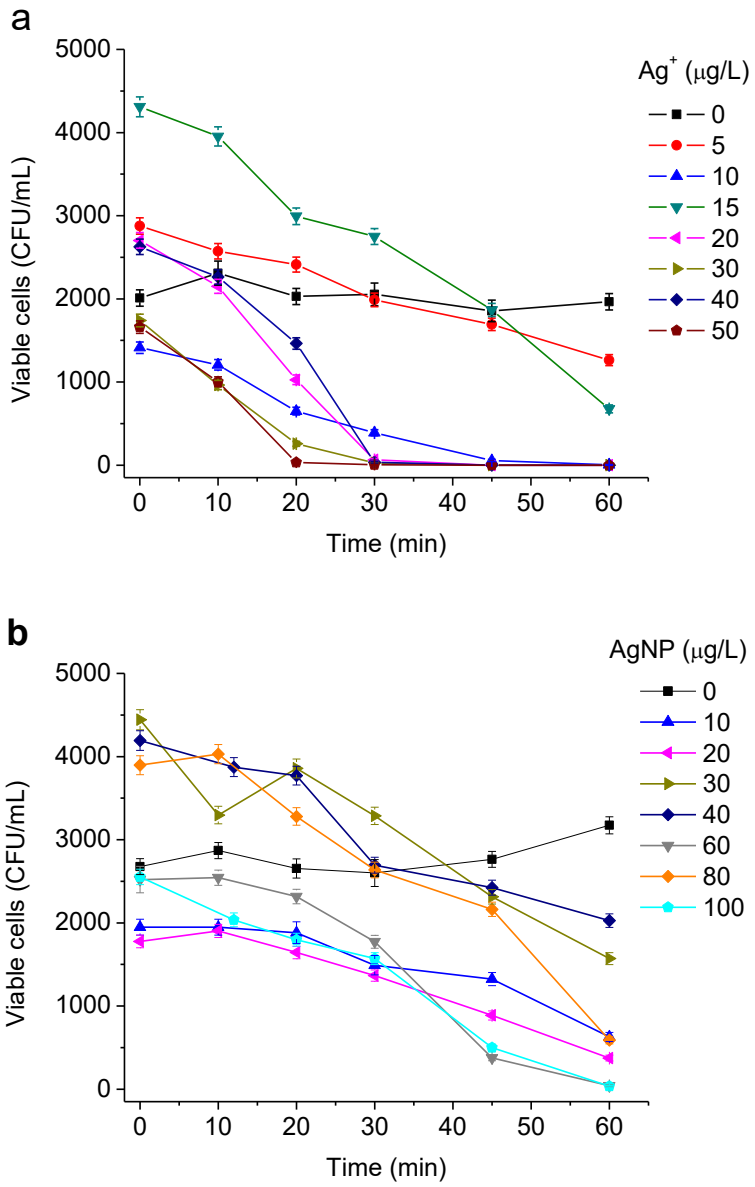

Figure 3.11 High-resolution inhibition kinetics

High-resolution inhibition kinetics for (a) Ag^+ and (b) AgNPs. The initial cell densities varied within the range of 1,400-4,500 CFU/mL. Error bars indicate SDs of viable counts.

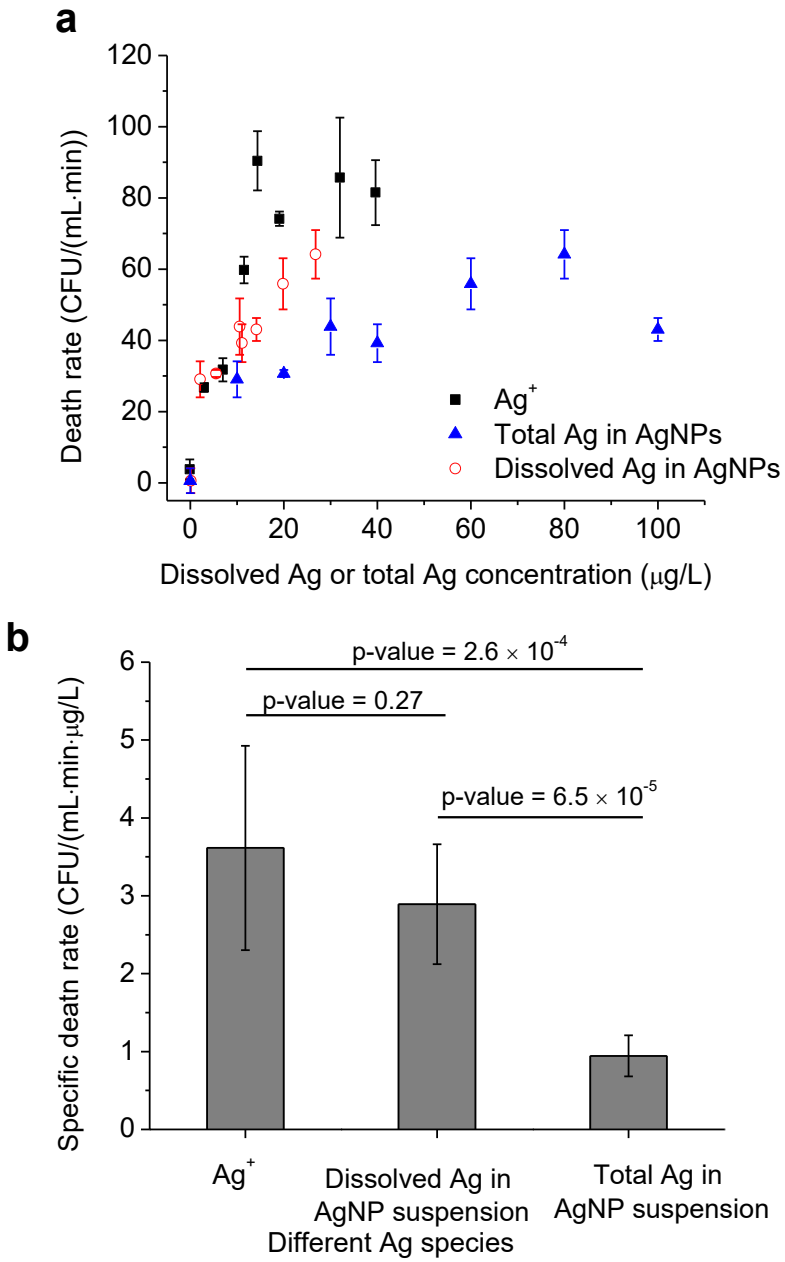

Figure 3.12 Dependence of death rates on silver concentrations
(a) Death rate versus initial concentrations of Ag^+, dissolved Ag in AgNP suspension or total Ag in AgNP suspension. The death rates were calculated by linear regression of cell viability against time shown in Figure 3.11. The error bars are standard errors of the regression slopes. **(b)** Specific death rates, defined as death rate per Ag concentration data in panel (a) (intercept = 0), within the range of 0-32 μg/L for Ag^+, 0-80 μg/L for total Ag in AgNPs and 0-27 μg/L for dissolved Ag in AgNPs. The error bars are 95% confidence intervals. The p-values of comparing the difference among the three specific death rates were carried out with t-test using R (Version 2.9.2).

Table 3.4 Specific death rate

Values of specific death rates, standard errors (SE) and p-values of linear regression with analysis of variance (ANOVA) by F-test using OriginLab (OriginPro, v8.0724, Northampton, USA)

Silver species	Specific death rate (CFU/(mL·min·g/L))	SE	p-value
Ag^+	3.61	0.54	5.2×10^{-4}
Dissolved Ag in AgNP suspension	2.89	0.33	4.7×10^{-5}
Total Ag in AgNP suspension	0.94	0.11	1.2×10^{-4}

3.4 Discussion

3.4.1 Formation and stability of uncapped AgNPs

This study demonstrated that stable, uncoated AgNPs could be obtained when the $AgNO_3$ concentration was decreased and the BH_4^-/Ag^+ concentration ratio was increased (Figure 3.2). The dissolution of AgNPs could be prevented in an anoxic environment. There are two steps involved in the dissolution of AgNPs [245]. The first step is the thermodynamically favourable oxidation of AgNPs, forming Ag_xO_y on the surface of the nanoparticle. The second step is hydrolysis of the Ag_xO_y layer in H_2O, resulting in Ag^+ release into the surrounding liquid. The high surface energy of AgNPs promotes oxidation and dissolution, leading to quicker dissolution of smaller AgNPs [79, 119, 123]. Oxidation of AgNPs is prevented in N_2, thereby also avoiding dissolution (Figure 3.3). Storing AgNP suspensions under nitrogen atmosphere ensures stability of AgNPs and should reduce variation between batches.

3.4.2 Aggregation of AgNPs in mineral growth medium

Higher AgNP concentrations favour aggregation by increasing the chances of effective collision that enables nanoparticles to overcome the energy barrier to form aggregates [138, 140]. The relatively small changes of hydrodynamic size and stable UV-Vis absorption spectra suggested that low concentrations of AgNPs were relatively stable in DMM, a defined, mineral growth medium (Figure 3.5). Sedimentation of AgNPs in cultures or assays was not observed and was not likely to take place in this study [238] since the aggregates were not large enough to settle rapidly [227].

3.4.3 Dissolution of AgNPs in H_2O and mineral growth medium

Silver nanoparticles spontaneously dissolve in the presence of oxygen in biological media. Their aggregation state and surface modification might contribute to the slow dissolution of uncoated AgNPs in DMM. Aggregates of nanoparticles have fewer active sites on their surface, which reduces oxidation and dissolution [124]. This could explain the higher dissolution rate of lower AgNP concentrations as they would have a lower degree of aggregation (Table 3.2). However, this aggregation effect is unlikely to be sufficient to explain the decrease of dissolution rates by two orders of magnitude since the aggregation of low concentrations of AgNPs in DMM was not strong (Figure 3.5). Instead, the much reduced AgNP dissolution in DMM suggests that chemicals in the medium not only affect aggregation of AgNPs but also govern their surface chemistry, which has a fundamental role in dissolution. Complexation and removal of Ag^+ from AgNP's surface by chloride can drive Ag release [106], whereas Ag_2S formation inhibits the dissolution of AgNPs [127]. In this study, an influence of Cl^- or S^{2-} is unlikely as precipitation equilibrium calculations by MINTEQ predict no precipitation, but Cl^-, phosphate and sulphate may decrease surface activity. A similar, rapid Zn^{2+} release in H_2O but slow dissolution in phosphate solution has been reported for ZnO nanoparticles as a result of phosphate reacting with the particle surface [246]. Given the high concentrations of phosphate (55 mM) and sulphate (8.4 mM) in DMM, Ag_3PO_4 or Ag_2SO_4 complexes might have formed on the AgNP surface, slowing down Ag^+ release.

Silver sorption to culture vessels cannot be excluded under our experimental conditions. The chemical properties of solutes in the medium and the vessel geometry, surface chemistry and material all affect Ag sorption [247-250]. The original Ag^+ concentration and the Ag^+ contents in the bulk liquid were measured during the dissolution studies. Silver loss might occur by adsorption to the vessel wall and membrane. It is desirable to quantify the lost Ag^+ with mass balance calculation that includes the AgNPs, free Ag^+ and attached Ag^+. Further experiments will be needed to quantify the attached Ag^+, which was not feasible in this study. While we could not quantify Ag sorption to the vessels or bacterial cells, we could measure the concentration of dissolved Ag^+ in the media and show that it was mainly responsible for the toxicity of AgNPs.

3.4.4 Cell density effects

Silver ions were more toxic in *P. putida* than AgNPs. The MICs for Ag^+ and AgNPs were dependent on initial cell densities (Figure 3.8). Such an inoculum effect has been previously observed with antibiotics [251] and can be simulated via a direct antibiotic-biomolecule reaction [252]. Compared to essential cellular metals (e.g., K, Zn, Fe, Mg), Ag has a higher affinity to various biomolecules, especially those containing thiol groups [253, 254]. It is therefore expected that bacterial components such as extracellular polysaccharides, lipoproteins and proteins complex Ag [170, 254, 255]. The interactions between Ag and bacteria can be understood as metal-cell complexation, through which Ag interrupts molecular structure and function, imposing stress on bacterial cells while leading to the chelation of free Ag. The cell density effect was

proposed to be due to titration of Ag by the biomass. The higher the bacterial density was, the larger the fraction of Ag that will be sequestered by the inhibited or killed cells. This lowering of the active concentration of Ag^+ apparently reduces Ag^+ toxicity.

3.4.5 Inhibition kinetics of Ag^+ and AgNPs

The kinetics of inhibition or death were complicated by the simultaneous decline of dissolved Ag concentration. The decrease of Ag might be attributed to Ag titration by bacterial cells and the sorption of Ag to the flask surface. Silver titration can also explain the cell density effect. Ag sorption to the flasks leads to a drop of Ag concentration only at the start of experiments (Figure 3.6).

Some bacteria survived long exposures to Ag and the population subsequently regrew (Table 3.3), suggesting the presence of persisters in the population [256]. At higher initial concentrations of Ag^+, there will still be enough Ag^+ left to kill any persisters, explaining the absence of regrowth at high Ag concentrations. For AgNPs, toxicity effects are complicated by the continuous dissolution of AgNPs replenishing dissolved Ag (Figure 3.10), which would be an advantage for killing persisters.

3.4.6 Quantifying the toxicity of Ag^+ and AgNPs

Larger concentrations of Ag^+ or AgNPs caused faster cell death (Figure 3.12). Silver ions had stronger toxicity towards *P. putida* than AgNPs (Figures 3.10, 3.12). The toxicity of AgNPs with different coatings and sizes in bacteria is believed to be exclusively due to the dissolved Ag^+ in anoxic environments [201]. To our knowledge, there is no evidence that AgNPs can penetrate the bacterial cell wall as intact particles

(they could form inside the cell by reduction of Ag^+). It is the intracellular dissolved Ag that ultimately causes the toxicity of AgNPs [207]. Silver nanoparticles thus only function as a Ag reservoir releasing Ag^+. On the other hand, larger concentrations of ions accumulate on the surface of AgNPs compared to the concentration of homogeneous ions in the bulk liquid [225]. Therefore, AgNPs trapped by the cell wall could deliver higher concentrations of Ag^+ at the cell surface, which could enhance the toxic effects of AgNPs. Our results suggest that the concentration of dissolved Ag^+ in AgNP suspensions is sufficient to explain the bactericidal effects of AgNPs since there was no significant difference between the toxicity of Ag^+ and the dissolved Ag^+ in the AgNP suspensions (Figure 3.12b) from the t-test.

3.5 Conclusions

In this study, the time-resolved transformations of AgNPs in microbial media was captured and the bacterial response was quantified, revealing the dynamic interactions between AgNPs and cells, which have important implications for application and environmental risk assessment of AgNPs. Preventing exposure of AgNPs to oxygen reduced the dissolution of AgNPs and their morphological transformations. Uncoated AgNPs underwent aggregation in a defined, mineral medium, which slowed down their dissolution. Higher concentrations of Ag^+ or AgNPs resulted in higher death rates. The MICs of Ag^+ or AgNPs increased with initial cell densities. Silver ions were more toxic than the same concentration of AgNPs in terms of total Ag mass per volume. The continuous release of Ag^+ from AgNPs replenishes dissolved Ag facilitating longer-term inhibition. The bactericidal effects of AgNPs could be mostly attributed to the concentration of dissolved Ag in AgNP suspensions.

4 Chapter Four

Experimental Evolution of *Pseudomonas putida* under Silver Ion and Nanoparticle Stress

This chapter is in preparation for publication. **Feng Dong**, Eugenia Valsami-Jones, Jan-Ulrich Kreft. Experimental evolution of *Pseudomonas putida* under silver ion and nanoparticle stress. 2016.

4.1 Introduction

Silver (Ag) is not an essential element for microorganisms. It has been used as an antimicrobial agent to preserve food and control infections [28]. The antimicrobial properties of Ag result from its high affinity to a variety of biomolecules [253]. Silver targets proteins in both Gram-positive and -negative bacteria [155], disrupts cellular metabolism such as respiration [30], interacts with ribosomes [31], disturbs iron homeostasis and inhibits protein disulfide bond formation [150], induces ROS stress [257], damages the membrane [156], and ultimately leads to cell death. During the last decades, Ag in the nano form such as AgNPs has received increasing interest for antimicrobial applications [9, 51]. Silver nanoparticles are toxic to microorganisms, plants and animals, posing potential ecological risks [237, 258, 259]. Silver nanoparticles have the same bactericidal effects as Ag^+ on different species [214, 260]. The dissolved Ag released from AgNPs is considered to be the only factor that causes cell death [201]. It is unknown whether AgNPs themselves have a direct role in killing bacteria. Different sensibilities of single-gene mutants [205] and different gene regulation [206] have been observed when bacteria were treated with Ag^+ and AgNPs, suggesting that AgNPs and Ag^+ might have somewhat different toxicity pathways.

Considering that Ag binds non-selectively to a broad range of biomolecules, it is generally accepted that evolution of Ag resistance in bacteria is uncommon, yet Ag resistance has been reported under prolonged Ag-exposure such as Ag-treated burn patients [162] and in silver mines [90], where bacteria can tolerate Ag^+ at concentrations

up to 10 and 50 mM, respectively. This is much higher than the MICs for wild type strains (0.06-0.3 mM) [175]. There are several bacterial Ag resistance mechanisms, including efflux [179, 261], reducing Ag^+ to less toxic metallic Ag [90, 262], and deactivating Ag through binding, adsorption or chelation [147, 169, 263].

Bacteria steadily evolve gaining advantages over the competition for environmental resources [264] or surviving harsh environments [160]. For instance, many bacteria have evolved resistance to antibiotics [210]. The mutations reveal the targets and mechanisms of antibiotic action [265]. Evolutionary experiments have been used to investigate the mechanisms of killing and resistance for antibiotics [266, 267]. The trajectories of evolution may diverge in different environments [268] and bacteria may adapt in different ways under different environmental stresses [267].

In this study, we hypothesised that bacteria will evolve differently in the presence of Ag^+ and AgNPs if they have different antibacterial models. We found some differential mutations in cell surface structures suggesting that AgNPs affect cells in ways that are independent from the release of Ag^+.

4.2 Materials and methods

4.2.1 Preparation of AgNPs

Uncoated AgNPs were produced according to the method described in section 2.2.1. Within 4 d after the synthesis, the AgNP suspension was washed with DI water to remove dissolved Ag and reactants (BH_4^-, $B(OH)_4^-$, NO_3^- and Na^+). Briefly, AgNP stock was filtered through a membrane with pore size of 3 kDa (Ultracel® 3 KDa Ultrafiltration Discs, Millipore, Billerica, USA) under the pressure of nitrogen gas (1 bar) using an Amicon® stirrer cell (400 mL, Millipore, Billerica, USA). Fresh DI water was added when the volume of the AgNP suspension had decreased to 1/3-1/2 of the original volume. After 10 such cycles, the dissolved chemicals in AgNP suspension should have been diluted at least 1,000 fold (2^{10}). The trace amounts of $B(OH)_4^-$ (<1.5 μM), Na^+ (<1.5 μM) and NO_3^- (<0.06 μM) left were assumed not to interfere with bacterial evolution. Some Ag^+ unavoidably remained in the suspension due to the ongoing dissolution of AgNPs. The washed AgNP suspension was sterilized by filtration through a membrane with a pore size of 0.2 μm. To prevent oxidation, the AgNP containing bottle was flushed with copious amounts of nitrogen gas (passed through a 0.2 μm pore size filter). The concentration of total and dissolved Ag in the AgNP stock was 3,228 ± 469 and 537 ± 13 μg/L after the washing, respectively.

4.2.2 Characterization of AgNPs

The size distribution of washed AgNPs was measured by DLS (Zetasizer Nano, Malvern Instruments, Malvern, UK) and DCS (DC24000, CPS Instruments Europe,

Oosterhout, Netherlands). Localized surface plasmon resonance of uncoated AgNPs in suspension was measured by UV-Vis absorption spectrometry (UV-Vis 6800, Jenway, Staffordshire, UK). Zeta potential was measured by Malvern Zetasizer Nano. The morphology of AgNPs was examined by TEM (JEOL 1200EX, Tokyo, Japan). The sample preparation of TEM is described in section 2.2.2.

To examine the stability of AgNPs during storage, the concentration of dissolved Ag in the AgNP stock suspension was monitored during the evolution experiment based on a combined aggregation-centrifugation method described in Chapter 2. The aggregation kinetics of washed AgNPs in different concentrations of $Ca(NO_3)_2$ were examined. The procedures were described in section 2.2.3. Since a $Ca(NO_3)_2$ concentration of 20 mM was needed to quickly aggregate washed AgNPs, The AgNP suspension (0.5 mL) was mixed with 20 mM $Ca(NO_3)_2$ (0.5 mL) for aggregation (final Ca^{2+} concentration, 10 mM). After 10 min, the mixture was centrifuged at 20,100 g for 30 min to separate AgNPs from Ag^+ (Centrifuge 5804R, Eppendorf, Engelsdorf, Germany). Supernatant (0.5 mL) was carefully taken and stored at -20 °C. The method for sample preparation and measurement of concentrations of dissolved Ag was described in section 2.2.2 and 2.2.4.

To examine the aggregation state of AgNPs in the microbial media, the AgNP stock (0.5 mL) was mixed with DMM (0.5 mL) in a cuvette using the pipette and the changes of hydrodynamic diameter were immediately recorded for 2 h by the Malvern Zetasizer Nano.

4.2.3 Bacterial strains and media

The strain for the evolution experiment was a wild type *Pseudomonas putida* KT2440 that was kindly donated by Víctor de Lorenzo (Centro Nacional de Biotecnología, CNB-CSIC, Madrid, Spain). A *Pseudomonas putida* KT2440 tagged with GFP was used as the reference ancestor in competition assays between evolved bacterial population and the reference and also kindly donated by Víctor de Lorenzo. Davis minimal medium (include SL10 trace elements as described in section 3.2.4) supplemented with citrate instead of glucose as the sole carbon and energy source was used to grow cells.

4.2.4 Evolution experiment

The evolution experiment was divided into two stages: pre-evolution and main evolution (Figure 4.1). The *P. putida* KT2440 strain will have experienced various environments and selective pressures before the evolution experiment. Therefore, a pre-evolution was carried out to ensure this strain effective adaption to the conditions of the evolution experiment in the absence of silver stress.

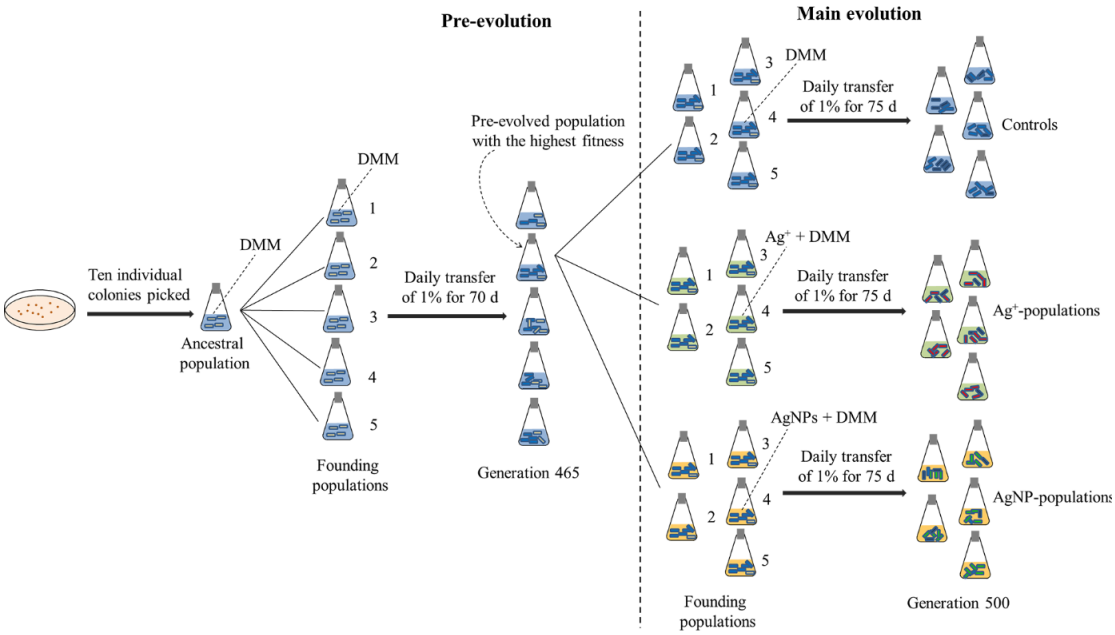

Figure 4.1 Schematic diagram of evolution experiment
Ten individual *Pseudomonas putida* colonies were picked from LB plates and grew in DMM into stationary phase, designated as ancestral population. The evolution experiment was divided into two stages: pre-evolution and main evolution. In pre-evolution experiment, five parallel populations that were seeded from the ancestral population evolved independently for 70 d in DMM. In the main evolution experiment, the fittest population amongst the five pre-evolved populations was divided into 15 populations and evolved 75 d in the presence of Ag^+ (5 μg/L), AgNPs (20 μg/L) or in Ag-free condition. Five replicates were carried out for each condition.

Ten individual *P. putida* colonies on LB plates were picked and grown in 20 mL DMM overnight. This culture was designated as the ancestral population. Ancestor culture (0.1 mL) was transferred into 9.9 mL fresh DMM and grown in a 100 mL glass flask at 30 °C. Cultures were aerated by shaking at 150 rpm in a water bath shaker. Every 24 h, 0.1 mL of the evolving cultures in stationary phase were transferred into 9.9 mL fresh DMM. This 100-fold dilution resulted in an initial cell density of ~10^7 CFU/mL and 6.64 ($\log_2 100$) generations each day. Five parallel populations inoculated from the same ancestor culture were transferred independently for 70 d (465 generations). To store the bacterial populations, whole evolved cultures were collected by centrifugation (4000 g,

8 min) and resuspended in 15% glycerol, split into several microtubes and frozen at -80 °C. Evolved populations were frozen every 3 d at the early stage (1-27 d) and every 7 d later.

Before the main evolution experiment, MICs for Ag^+ and AgNPs were measured according to the standard protocol [243]. Overnight cultures (ancestral cells) were grown into mid-exponential phase and diluted to a cell density of ~10^6 CFU/mL. This diluted culture was then treated with Ag^+ or AgNPs in a concentration series in a 96-well plate (Corning Incorporated, New York, USA), where 100 µL inoculum was mixed with 100 µL Ag^+ solution or AgNP suspension synthesized according to Sally *et al*. [94] (total Ag 5,200 µg/L, dissolved Ag 124 µg/L). The plate, covered with a lid, was incubated at 30 °C for 16-24 h. OD at 600 nm was measured to determine the MIC as the lowest concentration of Ag^+ or AgNPs that completely inhibited bacterial growth (OD < 0.05).

The population with the highest fitness amongst the five parallel cultures after 465 generations of the pre-evolution experiment was chosen as the founding population for the main evolution experiment. This pre-evolved population was revived in DMM overnight and 100 µL culture was transferred into 9.9 mL fresh DMM that contained 5 µg/L Ag^+ ($AgNO_3$) or 20 µg/L AgNPs (nanoparticulate Ag 16.7 ± 3 µg/L, dissolved Ag3.3 ± 0.1 µg/L) to start the main evolution. They were designated as the Ag^+-population and AgNP-population, respectively. Another five parallel cultures evolved in DMM devoid of Ag^+ and AgNPs, designated as the control. The 15 populations were propagated independently for 75 d (500 generations) in the same way as in the pre-

evolution experiment apart from the Ag or AgNP additions to the medium.

To ensure the consistency of the Ag^+ or AgNP stress during the main evolution experiment, the same $AgNO_3$ and AgNP stocks were used throughout and the AgNP stock was kept under N_2 to prevent dissolution.

4.2.5 Fitness assay

In this study, fitness differences between evolved and ancestral populations, or relative fitness, was assessed by competition in the same medium [269]. The evolved population was competed against a GFP tagged *P. putida* KT2440 reference strain. Viable cells were counted before and after the 24 h competition experiment. The constitutive expression of the chromosomally inserted GFP gene enabled us to distinguish evolved and reference strains on the same LB agar plates. The competitions were prepared by reviving frozen stock cultures of the two populations in DMM overnight. These were then mixed together in approximately equal numbers. The relative fitness F is defined as

$$F = \frac{\log(N_{e24} / N_{e0})}{\log(N_{r24} / N_{r0})} \tag{4.1}$$

where N_{e0} and N_{e24} are the initial and final (24 h) cell densities for the evolved population, respectively, and N_{r0} and N_{r24} are the initial and final (24 h) cell densities for the reference population, respectively. The GFP tagged reference strain had the same fitness (1.01 ± 0.03, mean ± SD, n = 9) as the ancestral cells when they were competed in DMM.

The reproducibility of the fitness assay was examined by competing one evolved

population (culture 1 from the control conditions of the main evolution experiment, generation 500) against the reference strain in six replicates as described above. After 6 h of growth, when the two populations were expected to be at the end of the exponential phase, 1 mL of the competitor mix was collected, pelleted (centrifuged at 5,100 g for 10 min), resuspended in DMM without carbon source, and stored at 4 °C. Viable cell counting was carried out by spreading on LB plates the next day. The initial population was counted in triplicate to estimate the variance due to viable counting. Additionally, the whole procedure was repeated one week later.

To assess the fitnesses of cultures from the main evolution experiment, the competitions were carried out as described above but in DMM containing either no silver, 5 μg/L Ag^+ or 20 μg/L AgNPs. Due to the large number of combinations of three evolved populations (control, Ag^+-population and AgNP-population assayed under three types of stress (Ag^+, AgNPs and Ag-free) it was necessary to pool all five parallel cultures for competition with the reference strain. After reviving the 15 frozen cultures in DMM overnight, the five populations from the same treatment were pooled and mixed before competing against the reference culture as described above.

4.2.6 Whole genome sequencing

Reviving the frozen populations was performed by streaking the stock cultures on LB plates. Bacteria from these plates were harvested with a sterile loop and transferred into Microbank tubes (Microbank™, Pro-Lab Diagnostics, Canada) that contain beads for binding the bacterial cells. For DNA extraction, three beads from each tube were

washed with extraction buffer containing lysozyme and RNase A and incubated for 25 min at 37 °C. Then, proteinase K and RNaseA were added and the mixture incubated for another 5 min at 65 °C. Genomic DNA was purified using SPRI beads and resuspended in an elution buffer.

DNA library preparation, whole-genome sequencing and aligning the reads to the KT2440 reference genome were performed by the microbesNG service at the University of Birmingham. DNA samples were quantified with the Quantit dsDNA HS assay in triplicate with a plate reader (Eppendorf AF2200). Genomic DNA libraries were prepared for Illumina sequencing using Nextera XT Library Prep Kit (Illumina, San Diego, USA) according to the manufacturer's protocol with the following modifications: two nanograms of DNA instead of one were used as input, and PCR elongation time was increased to 1 min from 30 seconds. DNA quantification and library preparation were carried out on a Hamilton Microlab STAR automated liquid handling system. Pooled libraries were quantified using the Kapa Biosystems Library Quantification Kit on a Roche light cycler 96 qPCR machine. Libraries were sequenced by Illumina MiSeq using a 250 bp paired end protocol.

4.2.7 Variant calling

The raw reads were trimmed with the tool Trimmomatic to remove adapters and bases with quality scores <15. The reads were aligned to the *Pseudomonas putida* KT2440 (NC_002947.4, GenBank) reference genome using Burrows-Wheeler Aligner (BWA) and SAMtools. Variant calling (defined as identifying the existence of single nucleotide

variants by comparing the nucleotide at a given position in an individual genome or transcriptome with the reference in the next generation sequencing) was performed by VarScan with the following settings: Phred score ≥ 15, depth of variant-supporting bases ≥ 3, variant allele frequency ≥ 0.1, p-value for calling variants ≤ 0.05. A manual filtration was performed as 0.1 ≤ frequency of variants-supporting bases on one strand ≤ 0.9. SNPs in a homopolymer tract of length ≥ 8 bp were then manually excluded.

4.2.8 Association of mutations with selective pressures

Any association between mutations (wild type vs mutant) and selective pressures (Ag, AgNP or control) was tested with a modified version of Fisher's exact test that accounts for the discrete nature of the results by calculating mid-p-values [270]. Such mid-p-values for the two-tailed test were calculated with the oddsratio.fisher function in R (part of the epitools package) (Table 4.1).

Table 4.1 Mid-p-values calculated with a modified Fisher's exact test for association between mutation and condition

Mid-p-values for all possible combinations of mutant frequencies in the parallel cultures evolved under different conditions calculated with a modified Fisher's exact test[270] for association between mutation and condition. WT indicates the number of cultures evolved in parallel without mutation (from 0 to 5). Likewise, mutant indicates the number of cultures evolved in parallel with the mutation (from 0 to 5).

WT, Mutant		Condition 2					
		0, 5	1, 4	2, 3	3, 2	4, 1	5, 0
Condition 1	5, 0	0.0040	0.0238	0.0833	0.2222	0.5	1
	4, 1	0.0238	0.1071	0.2857	0.5833	1	0.5
	3, 2	0.0833	0.2857	0.6032	1	0.5833	0.2222
	2, 3	0.2222	0.5833	1	0.6032	0.2857	0.0833
	1, 4	0.5	1	0.5833	0.2857	0.1071	0.0238
	0, 5	1	0.5	0.2222	0.0833	0.0238	0.0040

4.3 Results

4.3.1 Synthesis and stability of AgNPs

The uncoated AgNPs that were synthesized were spherical and monodispersed (Figure 4.2a). The average diameter was 12.4 ± 4 nm and more than 95% were between 5 and 25 nm based on the TEM image (Figure 4.2b). A similar size distribution measured by DCS confirmed the successful synthesis of uncoated AgNPs. Absence of detection of large particles by DLS indicated that the AgNPs had not aggregated. The AgNPs had a zeta potential of -23.0 ± 3.9 mV at a pH of 7.7 ± 0.6 in H_2O. The pH of the AgNP stock suspension was 7.2 ± 0.4.

The stability of the AgNPs during storage was also examined. The concentration of dissolved Ag in the AgNP stock stored under N_2 was approximately constant over 76 d (Figure 4.2c). Slight loss observed could be due to adsorption of Ag to the glass surface [249, 250]. The stability of AgNPs was also confirmed by UV-Vis absorption spectra, which did not change over 44 d (Figure 4.2d). No obvious aggregation was observed for the AgNP stock suspension (3,228 ± 469 μg/L) in the DMM growth medium over 2 h (Figure 4.2e). At the lower concentration of AgNPs (161-fold dilution) that was used for the main evolution experiment, aggregation would be less likely since dilution of AgNPs substantially reduces aggregation. A concentration of 20 mM $Ca(NO_3)_2$ was high enough to aggregate the washed AgNPs (Figure 4.2f). This concentration of $Ca(NO_3)_2$ was added into same volume of AgNP suspensions to trigger the aggregation of AgNPs for the measurements of dissolved Ag concentrations.

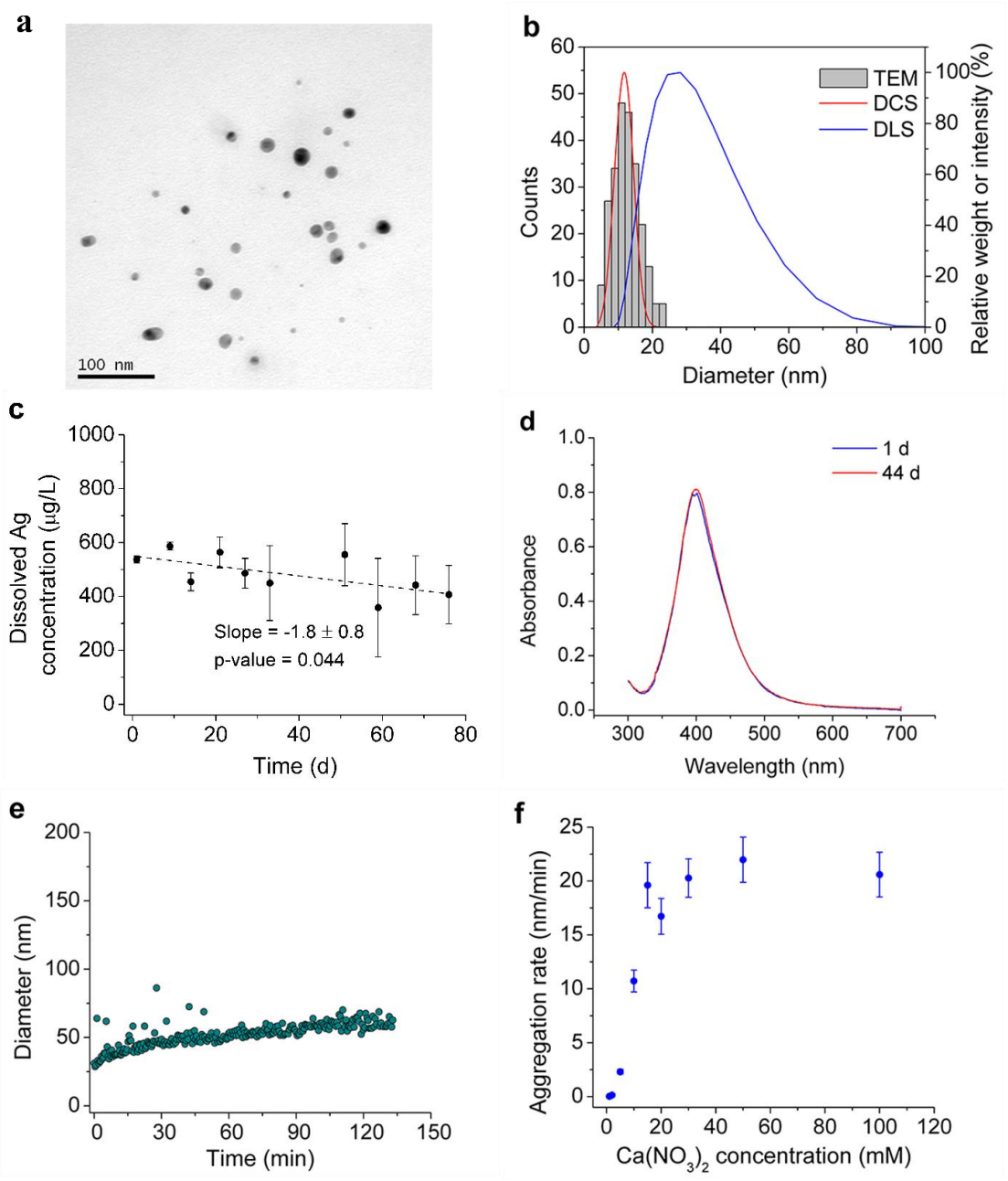

Figure 4.2 Properties of AgNPs for evolution experiment

Properties of AgNPs and their stability in H_2O or microbial minimal media. **(a)** Morphology obtained by TEM. **(b)** Diameter distribution based on TEM images analyzed by ImageJ [222] and measured by DLS and DCS. **(c)** The concentration of dissolved Ag in the AgNP stock over time during the main evolution experiment. **(d)** UV-Vis absorption spectra. **(e)** The change of hydrodynamic diameter of the AgNP stock suspension in DMM measured by DLS. **(f)** Aggregation rates of the washed AgNPs that were used for evolution experiment in different concentrations of $Ca(NO_3)_2$.

4.3.2 Fitness of evolved populations

Fitness of evolved populations is expected to become more competitive in the environment in which they evolve. The relative fitness was measured by competing evolved populations against a reference *P. putida* KT2440 strain tagged with GFP to distinguish it from the evolved cells (Figure 4.3). Because large variations of fitness values seemed to be characteristic of the competition assays, the reproducibility of the assay was examined (Figure 4.4a). The fitness values of 18 replicates were 1.38-1.64 and the coefficient of variation (standard deviation/mean) was 4.6%. The experiment with 18 replicates was repeated another week with very similar results (there was no significant difference in the mean and variance of fitness values for the two batches of experiments: p-value = 0.636 for mean, paired t-test; p-value = 0.798 for variance, F-test) (Figure 4.4a). This shows that the method is accurate (no systematic bias) but not precise (high variance) so fitness values have to be treated with caution.

The fitness of the GFP free KT2440 ancestor was 1.01 ± 0.03 relative to the GFP reference strain in DMM (Figure 4.4b), indicating that the GFP tag did not affect fitness. After propagating the five parallel cultures for 70 d (~465 generations), their fitness ranged from 1.16 ± 0.02 to 1.04 ± 0.02 and the mean fitness had increased to 1.10 ± 0.05 (Figure 4.4b). The fitness was significantly improved during the pre-evolution experiment.

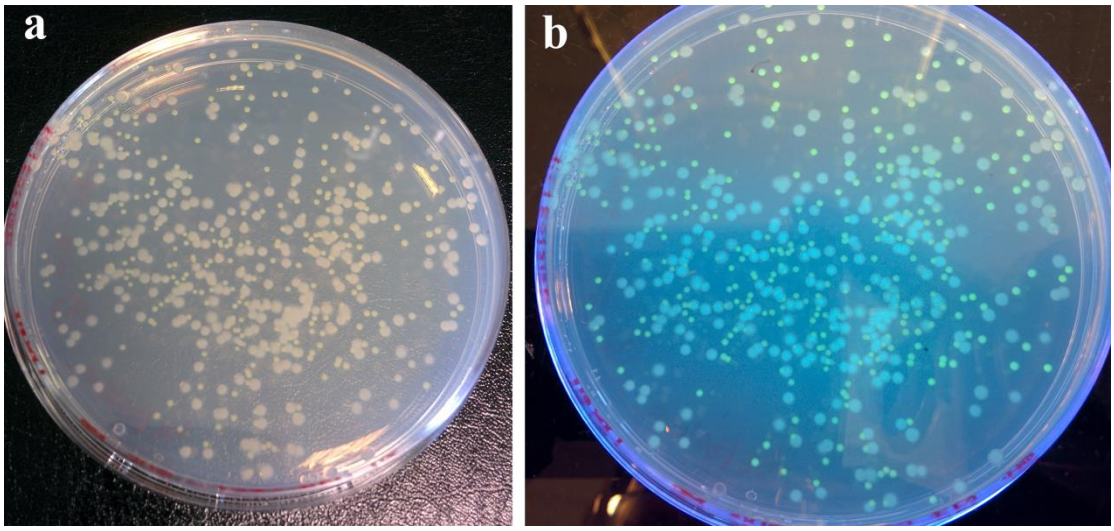

Figure 4.3 Evolved and reference cells on the same LB plate
The larger, white colonies represent evolved cells. Green colonies represent the GFP tagged reference cells. **(a)** Under natural light. **(b)** Illuminated by UV light.

The population with the largest fitness improvement in the pre-evolution experiment was chosen as the founding population for the main evolution experiment. The MICs for Ag^+ and AgNPs for the ancestor were 50 and 200 µg/L, respectively. Therefore, we chose 10% of these values, 5 µg/L Ag^+ or 20 µg/L AgNPs, to select for resistance to silver stress in the main evolution experiment as these low concentrations enabled the bacteria to grow and evolve.

Dissolution of the AgNPs was reduced by storage under a nitrogen atmosphere and the concentration of dissolved Ag^+ in the AgNP stock changed only slightly during the main evolution experiment. The concentration of dissolved Ag^+ added to the cultures with the 20 µg/L AgNP dosage was 2.2-3.6 µg/L. Moreover, silver nanoparticles will release Ag^+ upon addition to the bacterial culture at a rate of up to 0.03 µg Ag^+/(L·h), calculated from the maximal dissolution rate of AgNPs in DMM of $1.9 \pm 0.4 \times 10^{-3}$ µg Ag^+/(µg AgNP·h), corresponding to 0.72 µg Ag^+/L released in 24 h (see section 3.3.4). This

means that the AgNP stress was a combined Ag^+ and AgNP stress.

To measure the fitness of the populations in the main evolution experiment that *evolved* under Ag^+ or AgNP stress or in the silver-free control medium, *competitions* were set up under the same three conditions, giving 9 combinations. The five parallel populations were pooled to determine their fitness at the start and end of the main evolution experiment (generation 1 and 500) (Figure 4.4c). Considering the large variance of fitness values (Figure 4.4a, c), one has to interpret these results cautiously even when the error bars happen to be small. One would expect that the cultures that were evolving without silver stress in the main evolution experiment, therefore continuing to evolve under the same conditions as in the pre-evolution experiment, would only slightly increase further in fitness. Also, one would expect these control cultures to be fitter without silver stress than in the presence of Ag^+ or AgNPs. The results are consistent with these expectations. Further, one would expect that the cultures that were evolving under AgNP stress would have a higher fitness competing under AgNP stress than under Ag^+ stress or without stress. The results suggest that the AgNP evolved cultures have a higher fitness under AgNP stress than Ag^+ stress, but they appear to have also gained higher fitness without stress, compared to the cultures that evolved without stress. Likewise, one would expect that the cultures that were evolving under Ag^+ stress would have a higher fitness competing under Ag^+ stress than under AgNP stress or without stress. The results suggest that this is not the case as they seem to have a higher fitness under AgNP stress than under Ag^+ stress, and a higher fitness without silver stress than the cultures that had evolved without silver stress. It

seems that fitness values under Ag^{+} stress were consistently lower than under AgNP stress or without stress, regardless of which conditions the cultures had evolved in (Figure 4.4c).

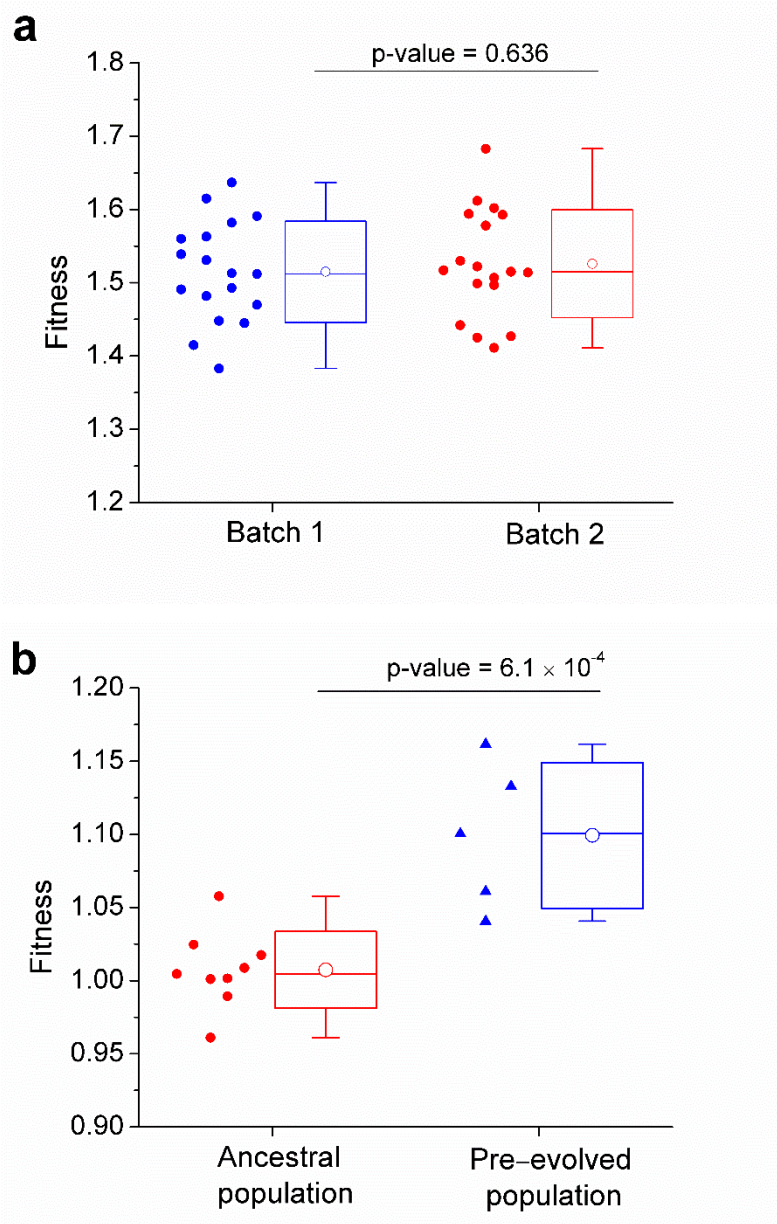

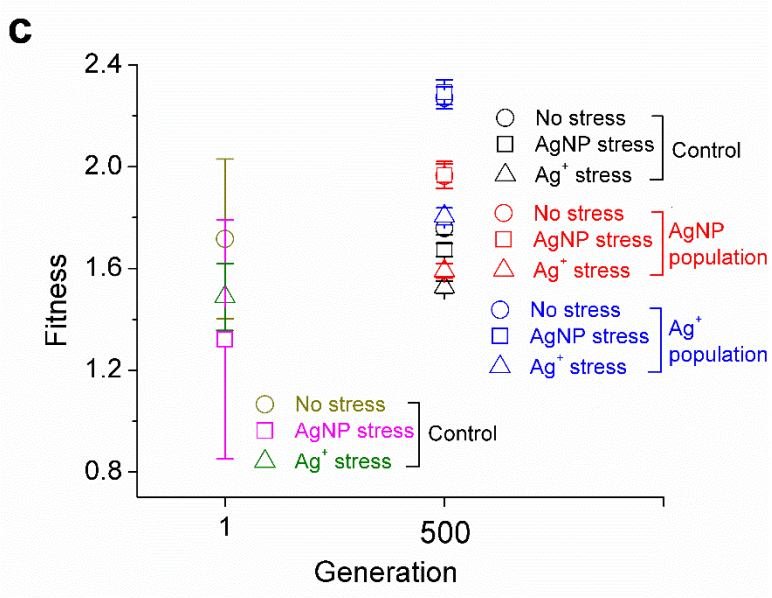

Figure 4.4 Reproducibility of the fitness assay and relative fitnesses of the evolved populations

(a) Reproducibility of the fitness assay for a population of the control in main evolution (culture 1, generation 500). Two batches of fitness tests with 18 replicates each were carried out in separate weeks. Data points are individual replicates. Boxes represent SDs, bars medians, open circles means, whiskers 5-95 percentiles. The p-value of comparing the mean fitness of ancestral and pre-evolved population was calculated with t-test. **(b)** Fitnesses of the ancestral and pre-evolved populations. The data points for the ancestral culture are replicate assays of the same ancestral population competing against the GFP tagged reference strain, showing that the GFP tag had no significant effect (mean fitness ± SD, 1.01 ± 0.03) and also indicating reproducibility of the assay. The data points for the pre-evolved cultures are fitness values for the five parallel populations after 465 generations of pre-evolution. Boxes refer to SDs, bars to medians, open circles to means, and whiskers to 5-95 percentiles.The p-value of comparing the mean fitness of batch 1 and 2 was calculated with t-test. **(c)** Fitnesses of three populations *evolved* in the presence of Ag^+, AgNPs or silver-free control medium and *competing* in the presence of Ag^+, AgNP or silver-free control medium. Error bars for generation 1 represent the SDs of three replicate measurements. Error bars for generation 500 represent SDs derived from the viable counts assuming that cells were randomly sampled and counts therefore Poisson distributed (Clegg et al. unpublished).

4.3.3 Mutations during the pre-evolution experiment

Contamination of sequenced cultures was not detected because the GC content distribution of the contigs was the same and because more than 99.9% of the reads mapped to the Pseudomonadaceae family. To identify the mutations in the pre-evolved

population, the quality filtered reads from the ancestral and pre-evolved populations were aligned with the *Pseudomonas putida* KT2440 reference genome that has been well characterized [271, 272] (Appendix 1). Twenty-four single nucleotide polymorphisms (SNPs) were identified in the pre-evolved population after 465 generations, 7 SNPs were located in intergenic regions, 13 SNPs were located in a putative surface adhesion protein gene (PP_0168), and 4 other SNPs were located in other coding regions (CDS) (*gacS*, *felQ*, *flgK* and PP_4920).

4.3.4 Mutations during the main evolution experiment

All 15 populations of the main evolution experiment were sequenced after 500 generations. The mutations are listed in Appendix 2. There were 198, 194 and 218 mutations in the population that evolved without stress, with Ag^+ and AgNPs stress, respectively. Most of these mutations did not occur in all parallel cultures that had evolved under the same conditions. Half of the mutations were only found in one population. Populations from the three selective conditions had similar distributions of the number of parallel mutations (Figure 4.5a).

The total number of mutations in the evolved lineages varied in the range from 52 to 124 (Figure 4.5b), with on average 91 mutations in the Ag^+-populations, 90 in the controls and 104 in the AgNP populations. Multiple mutations in gene PP_0168 and PP_5662 were found in all populations, which encode a putative surface adhesion protein and an apparent pseudogene, respectively, which accounted for 81-93% of the mutations in CDS. Figure 4.5c shows the total number of nonsynonymous mutations.

More mutations were located in coding regions for the populations treated with Ag^+ or AgNPs than for the controls, most of which caused amino acid substitutions. On average, 12.6 ± 4.1, 12.2 ± 2.2 and 10.2 ± 2.4 nonsynonymous mutations were identified for the populations treated with Ag^+, AgNPs, and the control, accounting for 14.2 ± 4.0%, 11.7 ± 1.7% and 11.3 ± 1.1% of the total mutations, respectively. There was no significant difference in the total number of mutations or the number of mutations in CDS among the control, Ag^+-population and AgNP-population.

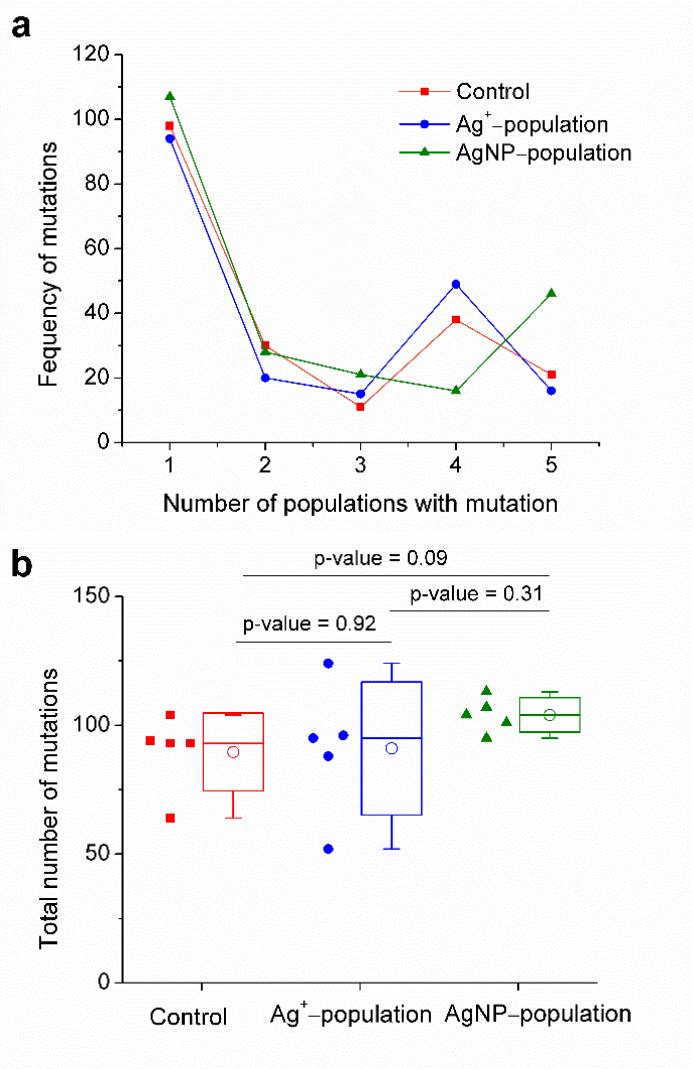

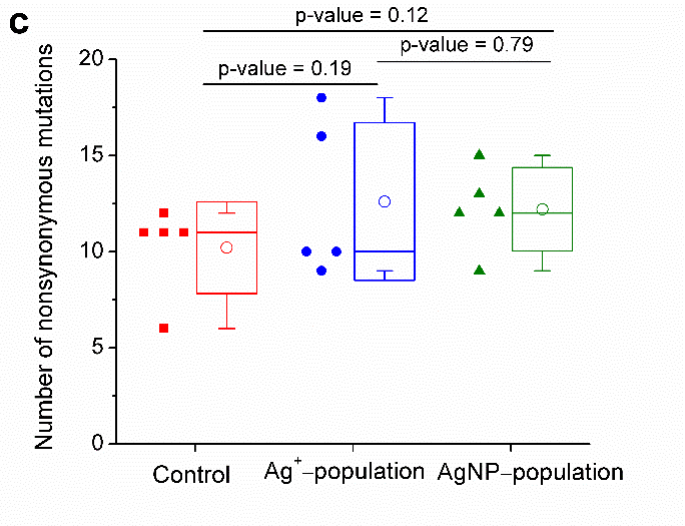

Figure 4.5 Number of mutations in populations in main evolution experiment
Number of mutations in populations that had evolved for 500 generations under Ag^+ or AgNP stress or without stress (control). Open circles are means. Boxes refer to SD. Bars in the boxes are medians. Whiskers are 5-95 percentiles. The p-values were calculated by comparing the means with t-test. **(a)** The frequency of mutations that occurred 1, 2, 3, 4 or 5 times in the five parallel cultures. **(b)** Total number of mutations in the 15 populations. **(c)** Number of nonsynonymous mutations in coding sequences in the 15 populations.

4.3.5 Mutations that differ between exposure to Ag^+ or AgNPs

All mutations were listed and compared to determine whether they were associated with different Ag stresses (Appendix 2). As shown in Figure 4.6a, the three evolved populations shared approximately half of the mutations at the same positions, some of which were nonsynonymous (Figure 4.6b). Many single mutations were found in various chromosomal locations in the three populations (Appendix 3). Despite most mutations occurred in only one of the 15 populations (Figure 4.6a, b), some mutations appeared repeatedly in parallel populations. A modified Fisher's exact test was used to determine how many times a mutation has to have occurred in one treatment versus another treatment to show a statistically significant association between mutation and treatment (Table 4.1). Nine such mutations were identified as statistically significant

with p-values ≤ 0.05, including two mutations in intergenic regions, one mutation in a 16S ribosomal RNA gene, and six mutations (genes *ftsZ*, *gacS*, *uvrY* and PP_2758) in protein coding sequences (Figure 4.6c). Other genes may well be associated with treatment but with only five parallel cultures these will remain uncertain.

In addition to the mutations with statistically significant associations to treatments, double and triple mutations in the same genes were found in several genes in the populations treated with Ag+ or AgNPs but mostly absent in the control populations (Figure 4.6c). CopA is a P-type ATPase Cu-transporter associated with Cu/Ag resistance [261, 273]. The multi-point mutation of *copA* in Ag^{+}- and AgNP-populations might be linked with positive adaptation. A triple mutation in *thiL* was only observed in one Ag+-population. The different double mutations in *envZ*, *tauB-II* and PP_2397 in Ag^{+}- and AgNP-populations further suggest that AgNPs and Ag^{+} had different mechanisms of toxicity selecting for different mutations.

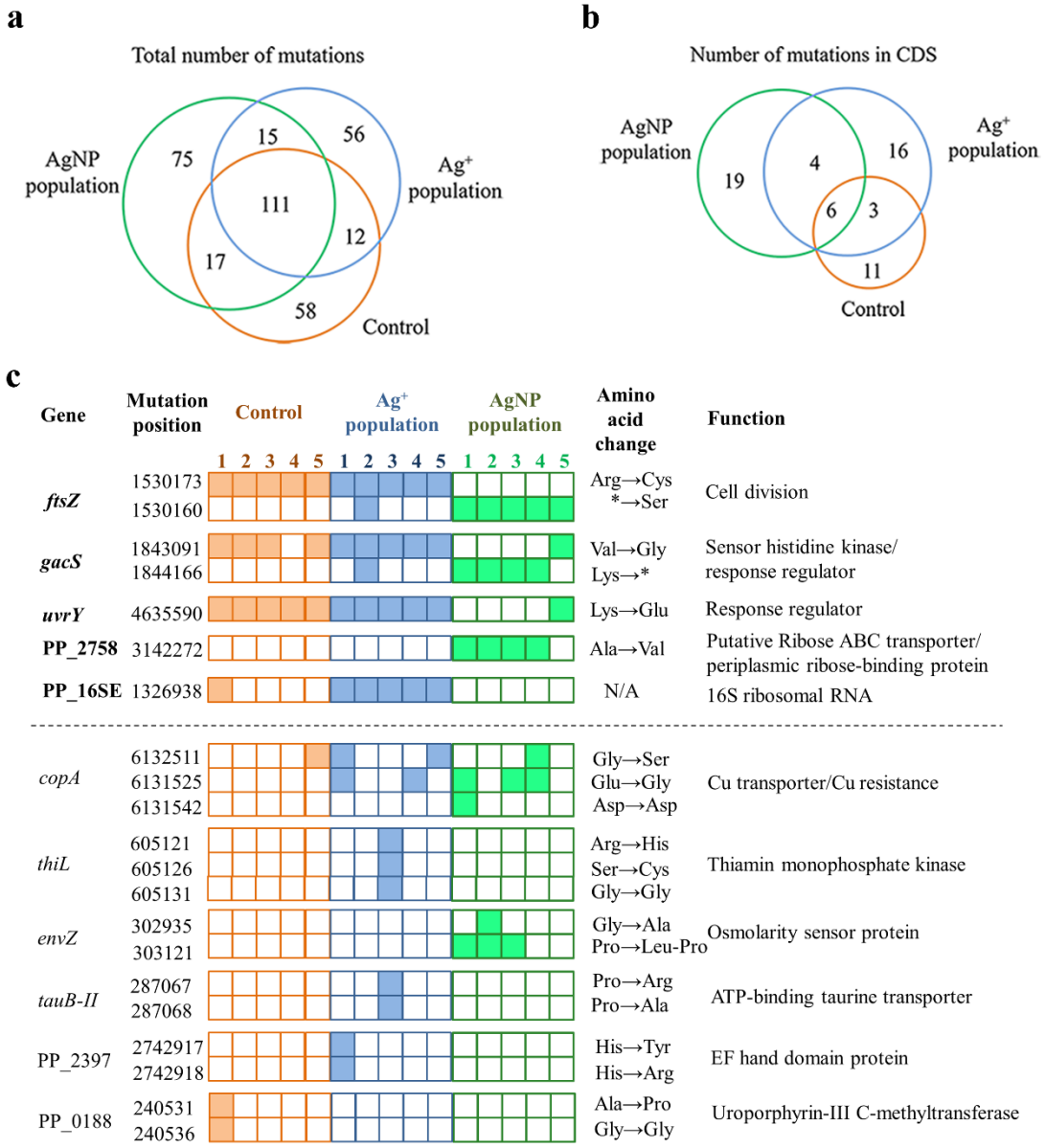

Figure 4.6 Mutations in the populations of the main evolution experiment
Venn diagram of counts of all mutations **(a)** and nonsynonymous mutations **(b)**. The numbers in the green, blue and red circles refer to the counts of mutations in the AgNP populations, Ag^+ populations and control, respectively. **(c)** List of non-synonymous mutations with mid-p-values ≤ 0.05 in Fisher's exact test (genes with the names in bold) and the genes with mutations in multiple positions. Five parallel populations had each evolved under three different conditions indicated by colors. The solid squares indicate mutation, and the open squares indicate no mutation. For amino acid changes, "*" refers to a stop codon.

4.4 Discussion

4.4.1 Silver nanoparticles for the evolution experiment

The AgNP suspension should change as little as possible to maintain similar selective conditions throughout the whole evolution experiment. The fraction of Ag^+ in AgNP suspensions should remain constant since they have different antibacterial activities [201, 205, 206]. Therefore, the AgNP stock suspension was stored under N_2 to prevent dissolution due to oxidation. As a result, the concentrations of Ag^+ and AgNPs remained almost constant. Uncoated AgNPs were used to avoid any effects that surface coatings such as PVP might have effect on the attachment of nanoparticles to bacterial cell walls [203]. Moreover, the dissolved chemicals left after synthesis were removed to avoid any confounding effects on the evolution of the bacteria. Overall, selective conditions in the AgNP treatment hardly changed during the extended exposures.

4.4.2 Pre-evolution experiment

To our knowledge, our study is the first to have carried out a pre-evolution experiment to adapt the ancestor to the selection regime without the specific stress of interest in order to disentangle selection for confounding conditions from selection for conditions of interest. We note that this attempt was not entirely successful. While the ancestor gained fitness by accumulating mutations in the pre-evolution experiment, the populations that continued to evolve under the same Ag stress free conditions did not appear to further increase fitness but did acquire further mutations.

4.4.3 Fitness improvements

Fitness is a phenotypic property reflecting genetic changes, which is dependent on the environment and can be used as an overall indicator to quantify bacterial evolution [274]. Positive adaption leads to an increase of population fitness. Lenski et al. showed that the increase of mean fitness over time in the long term evolution experiment of *Escherichia coli* in a constant environment fits a power law [275, 276]. Based on this power law model (Relative fitness = $(0.00515 \times \text{generations} + 1)^{0.0950}$), the mean fitness of *P. putida* populations after 465 generations of the pre-evolution experiment was predicted to be 1.12, close to the measured value of 1.10 ± 0.05. The relative SD of fitness of 4.5% among the five parallel populations was similar to the variance reported by Wiser and Lenski [277]. The rate of accumulation of beneficial mutations is faster at the beginning and then slows down increasingly [278]. Although fitness gains were not expected to cease, they might acquire sufficient adjustment to DMM within 465 generations.

We chose a low dosage of Ag^+ and AgNPs to make sure that the bacteria were able to grow and evolve. Such a low stress tends to enable bacteria to explore diverse mutation paths [279] rather than shorter paths leading to larger fitness gains, if they exist, under strong selection [280]. The unavoidable coexistence of Ag^+ and AgNPs in the AgNP treatment complicates the comparison of Ag^+ and AgNP treatments. Since the AgNP populations had the opportunity to adapt to both Ag^+ and AgNPs, one would expect these populations to have gained a higher fitness under Ag^+ stress than the control

populations, and higher fitness under AgNP stress than the Ag^+ and control populations. However, if the toxic effects of AgNPs result entirely from ionic Ag, the Ag^+ evolved population should have a similar fitness upon AgNP stress. The results were not quite as expected. The AgNP evolved populations had a higher fitness under AgNP stress than Ag^+ stress, suggesting that the AgNP effects are not entirely due to the release of Ag^+ but also due to some direct effects of AgNPs. On the other hand, the Ag^+ evolved populations had a higher fitness under AgNP stress than Ag^+ stress. Overall, the fitness results alone have not answered the question whether AgNPs have direct effects on cells.

4.4.4 Differential mutation profiles

While the fitness changes remained inconclusive, the differences in the mutation profiles of Ag^+ and AgNP evolved populations identified by whole-genome sequencing might be able to answer the question of whether bacteria have different mutational strategies in response to ionic or nanoparticulate Ag stress. Typically, bacteria have a spontaneous mutation rate of 10^{-9}-10^{-10} per base pair per replication [279]. Given an initial population density of 10^7 CFU/mL and a genome size of ~6 Mb for *P. putida* KT2440, the evolving population would have explored 0.3-3 × 10^7 *new* mutations after 465 generations of pre-evolution. Since only 24 mutations were detected in the population, 87.5% of which are likely to be more or less neutral as they did not alter the amino acid sequence, the overwhelming number of mutations appears to have been selected against. The long-term evolution study of Lenski et al. found an average mutation accumulation rate of 2-3 mutations/1000 generations at the early stage of *E.*

coli evolution in a batch environment [278]. The observed 2 nonsynonymous SNPs in our pre-evolution experiment were close to this mutation rate.

In the main evolution experiment, many identical mutations were found in parallel populations, despite the randomness of mutations and diversified evolutionary paths. Furthermore, multiple mutations in different positions of the same genes were identified, which is also much higher than expected from random mutations. This suggests strong selection of the identified mutations.

4.4.5 Differential mutations in response to AgNP versus Ag^+ stress

The populations that evolved under Ag^+ or AgNP treatment shared many similar mutations with the control populations, but some mutations appeared to be specific to the selective conditions. If at least four of the five parallel cultures acquired the same unique mutation (not present in cultures evolved in the other conditions), the association between mutation and treatment is statistically significant (Table 4.1). It is likely that more mutations would have shown significant associations if the sample size would have been higher than five. The treatment with Ag^+ had a similar mutation profile to the control with only one gene significantly associated with Ag^+ treatment (PP_16SE, Figure 4.6). By contrast, mutations in five genes were significantly associated with AgNP treatment (*ftsZ*, *gacS*, *uvrY*, PP_2758 and PP_16SE, Figure 4.6). This suggests that AgNPs affected the cells differently from Ag^+ in a way that different mutations were positively selected in response.

Multiple mutations in the same gene in the Ag^+ populations that were absent in the

control populations demonstrated that Ag^+ did select for specific genetic changes (*copA*, *thiL*, *tauB-II* and PP_2397, Figure 4.6). The AgNP selected populations were expected to have all the same mutations that appeared in the Ag^+ selected populations since the AgNP suspension contained Ag^+, but the genes with multiple mutations in Ag^+ and AgNP selected populations were different, i.e. the mutations in PP_2758 and *envZ* were only observed in the AgNP-populations and the mutations in *thiL*, *tauB-II* and PP_2397 were only found in the Ag^+-populations (Figure 4.6), further suggesting that AgNPs exerted different selective pressures.

4.4.6 Functions of mutated genes

Previous studies have demonstrated that the CusCFBA efflux system [166], the plasmid-related SilCFBA system [179], the outer membrane protein (porin) [168] and periplasmic proteins (SilE and engineered Ag-binding protein) [169, 263] participate in bacterial detoxification of Ag^+. A mutation in *cus* was not detected in any evolved populations. Instead, *copA*, which has a role in Ag efflux [261], was mutated in multiple positions in Ag^+ and AgNP stressed populations, providing direct evidence of adaptation. The other mutations found in the evolved populations have not been previously reported to be linked with Ag resistance, suggesting that novel mechanisms are involved in the bacterial response to Ag stress.

Faster growth rate and larger cell size are phenotypic changes of evolved cells in the long-term evolution experiment [281]. FtsZ, which is recruited to the cell membrane to form the Z-ring for cell division, is associated with bacterial growth rate [282]. In *ftsZ*,

all five parallel AgNP-populations acquired a mutation turning a stop codon into a codon for Ser (serine), while in all five Ag^+ populations, Arg (arginine) was substituted with Cys (cysteine). A similar phenomenon was observed in *gacS*, which encodes a transmembrane signal sensor protein that is coupled with the response regulator GacA, comprising a two-component system [283]. The mutation of *uvrY*, which is homologous to *gacA*, occurred in the Ag^+ and the control populations but was mostly absent in the AgNP-populations, suggesting different regulatory strategies in response to the different Ag species.

The two AgNP-specific mutations in *envZ* (encoding an inner membrane protein that activates the production of the outer membrane protein porin [284]) and in PP_2758 (encoding a putative periplasmic protein) could indicate a direct attack of AgNPs on the bacterial cell wall. The genes *thiL* and PP_2397, mutated in Ag^+-populations, encode a thiamin monophosphate kinase and an EF-hand domain protein, which are located in the cytosol and have magnesium and calcium binding domains, respectively. The mutation in *tau-II*, coding for the taurine ABC transmembrane transporter ATP-binding subunit that is located at the cytoplasmic side, might suggest that this transporter is facilitating the uptake of Ag^+ into the cytosol, selecting mutations that reduce uptake. The different adaption models of *P. putida* under the treatment of Ag^+ or AgNP were compared (Figure 4.7). Because AgNPs cannot penetrate the bacterial cell wall, the mutations selected by AgNPs were associated with proteins in the periplasm and outer membrane. In contrast, Ag^+ mostly selected for mutations in cytoplasmic proteins, indicating a response to intracellular Ag^+.

P. putida evolved somewhat different adaptations upon exposure to low doses of Ag^+ versus AgNPs. Silver nanoparticles might have direct effects on the outer membrane and periplasm while silver ions selected several mutations in cytoplasmic proteins, possibly adapting to effects of silver uptake.

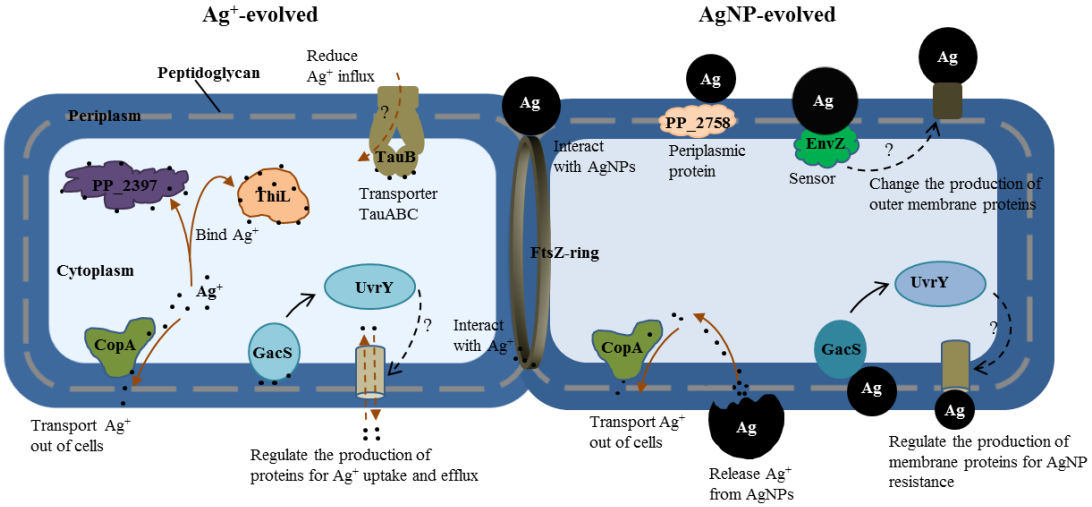

Figure 4.7 Different adaption models in *Pseudomonas putida* under the stress of Ag^+ or AgNPs

Adaption mechanisms in Ag^+-evolved (left side of the dividing cell) and AgNP-evolved populations (right side of the dividing cell) were compared. Silver ions and nanoparticles may interact with FtsZ to influence cell division in different pathways. In Ag^+-evolved populations, CopA transport Ag^+ in the cytoplasm into periplasmic space. GacS senses Ag^+ in the environment and may active UvrY to regulate the production of membrane proteins to reduce Ag^+ uptake or promote Ag^+ efflux. The cytoplasmic proteins PP_2397 and ThiL bind cytoplasmic Ag^+ to reduce the availability of intracellular Ag^+. The interaction between TauB and Ag^+ may induce the transporter TauABC complex to reduce Ag^+ influx. Silver nanoparticles cannot penetrate bacterial cells due to the physical barrier of bacterial membrane (i.e. the mean pore size of peptidoglycan in bacteria is < 5 nm [285]), but they might attach to bacterial outer membrane and release Ag^+ into cells. In AgNP-evolved populations, CopA transports Ag^+ that is released from AgNPs out of cells. The GacS/UvrY two-component system may control the production of membrane proteins for Ag resistance. The membrane protein EnvZ may also participate in regulating outer membrane protein for AgNP resistance. The periplasmic protein PP_2758 may deactivate AgNPs in the periplasmic region.

4.5 Conclusions

This study demonstrated the distinct evolution of *P. putida* upon prolonged exposure to low concentrations of Ag^+ or AgNPs. Fitness improved in the pre-evolution experiment and under the silver stresses in the main evolution experiment, including in conditions that were not selected for. The different mutation patterns in populations that evolved under Ag^+ or AgNP stress indicate somewhat different antibacterial activities of Ag^+ and AgNPs. Mutations unique to AgNP populations were mostly associated with the cell surface and two-component systems. By contrast, the mutations specific to Ag^+ populations were in uptake systems and metal-binding proteins in the cytosol. These results suggest different toxicity pathways for ionic and nanoparticulate Ag in bacteria. Significantly different mutations associated with the treatment of Ag^+ versus AgNPs were identified in the evolved populations, implying that nano-specific effects cannot be excluded in the toxicity of AgNPs, which has important implications for the application of AgNPs and their environmental risk assessment for the regulatory purpose.

5 Chapter Five

Conclusions and Future Work

5.1 Conclusions

Nanotechnology as a promising new science has already been applied in a variety of fields. Silver nanoparticles are one of the widely used nanomaterials, especially in killing pathogens, owing to their outstanding antimicrobial properties. But the mechanisms involved in the killing of bacteria by AgNPs are not clear. The studies in this thesis investigated the interactions between AgNPs and bacteria, including the synthesis of uncoated AgNPs, long-term storage, physicochemical transformations of AgNPs in microbial media, their dynamic toxicity in a bacterium *Pseudomonas putida*, and the bacterial response upon the prolonged exposure to low concentrations of AgNPs. The cellular and genetic mechanisms in the toxicity of AgNPs on bacteria are explored in this thesis.

Firstly, a rapid, convenient and inexpensive method of measuring the concentration of dissolved Ag^+ in AgNP suspensions was developed by combining aggregation with centrifugation (**Chapter 2**). Compared to several hours in conventional ultracentrifugation, the time to separate AgNPs from dissolved Ag was reduced to half hour with centrifugation based on pre-aggregating the AgNPs with Ca^{2+}. This method is especially helpful for real-time toxicity assays, in which quantification of the concentrations of Ag species is needed. To maintain the stability of AgNPs, storing AgNP stocks in an anoxic environment can prevent dissolution for three months. In addition to a concentration-dependent aggregation, AgNPs undergo slow dissolution in microbial media, influencing AgNP's state and their toxicity in bacteria (**Chapter 2** and

3).

In **Chapter 3**, the toxicity of AgNPs in an environmental model bacterium *Pseudomonas putida* was investigated. The MICs of Ag^+ and AgNPs are strongly correlated with initial cell densities. Silver ions are more toxic to bacteria than AgNPs. Accompanying the bacteria-killing, Ag^+ and AgNPs might be inactivated or fixed by cells, leading to a decrease of Ag concentration in cell culture, which might mitigate the Ag stress, allowing the recovery of the bacterial population. However, the dissolution of AgNPs results in continuous release of Ag^+, inhibiting the repopulation. The bacteria-killing ability of AgNPs is mainly attributed to the dissolved Ag.

The nano-specific effect of AgNPs was investigated in an experimental evolution study. The mutations in response to Ag^+ and AgNP stress were identified and compared. *P. putida* evolved in different patterns while they were treated by 5 and 20 μg/L Ag^+ and AgNPs (**Chapter 4**). The distinct mutation profiles in the populations stressed by different Ag species might indicate different toxicity models of action of Ag^+ and AgNPs. It was found that the toxicity of AgNPs is mostly associated with cell surface metabolism and Ag^+ is associated with the proteins for uptake and binding of metals in cytosol, demonstrating nano-specific effects in the antibacterial activities of AgNPs.

5.2 Future work

The properties of AgNPs have fundamental roles in their antibacterial activities. The surface chemistry, especially the ions around nanoparticle's core, determines the initial attachment of AgNPs to bacterial cells and the toxicity, which needs additional

investigation. The population-density related bacteria-killing by AgNPs found in this thesis should be considered for toxicity assays. Considering that bacteria typically live in the natural environment and medical settings as biofilm, it is necessary to measure the minimum biofilm eradication concentration such as crystal violent staining based assays to investigate the toxicity of AgNPs in more realistic environmental scenarios. Future studies of bacteria-killing kinetics by varying initial cell population densities will further provide evidences to support the inoculum effect in Ag^+/AgNP-cell interactions. The mechanisms of how Ag^+ penetrate into cells, AgNPs attach to cell surfaces, and their fate in bacterial cells are crucial to understand this inoculum effect, which needs further investigation. Further experiments are needed to differentiate the Ag adsorption by bacterial cells and those attached to the vessel surfaces with mass balance calculation, which can be explored to quantify the Ag^+ required to kill a given density of bacterial cells. The Ag degradation that leads to the decrease of the concentration of active Ag in the cell culture might weaken the Ag stress, but some bacteria are certainly less susceptible, allowing the recovery of bacteria populations. The heterogeneous susceptibility of individual cells might be linked with bacterial defences against Ag, which is unknown. To understand why partial bacterial population survive the Ag treatment, it will be helpful to isolate the potential resistant strains and measure their Ag tolerance, which will have important medical implications to optimize Ag dosage for infectious disease treatment. Although the evolved *P. putida* population gained fitness under the treatments of low concentrations of Ag^+ or AgNPs, it is not clear of whether the mutants can tolerate higher concentrations of Ag^+ or AgNPs.

Further experiments to measure the tolerance of mutated strains under higher concentrations of Ag^+ or AgNPs can be carried out to quantify the Ag tolerance in the evolved populations. As shown in the evolution experiment, *P. putida* evolved in different patterns in response to the stress of Ag^+ and AgNPs. Most of the mutated genes have not been reported to be linked with the toxicity of Ag^+ or AgNPs. An understanding of the relationship between these genes and the antibacterial activities of AgNPs as well as the potential for Ag resistance will be important for better design of AgNP products and their applications and for regulatory decisions regarding AgNP-containing medical and consumer products.

6 References

1. Petersen, E.J., et al., *Identification and Avoidance of Potential Artifacts and Misinterpretations in Nanomaterial Ecotoxicity Measurements.* Environmental Science & Technology, 2014. 48(8): p. 4226-4246.
2. Ghosh Chaudhuri, R. and S. Paria, *Core/Shell Nanoparticles: Classes, Properties, Synthesis Mechanisms, Characterization, and Applications.* Chemical Reviews, 2011. 112(4): p. 2373-2433.
3. Silvera Batista, C.A., R.G. Larson, and N.A. Kotov, *Nonadditivity of nanoparticle interactions.* Science, 2015. 350(6257).
4. Shulaker, M.M., et al., *Carbon nanotube computer.* Nature, 2013. 501(7468): p. 526-530.
5. Sun, C., J.S.H. Lee, and M. Zhang, *Magnetic nanoparticles in MR imaging and drug delivery.* Advanced Drug Delivery Reviews, 2008. 60(11): p. 1252-1265.
6. Kelly, K.L., et al., *The Optical Properties of Metal Nanoparticles: The Influence of Size, Shape, and Dielectric Environment.* The Journal of Physical Chemistry B, 2002. 107(3): p. 668-677.
7. Moghimi, S.M., A.C. Hunter, and J.C. Murray, *Nanomedicine: current status and future prospects.* The FASEB Journal, 2005. 19(3): p. 311-330.
8. Dreaden, E.C., et al., *The golden age: gold nanoparticles for biomedicine.* Chemical Society Reviews, 2012. 41(7): p. 2740-2779.
9. Chaloupka, K., Y. Malam, and A.M. Seifalian, *Nanosilver as a new generation of nanoproduct in biomedical applications.* Trends in Biotechnology, 2010. 28(11): p. 580-588.
10. Lohse, S.E. and C.J. Murphy, *Applications of Colloidal Inorganic Nanoparticles: From Medicine to Energy.* Journal of the American Chemical Society, 2012. 134(38): p. 15607-15620.
11. Zaera, F., *Shape-Controlled Nanostructures in Heterogeneous Catalysis.* ChemSusChem, 2013. 6(10): p. 1797-1820.
12. Howes, P.D., R. Chandrawati, and M.M. Stevens, *Colloidal nanoparticles as advanced biological sensors.* Science, 2014. 346(6205).
13. Boisselier, E. and D. Astruc, *Gold nanoparticles in nanomedicine: preparations, imaging, diagnostics, therapies and toxicity.* Chemical Society Reviews, 2009. 38(6): p. 1759-1782.
14. Zhu, X., et al., *Nanomedicine in the management of microbial infection – Overview and perspectives.* Nano Today, 2014. 9(4): p. 478-498.
15. Gabizon, A., et al., *Cancer nanomedicines: closing the translational gap.* The Lancet, 2014. 384(9961): p. 2175-2176.
16. Polte, J., et al., *Formation Mechanism of Colloidal Silver Nanoparticles: Analogies and Differences to the Growth of Gold Nanoparticles.* Acs Nano,

2012. 6(7): p. 5791-5802.
17. Scholl, J.A., A.L. Koh, and J.A. Dionne, *Quantum plasmon resonances of individual metallic nanoparticles.* Nature, 2012. 483(7390): p. 421-U68.
18. Homan, K.A., et al., *Silver Nanoplate Contrast Agents for in Vivo Molecular Photoacoustic Imaging.* ACS Nano, 2012. 6(1): p. 641-650.
19. Wiley, B.J., et al., *Synthesis and Optical Properties of Silver Nanobars and Nanorice.* Nano Letters, 2007. 7(4): p. 1032-1036.
20. Sun, Y.G. and Y.N. Xia, *Shape-controlled synthesis of gold and silver nanoparticles.* Science, 2002. 298(5601): p. 2176-2179.
21. Xie, J., et al., *The Synthesis of SERS-Active Gold Nanoflower Tags for In Vivo Applications.* ACS Nano, 2008. 2(12): p. 2473-2480.
22. Niu, W., et al., *Selective Synthesis of Single-Crystalline Rhombic Dodecahedral, Octahedral, and Cubic Gold Nanocrystals.* Journal of the American Chemical Society, 2009. 131(2): p. 697-703.
23. Shin, H., et al., *High resolution imaging analysis of CdSe/ZnS core-shell quantum dots (QDs) using Cs-corrected HR-TEM/STEM.* Journal of Materials Science-Materials in Electronics, 2013. 24(10): p. 3744-3748.
24. Henning, A.M., et al., *Gold–Palladium Core–Shell Nanocrystals with Size and Shape Control Optimized for Catalytic Performance.* Angewandte Chemie International Edition, 2013. 52(5): p. 1477-1480.
25. Huang, J., et al., *Effects of Nanoparticle Size on Cellular Uptake and Liver MRI with Polyvinylpyrrolidone-Coated Iron Oxide Nanoparticles.* Acs Nano, 2010. 4(12): p. 7151-7160.
26. Garnett, E.C. and P. Yang, *Silicon Nanowire Radial p−n Junction Solar Cells.* Journal of the American Chemical Society, 2008. 130(29): p. 9224-9225.
27. Odom, T.W., et al., *Atomic structure and electronic properties of single-walled carbon nanotubes.* Nature, 1998. 391(6662): p. 62-64.
28. Russell, A.D. and W.B. Hugo, *Antimicrobial activity and action of silver.* Progress in medicinal chemistry, 1994. 31: p. 351-70.
29. Chernousova, S. and M. Epple, *Silver as Antibacterial Agent: Ion, Nanoparticle, and Metal.* Angewandte Chemie-International Edition, 2013. 52(6): p. 1636-1653.
30. Holt, K.B. and A.J. Bard, *Interaction of Silver(I) Ions with the Respiratory Chain of Escherichia coli: An Electrochemical and Scanning Electrochemical Microscopy Study of the Antimicrobial Mechanism of Micromolar Ag^+.* Biochemistry, 2005. 44(39): p. 13214-13223.
31. Yamanaka, M., K. Hara, and J. Kudo, *Bactericidal actions of a silver ion solution on Escherichia coli, studied by energy-filtering transmission electron microscopy and proteomic analysis.* Appl Environ Microbiol, 2005. 71(11): p. 7589-93.
32. Jung, W.K., et al., *Antibacterial activity and mechanism of action of the silver*

ion in Staphylococcus aureus and Escherichia coli. Appl Environ Microbiol, 2008. 74(7): p. 2171-8.
33. Rizzello, L., R. Cingolani, and P.P. Pompa, *Nanotechnology tools for antibacterial materials.* Nanomedicine, 2013. 8(5): p. 807-821.
34. Xia, X.H., et al., *Recent Developments in Shape-Controlled Synthesis of Silver Nanocrystals.* Journal of Physical Chemistry C, 2012. 116(41): p. 21647-21656.
35. Xia, Y.N., et al., *Shape-Controlled Synthesis of Metal Nanocrystals: Simple Chemistry Meets Complex Physics?* Angewandte Chemie-International Edition, 2009. 48(1): p. 60-103.
36. Benn, T.M. and P. Westerhoff, *Nanoparticle silver released into water from commercially available sock fabrics.* Environmental Science & Technology, 2008. 42(11): p. 4133-4139.
37. Huang, Y.S., et al., *A randomized comparative trial between Acticoat and SD-Ag in the treatment of residual burn wounds, including safety analysis.* Burns, 2007. 33(2): p. 161-166.
38. Lin, S., et al., *Silver nanoparticle-alginate composite beads for point-of-use drinking water disinfection.* Water Research, 2013. 47(12): p. 3959-3965.
39. Cui, Z., et al., *Impact of antibiotic- and silver-impregnated external ventricular drains on the risk of infections: A systematic review and meta-analysis.* American Journal of Infection Control, 2015. 43(7): p. e23-e32.
40. Darouiche, R.O., et al., *A Comparison of Two Antimicrobial-Impregnated Central Venous Catheters.* New England Journal of Medicine, 1999. 340(1): p. 1-8.
41. Bonne, S., et al., *Effectiveness of Minocycline and Rifampin vs Chlorhexidine and Silver Sulfadiazine-Impregnated Central Venous Catheters in Preventing Central Line-Associated Bloodstream Infection in a High-Volume Academic Intensive Care Unit: A Before and after Trial.* Journal of the American College of Surgeons, 2015. 221(3): p. 739-747.
42. Antonelli, M., et al., *Comparison of triple-lumen central venous catheters impregnated with silver nanoparticles (AgTive®) vs conventional catheters in intensive care unit patients.* Journal of Hospital Infection, 2012. 82(2): p. 101-107.
43. Atkinson, R.A., et al., *Silver-impregnated external-ventricular-drain-related cerebrospinal fluid infections: a meta-analysis.* Journal of Hospital Infection, 2016. 92(3): p. 263-272.
44. Vlachou, E., et al., *The safety of nanocrystalline silver dressings on burns: A study of systemic silver absorption.* Burns, 2007. 33(8): p. 979-985.
45. Roe, D., et al., *Antimicrobial surface functionalization of plastic catheters by silver nanoparticles.* Journal of Antimicrobial Chemotherapy, 2008. 61(4): p. 869-876.
46. Gilabert-Porres, J., et al., *Design of a Nanostructured Active Surface against*

Gram-Positive and Gram-Negative Bacteria through Plasma Activation and in Situ Silver Reduction. ACS Applied Materials & Interfaces, 2016. 8(1): p. 64-73.
47. Taheri, S., et al., *Substrate independent silver nanoparticle based antibacterial coatings.* Biomaterials, 2014. 35(16): p. 4601-4609.
48. Nel, A.E., et al., *Understanding biophysicochemical interactions at the nano-bio interface.* Nature Materials, 2009. 8(7): p. 543-557.
49. Qu, X., et al., *Nanotechnology for a Safe and Sustainable Water Supply: Enabling Integrated Water Treatment and Reuse.* Accounts of Chemical Research, 2013. 46(3): p. 834-843.
50. Qu, X.L., P.J.J. Alvarez, and Q.L. Li, *Applications of nanotechnology in water and wastewater treatment.* Water Research, 2013. 47(12): p. 3931-3946.
51. Sankar, M.U., et al., *Biopolymer-reinforced synthetic granular nanocomposites for affordable point-of-use water purification.* Proceedings of the National Academy of Sciences, 2013. 110(21): p. 8459-8464.
52. Zhang, M., R.W. Field, and K. Zhang, *Biogenic silver nanocomposite polyethersulfone UF membranes with antifouling properties.* Journal of Membrane Science, 2014. 471: p. 274-284.
53. Adeleye, A.S., et al., *Engineered nanomaterials for water treatment and remediation: Costs, benefits, and applicability.* Chemical Engineering Journal, 2016. 286: p. 640-662.
54. Valsami-Jones, E. and I. Lynch, *How safe are nanomaterials?* Science, 2015. 350(6259): p. 388-389.
55. Le Ouay, B. and F. Stellacci, *Antibacterial activity of silver nanoparticles: A surface science insight.* Nano Today, 2015. 10(3): p. 339-354.
56. Ogar, A., G. Tylko, and K. Turnau, *Antifungal properties of silver nanoparticles against indoor mould growth.* Science of The Total Environment, 2015. 521–522: p. 305-314.
57. Navarro, E., et al., *Effects of Differently Coated Silver Nanoparticles on the Photosynthesis of Chlamydomonas reinhardtii.* Environmental Science & Technology, 2015. 49(13): p. 8041-8047.
58. Schwab, F., et al., *Barriers, pathways and processes for uptake, translocation and accumulation of nanomaterials in plants – Critical review.* Nanotoxicology, 2016. 10(3): p. 257-278.
59. Osborne, O.J., et al., *Organ-Specific and Size-Dependent Ag Nanoparticle Toxicity in Gills and Intestines of Adult Zebrafish.* ACS Nano, 2015. 9(10): p. 9573-9584.
60. Wang, H., et al., *Toxicity, Bioaccumulation, and Biotransformation of Silver Nanoparticles in Marine Organisms.* Environmental Science & Technology, 2014. 48(23): p. 13711-13717.
61. Eckelman, M.J. and T.E. Graedel, *Silver emissions and their environmental*

impacts: A multilevel assessment. Environmental Science & Technology, 2007. 41(17): p. 6283-6289.
62. Mueller, N.C. and B. Nowack, *Exposure modeling of engineered nanoparticles in the environment.* Environmental Science & Technology, 2008. 42(12): p. 4447-4453.
63. Lem, K.W., et al., *Use of Nanosilver in Consumer Products.* Recent Patents on Nanotechnology, 2012. 6(1): p. 60-72.
64. Piccinno, F., et al., *Industrial production quantities and uses of ten engineered nanomaterials in Europe and the world.* Journal of Nanoparticle Research, 2012. 14(9).
65. Nowack, B., *Nanosilver Revisited Downstream.* Science, 2010. 330(6007): p. 1054-1055.
66. Mitrano, D.M., et al., *Durability of nano-enhanced textiles through the life cycle: releases from landfilling after washing.* Environmental Science: Nano, 2016.
67. Shafer, M.M., J.T. Overdier, and D.E. Armstong, *Removal, partitioning, and fate of silver and other metals in wastewater treatment plants and effluent-receiving streams.* Environmental Toxicology and Chemistry, 1998. 17(4): p. 630-641.
68. Lombi, E., et al., *Transformation of four silver/silver chloride nanoparticles during anaerobic treatment of wastewater and post-processing of sewage sludge.* Environmental Pollution, 2013. 176: p. 193-197.
69. Kim, B., et al., *Discovery and Characterization of Silver Sulfide Nanoparticles in Final Sewage Sludge Products.* Environmental Science & Technology, 2010. 44(19): p. 7509-7514.
70. Walser, T., et al., *Persistence of engineered nanoparticles in a municipal solid-waste incineration plant.* Nat Nano, 2012. 7(8): p. 520-524.
71. Li, L., et al., *To What Extent Can Full-Scale Wastewater Treatment Plant Effluent Influence the Occurrence of Silver-Based Nanoparticles in Surface Waters?* Environmental Science & Technology, 2016.
72. Ranville, M.A. and A.R. Flegal, *Silver in the North Pacific ocean.* Geochemistry Geophysics Geosystems, 2005. 6.
73. Ndungu, K., *Dissolved silver in the Baltic Sea.* Environmental Research, 2011. 111(1): p. 45-49.
74. Barriada, J.L., et al., *Dissolved silver measurements in seawater.* Trac-Trends in Analytical Chemistry, 2007. 26(8): p. 809-817.
75. Flegal, A.R., et al., *Spatial and temporal variations in silver contamination and toxicity in San Francisco Bay.* Environmental Research, 2007. 105(1): p. 34-52.
76. Gottschalk, F., et al., *Engineered nanomaterials in rivers - Exposure scenarios for Switzerland at high spatial and temporal resolution.* Environmental Pollution, 2011. 159(12): p. 3439-3445.
77. Hou, H., et al., *Concentrations of Ag, In, Sn, Sb and Bi, and their chemical*

fractionation in typical soils in Japan. European Journal of Soil Science, 2006. 57(2): p. 214-227.
78. Lottermoser, B.G., *Effect of long-term irrigation with sewage effluent on the metal content of soils, Berlin, Germany.* Environmental Geochemistry and Health, 2012. 34(1): p. 67-76.
79. Peng, X., J. Wickham, and A.P. Alivisatos, *Kinetics of II-VI and III-V Colloidal Semiconductor Nanocrystal Growth: "Focusing" of Size Distributions.* Journal of the American Chemical Society, 1998. 120(21): p. 5343-5344.
80. Woehl, T.J., et al., *Direct Observation of Aggregative Nanoparticle Growth: Kinetic Modeling of the Size Distribution and Growth Rate.* Nano Letters, 2013.
81. Wang, F., et al., *Kinetics and Mechanisms of Aggregative Nanocrystal Growth.* Chemistry of Materials, 2013. 26(1): p. 5-21.
82. Washio, I., et al., *Reduction by the end groups of poly(vinyl pyrrolidone): A new and versatile route to the kinetically controlled synthesis of Ag triangular nanoplates.* Advanced Materials, 2006. 18(13): p. 1745-1749.
83. Slonczewski, J. and J.W. Foster, *Microbiology : an evolving science*. 1st ed. 2009, New York: W.W. Norton & Co.
84. Zhang, Q., et al., *A Systematic Study of the Synthesis of Silver Nanoplates: Is Citrate a "Magic" Reagent?* Journal of the American Chemical Society, 2011. 133(46): p. 18931-18939.
85. Chandni, et al., *A growth kinetic study of ultrafine monodispersed silver nanoparticles.* Rsc Advances, 2013. 3(4): p. 1127-1136.
86. Raveendran, P., J. Fu, and S.L. Wallen, *Completely "green" synthesis and stabilization of metal nanoparticles.* Journal of the American Chemical Society, 2003. 125(46): p. 13940-13941.
87. Nam, K.T., et al., *Peptide-Mediated Reduction of Silver Ions on Engineered Biological Scaffolds.* ACS Nano, 2008. 2(7): p. 1480-1486.
88. Kumar, V. and S.K. Yadav, *Synthesis of different-sized silver nanoparticles by simply varying reaction conditions with leaf extracts of Bauhinia variegata L.* Iet Nanobiotechnology, 2012. 6(1): p. 1-8.
89. Naik, R.R., et al., *Biomimetic synthesis and patterning of silver nanoparticles.* Nat Mater, 2002. 1(3): p. 169-172.
90. Klaus, T., et al., *Silver-based crystalline nanoparticles, microbially fabricated.* Proceedings of the National Academy of Sciences of the United States of America, 1999. 96(24): p. 13611-13614.
91. Leclerc, S. and K.J. Wilkinson, *Bioaccumulation of Nanosilver by Chlamydomonas reinhardtii—Nanoparticle or the Free Ion?* Environmental Science & Technology, 2013.
92. Hou, W.-C., et al., *Sunlight-Driven Reduction of Silver Ions by Natural Organic Matter: Formation and Transformation of Silver Nanoparticles.* Environmental Science & Technology, 2013.

93. Yin, Y., J. Liu, and G. Jiang, *Sunlight-Induced Reduction of Ionic Ag and Au to Metallic Nanoparticles by Dissolved Organic Matter.* Acs Nano, 2012. 6(9): p. 7910-7919.
94. Mulfinger, L., et al., *Synthesis and Study of Silver Nanoparticles.* Journal of Chemical Education, 2007. 84(2): p. 322-325.
95. Zhang, Z.T., B. Zhao, and L.M. Hu, *PVP protective mechanism of ultrafine silver powder synthesized by chemical reduction processes.* Journal of Solid State Chemistry, 1996. 121(1): p. 105-110.
96. Boles, M.A., et al., *The surface science of nanocrystals.* Nat Mater, 2016. 15(2): p. 141-153.
97. Sotiriou, G.A., et al., *Quantifying the Origin of Released Ag+ Ions from Nanosilver.* Langmuir, 2012. 28(45): p. 15929-15936.
98. Liu, J.Y., K.G. Pennell, and R.H. Hurt, *Kinetics and Mechanisms of Nanosilver Oxysulfidation.* Environmental Science & Technology, 2011. 45(17): p. 7345-7353.
99. Römer, I., et al., *High Resolution STEM-EELS Study of Silver Nanoparticles Exposed to Light and Humic Substances.* Environmental Science & Technology, 2016. 50(5): p. 2183-2190.
100. Jang, M.-H., et al., *Uptake, Tissue Distribution, and Depuration of Total Silver in Common Carp (Cyprinus carpio) after Aqueous Exposure to Silver Nanoparticles.* Environmental Science & Technology, 2014. 48(19): p. 11568-11574.
101. Van Aert, S., et al., *Three-dimensional atomic imaging of crystalline nanoparticles.* Nature, 2011. 470(7334): p. 374-377.
102. Jadzinsky, P.D., et al., *Structure of a thiol monolayer-protected gold nanoparticle at 1.1 angstrom resolution.* Science, 2007. 318(5849): p. 430-433.
103. Peretyazhko, T.S., Q. Zhang, and V.L. Colvin, *Size-Controlled Dissolution of Silver Nanoparticles at Neutral and Acidic pH Conditions: Kinetics and Size Changes.* Environmental Science & Technology, 2014. 48(20): p. 11954-11961.
104. Cha, S.-H., et al., *Shape-Dependent Biomimetic Inhibition of Enzyme by Nanoparticles and Their Antibacterial Activity.* Acs Nano, 2015. 9(9): p. 9097-9105.
105. Baalousha, M., A. Prasad, and J.R. Lead, *Quantitative measurement of the nanoparticle size and number concentration from liquid suspensions by atomic force microscopy.* Environmental Science: Processes & Impacts, 2014. 16(6): p. 1338-1347.
106. Kent, R.D. and P.J. Vikesland, *Controlled Evaluation of Silver Nanoparticle Dissolution Using Atomic Force Microscopy.* Environmental Science & Technology, 2012. 46(13): p. 6977-6984.
107. Zucker, R.M., et al., *Detection of silver nanoparticles in cells by flow cytometry using light scatter and far-red fluorescence.* Cytometry Part A, 2013. 83(10): p.

962-972.
108. Peng, S., et al., *Reversing the size-dependence of surface plasmon resonances.* Proceedings of the National Academy of Sciences, 2010. 107(33): p. 14530-14534.
109. Zhao, J., et al., *Methods for Describing the Electromagnetic Properties of Silver and Gold Nanoparticles.* Accounts of Chemical Research, 2008. 41(12): p. 1710-1720.
110. Haiss, W., et al., *Determination of Size and Concentration of Gold Nanoparticles from UV−Vis Spectra.* Analytical Chemistry, 2007. 79(11): p. 4215-4221.
111. Quinten, M., *Local fields close to the surface of nanoparticles and aggregates of nanoparticles.* Applied Physics B, 2014. 73(3): p. 245-255.
112. Messersmith, R.E., G.J. Nusz, and S.M. Reed, *Using the Localized Surface Plasmon Resonance of Gold Nanoparticles To Monitor Lipid Membrane Assembly and Protein Binding.* The Journal of Physical Chemistry C, 2013. 117(50): p. 26725-26733.
113. Haynes, C.L., A.D. McFarland, and R.P.V. Duyne, *Surface-Enhanced Raman Spectroscopy.* Analytical Chemistry, 2005. 77(17): p. 338 A-346 A.
114. Biedermann, G. and L.G. Sillen, *Studies on the hydrolysis of metal ions .30. A critical survey of the solubility equilibria of Ag_2O.* Acta Chemica Scandinavica, 1960. 14(3): p. 717-725.
115. Loza, K., et al., *The dissolution and biological effects of silver nanoparticles in biological media.* Journal of Materials Chemistry B, 2014. 2(12): p. 1634-1643.
116. Liu, J. and R.H. Hurt, *Ion Release Kinetics and Particle Persistence in Aqueous Nano-Silver Colloids.* Environmental Science & Technology, 2010. 44(6): p. 2169-2175.
117. Grillet, N., et al., *Photo-Oxidation of Individual Silver Nanoparticles: A Real-Time Tracking of Optical and Morphological Changes.* Journal of Physical Chemistry C, 2013. 117(5): p. 2274-2282.
118. Levard, C., et al., *Environmental Transformations of Silver Nanoparticles: Impact on Stability and Toxicity.* Environmental Science & Technology, 2012. 46(13): p. 6900-6914.
119. Peter, M., et al., *Trends in the Binding Strength of Surface Species on Nanoparticles: How Does the Adsorption Energy Scale with the Particle Size?* Angewandte Chemie International Edition, 2013. 52(19): p. 5175-5179.
120. Kuzma, A., et al., *Influence of surface oxidation on plasmon resonance in monolayer of gold and silver nanoparticles.* Journal of Applied Physics, 2012. 112(10).
121. Zhang, W., et al., *Modeling the Primary Size Effects of Citrate-Coated Silver Nanoparticles on Their Ion Release Kinetics.* Environmental Science & Technology, 2011. 45(10): p. 4422-4428.

122. Ma, R., et al., *Size-Controlled Dissolution of Organic-Coated Silver Nanoparticles.* Environmental Science & Technology, 2012. 46(2): p. 752-759.
123. He, D., M.W. Bligh, and T.D. Waite, *Effects of Aggregate Structure on the Dissolution Kinetics of Citrate-Stabilized Silver Nanoparticles.* Environmental Science & Technology, 2013. 47(16): p. 9148-9156.
124. Kittler, S., et al., *Toxicity of Silver Nanoparticles Increases during Storage Because of Slow Dissolution under Release of Silver Ions.* Chemistry of Materials, 2010. 22(16): p. 4548-4554.
125. Gorham, J., et al., *Storage Wars: how citrate-capped silver nanoparticle suspensions are affected by not-so-trivial decisions.* Journal of Nanoparticle Research, 2014. 16(4): p. 1-14.
126. Liu, J., et al., *Controlled Release of Biologically Active Silver from Nanosilver Surfaces.* Acs Nano, 2010. 4(11): p. 6903-6913.
127. Chambers, B.A., et al., *Effects of Chloride and Ionic Strength on Physical Morphology, Dissolution, and Bacterial Toxicity of Silver Nanoparticles.* Environmental Science & Technology, 2013. 48(1): p. 761-769.
128. Levard, C., et al., *Effect of Chloride on the Dissolution Rate of Silver Nanoparticles and Toxicity to E. coli.* Environmental Science & Technology, 2013. 47(11): p. 5738-5745.
129. Levard, C., et al., *Sulfidation Processes of PVP-Coated Silver Nanoparticles in Aqueous Solution: Impact on Dissolution Rate.* Environmental Science & Technology, 2011. 45(12): p. 5260-5266.
130. Thalmann, B., et al., *Sulfidation Kinetics of Silver Nanoparticles Reacted with Metal Sulfides.* Environmental Science & Technology, 2014. 48(9): p. 4885-4892.
131. Reinsch, B.C., et al., *Sulfidation of Silver Nanoparticles Decreases Escherichia coli Growth Inhibition.* Environmental Science & Technology, 2012. 46(13): p. 6992-7000.
132. Lowry, G.V., et al., *Long-Term Transformation and Fate of Manufactured Ag Nanoparticles in a Simulated Large Scale Freshwater Emergent Wetland.* Environmental Science & Technology, 2012. 46(13): p. 7027-7036.
133. Albanese, A. and W.C.W. Chan, *Effect of Gold Nanoparticle Aggregation on Cell Uptake and Toxicity.* ACS Nano, 2011. 5(7): p. 5478-5489.
134. Lok, C.-N., et al., *Silver nanoparticles: partial oxidation and antibacterial activities.* JBIC Journal of Biological Inorganic Chemistry, 2007. 12(4): p. 527-534.
135. Cosgrove, T., *Colloid Sciences - Principles, Methods and Application*. 2005: Blackwell Publishing. 36-45.
136. Gambinossi, F., S.E. Mylon, and J.K. Ferri, *Aggregation kinetics and colloidal stability of functionalized nanoparticles.* Advances in Colloid and Interface Science, 2015. 222: p. 332-349.

137. Zhang, W., et al., *Attachment Efficiency of Nanoparticle Aggregation in Aqueous Dispersions: Modeling and Experimental Validation.* Environmental Science & Technology, 2012. 46(13): p. 7054-7062.
138. El Badawy, A.M., et al., *Impact of Environmental Conditions (pH, Ionic Strength, and Electrolyte Type) on the Surface Charge and Aggregation of Silver Nanoparticles Suspensions.* Environmental Science & Technology, 2010. 44(4): p. 1260-1266.
139. Huynh, K.A. and K.L. Chen, *Aggregation Kinetics of Citrate and Polyvinylpyrrolidone Coated Silver Nanoparticles in Monovalent and Divalent Electrolyte Solutions.* Environmental Science & Technology, 2011. 45(13): p. 5564-5571.
140. Kazim, S., et al., *Morphology and Kinetics of Aggregation of Silver Nanoparticles Induced with Regioregular Cationic Polythiophene.* Langmuir, 2016. 32(1): p. 2-11.
141. El Badawy, A.M., et al., *The impact of stabilization mechanism on the aggregation kinetics of silver nanoparticles.* Science of the Total Environment, 2012. 429: p. 325-331.
142. Chen, K.L. and M. Elimelech, *Influence of humic acid on the aggregation kinetics of fullerene (C60) nanoparticles in monovalent and divalent electrolyte solutions.* Journal of Colloid and Interface Science, 2007. 309(1): p. 126-134.
143. Dupont, C.L., et al., *History of biological metal utilization inferred through phylogenomic analysis of protein structures.* Proceedings of the National Academy of Sciences, 2010. 107(23): p. 10567-10572.
144. Finney, L.A. and T.V. O'Halloran, *Transition Metal Speciation in the Cell: Insights from the Chemistry of Metal Ion Receptors.* Science, 2003. 300(5621): p. 931-936.
145. Boening, D.W., *Ecological effects, transport, and fate of mercury: a general review.* Chemosphere, 2000. 40(12): p. 1335-1351.
146. Harrison, J.J., H. Ceri, and R.J. Turner, *Multimetal resistance and tolerance in microbial biofilms.* Nature Reviews Microbiology, 2007. 5(12): p. 928-938.
147. Imlay, J.A., *The molecular mechanisms and physiological consequences of oxidative stress: lessons from a model bacterium.* Nat Rev Micro, 2013. 11(7): p. 443-454.
148. Macomber, L. and J.A. Imlay, *The iron-sulfur clusters of dehydratases are primary intracellular targets of copper toxicity.* Proceedings of the National Academy of Sciences, 2009. 106(20): p. 8344-8349.
149. Morones-Ramirez, J.R., et al., *Silver Enhances Antibiotic Activity Against Gram-Negative Bacteria.* Science Translational Medicine, 2013. 5(190): p. 190ra81.
150. Park, H.-J., et al., *Silver-ion-mediated reactive oxygen species generation affecting bactericidal activity.* Water Research, 2009. 43(4): p. 1027-1032.

151. Gordon, O., et al., *Silver Coordination Polymers for Prevention of Implant Infection: Thiol Interaction, Impact on Respiratory Chain Enzymes, and Hydroxyl Radical Induction.* Antimicrobial Agents and Chemotherapy, 2010. 54(10): p. 4208-4218.
152. Xiu, Z.M., J. Ma, and P.J.J. Alvarez, *Differential Effect of Common Ligands and Molecular Oxygen on Antimicrobial Activity of Silver Nanoparticles versus Silver Ions.* Environmental Science & Technology, 2011. 45(20): p. 9003-9008.
153. Romanov, V., et al., *Binding Energies of the Silver Ion to Alcohols and Amides: A Theoretical and Experimental Study.* The Journal of Physical Chemistry A, 2008. 112(43): p. 10912-10920.
154. Bovenkamp, G.L., et al., *X-Ray Absorption Near-Edge Structure (XANES) Spectroscopy Study of the Interaction of Silver Ions with Staphylococcus aureus, Listeria monocytogenes, and Escherichia coli.* Applied and Environmental Microbiology, 2013. 79(20): p. 6385-6390.
155. Randall, C.P., et al., *The silver cation (Ag): antistaphylococcal activity, mode of action and resistance studies.* Journal of Antimicrobial Chemotherapy, 2013. 68(1): p. 131-138.
156. Dibrov, P., et al., *Chemiosmotic mechanism of antimicrobial activity of Ag^+ in Vibrio cholerae.* Antimicrobial Agents and Chemotherapy, 2002. 46(8): p. 2668-2670.
157. Asakura, K., et al., *Genotoxicity Studies of Heavy Metals: Lead, Bismuth, Indium, Silver and Antimony.* Journal of Occupational Health, 2009. 51(6): p. 498-512.
158. Butler, K.S., et al., *Silver nanoparticles: correlating nanoparticle size and cellular uptake with genotoxicity.* Mutagenesis, 2015. 30(4): p. 577-591.
159. Brown, E.D. and G.D. Wright, *Antibacterial drug discovery in the resistance era.* Nature, 2016. 529(7586): p. 336-343.
160. Piddock, L.J.V., *The crisis of no new antibiotics—what is the way forward?* The Lancet Infectious Diseases, 2012. 12(3): p. 249-253.
161. Larkin Mchugh, G., et al., *Salmonella typhimurium resistant to silver nitrate, chloramphenicol, and ampicillin.* The Lancet, 1975. 305(7901): p. 235-240.
162. Gupta, A., et al., *Molecular basis for resistance to silver cations in Salmonella.* Nature Medicine, 1999. 5(2): p. 183-188.
163. Chopra, I., *The increasing use of silver-based products as antimicrobial agents: a useful development or a cause for concern?* Journal of Antimicrobial Chemotherapy, 2007. 59(4): p. 587-590.
164. Stoyanov, J.V., D. Magnani, and M. Solioz, *Measurement of cytoplasmic copper, silver, and gold with a lux biosensor shows copper and silver, but not gold, efflux by the CopA ATPase of Escherichia coli.* FEBS Letters, 2003. 546(2–3): p. 391-394.
165. Randall, C.P., et al., *Silver resistance in Gram-negative bacteria: a dissection*

of endogenous and exogenous mechanisms. Journal of Antimicrobial Chemotherapy, 2015. 70(4): p. 1037-1046.
166. Kim, E.-H., et al., *Switch or Funnel: How RND-Type Transport Systems Control Periplasmic Metal Homeostasis.* Journal of Bacteriology, 2011. 193(10): p. 2381-2387.
167. Li, X.Z., H. Nikaido, and K.E. Williams, *Silver-resistant mutants of Escherichia coli display active efflux of Ag^+ and are deficient in porins.* Journal of Bacteriology, 1997. 179(19): p. 6127-32.
168. Sedlak, R.H., et al., *Engineered Escherichia coli Silver-Binding Periplasmic Protein That Promotes Silver Tolerance.* Applied and Environmental Microbiology, 2012. 78(7): p. 2289-2296.
169. Wakshlak, R.B.-K., R. Pedahzur, and D. Avnir, *Antibacterial activity of silver-killed bacteria: the "zombies" effect.* Sci. Rep., 2015. 5.
170. Kang, F., P.J. Alvarez, and D. Zhu, *Microbial Extracellular Polymeric Substances Reduce Ag^+ to Silver Nanoparticles and Antagonize Bactericidal Activity.* Environmental Science & Technology, 2013. 48(1): p. 316-322.
171. Flemming, H.C. and J. Wingender, *The biofilm matrix.* Nature Reviews Microbiology, 2010. 8(9): p. 623-633.
172. Stewart, P.S. and M.J. Franklin, *Physiological heterogeneity in biofilms.* Nature Reviews Microbiology, 2008. 6(3): p. 199-210.
173. Vlamakis, H., et al., *Sticking together: building a biofilm the Bacillus subtilis way.* Nature Reviews Microbiology, 2013. 11(3): p. 157-168.
174. Harrison, J.J., et al., *Biofilm susceptibility to metal toxicity.* Environmental Microbiology, 2004. 6(12): p. 1220-1227.
175. Harrison, J.J., R.J. Turner, and H. Ceri, *Persister cells, the biofilm matrix and tolerance to metal cations in biofilm and planktonic Pseudomonas aeruginosa.* Environmental Microbiology, 2005. 7(7): p. 981-994.
176. Schultz, D., J.N. Onuchic, and E. Ben-Jacob, *Turning death into creative force during biofilm engineering.* Proceedings of the National Academy of Sciences of the United States of America, 2012. 109(46): p. 18633-18634.
177. Wirth, S.M., et al., *Inhibition of bacterial surface colonization by immobilized silver nanoparticles depends critically on the planktonic bacterial concentration.* Journal of Colloid and Interface Science, 2016. 467: p. 17-27.
178. Gupta, A., et al., *Molecular basis for resistance to silver cations in Salmonella.* Nat Med, 1999. 5(2): p. 183-188.
179. Nel, A., et al., *Toxic potential of materials at the nanolevel.* Science, 2006. 311(5761): p. 622-627.
180. Hajipour, M.J., et al., *Antibacterial properties of nanoparticles.* Trends in Biotechnology, 2012. 30(10): p. 499-511.
181. Oh, E., et al., *Meta-analysis of cellular toxicity for cadmium-containing quantum dots.* Nat Nano, 2016. advance online publication.

182. Manshian, B.B., et al., *High-Content Imaging and Gene Expression Approaches To Unravel the Effect of Surface Functionality on Cellular Interactions of Silver Nanoparticles.* Acs Nano, 2015. 9(10): p. 10431-10444.
183. Verma, A., et al., *Surface-structure-regulated cell-membrane penetration by monolayer-protected nanoparticles.* Nat Mater, 2008. 7(7): p. 588-595.
184. Zhu, M., et al., *Physicochemical Properties Determine Nanomaterial Cellular Uptake, Transport, and Fate.* Accounts of Chemical Research, 2013. 46(3): p. 622-631.
185. Jiang, W., et al., *Nanoparticle-mediated cellular response is size-dependent.* Nature Nanotechnology, 2008. 3(3): p. 145-150.
186. AshaRani, P.V., et al., *Cytotoxicity and Genotoxicity of Silver Nanoparticles in Human Cells.* Acs Nano, 2009. 3(2): p. 279-290.
187. von Moos, N. and V.I. Slaveykova, *Oxidative stress induced by inorganic nanoparticles in bacteria and aquatic microalgae – state of the art and knowledge gaps.* Nanotoxicology, 2014. 8(6): p. 605-630.
188. Choi, O. and Z.Q. Hu, *Size dependent and reactive oxygen species related nanosilver toxicity to nitrifying bacteria.* Environmental Science & Technology, 2008. 42(12): p. 4583-4588.
189. Lok, C.N., et al., *Proteomic analysis of the mode of antibacterial action of silver nanoparticles.* Journal of Proteome Research, 2006. 5(4): p. 916-924.
190. Li, W.-R., et al., *Antibacterial activity and mechanism of silver nanoparticles on Escherichia coli.* Applied Microbiology and Biotechnology, 2010. 85(4): p. 1115-1122.
191. Morones, J.R., et al., *The bactericidal effect of silver nanoparticles.* Nanotechnology, 2005. 16(10): p. 2346-2353.
192. Liu, S., et al., *Antibacterial Activity of Graphite, Graphite Oxide, Graphene Oxide, and Reduced Graphene Oxide: Membrane and Oxidative Stress.* Acs Nano, 2011. 5(9): p. 6971-6980.
193. Ivask, A., et al., *Size-Dependent Toxicity of Silver Nanoparticles to Bacteria, Yeast, Algae, Crustaceans and Mammalian Cells In Vitro.* PLoS ONE, 2014. 9(7): p. e102108.
194. Käosaar, S., et al., *Profiling of the toxicity mechanisms of coated and uncoated silver nanoparticles to yeast Saccharomyces cerevisiae BY4741 using a set of its 9 single-gene deletion mutants defective in oxidative stress response, cell wall or membrane integrity and endocytosis.* Toxicology in Vitro, 2016. 35: p. 149-162.
195. Bertrand, C., et al., *The influence of salinity on the fate and behavior of silver standardized nanomaterial and toxicity effects in the estuarine bivalve Scrobicularia plana.* Environmental Toxicology and Chemistry, 2016. 35(10): p. 2550-2561.
196. Li, L., et al., *Both released silver ions and particulate Ag contribute to the*

toxicity of AgNPs to earthworm Eisenia fetida. Nanotoxicology, 2015. 9(6): p. 792-801.
197. Yameen, B., et al., *Insight into nanoparticle cellular uptake and intracellular targeting.* Journal of Controlled Release, 2014. 190: p. 485-499.
198. Zhao, C.M. and W.X. Wang, *Size-Dependent Uptake of Silver Nanoparticles in Daphnia magna.* Environmental Science & Technology, 2012. 46(20): p. 11345-11351.
199. Misra, S.K., et al., *The complexity of nanoparticle dissolution and its importance in nanotoxicological studies.* Science of the Total Environment, 2012. 438(0): p. 225-232.
200. Xiu, Z.-m., et al., *Negligible Particle-Specific Antibacterial Activity of Silver Nanoparticles.* Nano Letters, 2012. 12(8): p. 4271-4275.
201. Raghupathi, K.R., R.T. Koodali, and A.C. Manna, *Size-Dependent Bacterial Growth Inhibition and Mechanism of Antibacterial Activity of Zinc Oxide Nanoparticles.* Langmuir, 2011. 27(7): p. 4020-4028.
202. El Badawy, A.M., et al., *Surface Charge-Dependent Toxicity of Silver Nanoparticles.* Environmental Science & Technology, 2011. 45(1): p. 283-287.
203. Huehn, D., et al., *Polymer-Coated Nanoparticles Interacting with Proteins and Cells: Focusing on the Sign of the Net Charge.* Acs Nano, 2013. 7(4): p. 3253-3263.
204. Ivask, A., et al., *Toxicity Mechanisms in Escherichia coli Vary for Silver Nanoparticles and Differ from Ionic Silver.* Acs Nano, 2013. 8(1): p. 374-386.
205. McQuillan, J.S. and A.M. Shaw, *Differential gene regulation in the Ag nanoparticle and Ag^+-induced silver stress response in Escherichia coli: A full transcriptomic profile.* Nanotoxicology, 2014. 8(S1): p. 177-184.
206. Bondarenko, O., et al., *Particle-Cell Contact Enhances Antibacterial Activity of Silver Nanoparticles.* PLoS ONE, 2013. 8(5): p. e64060.
207. McQuillan, J.S., et al., *Silver nanoparticle enhanced silver ion stress response in Escherichia coli K12.* Nanotoxicology, 2012. 6(8): p. 857-866.
208. Kim, B.Y.S., J.T. Rutka, and W.C.W. Chan, *Current Concepts: Nanomedicine.* New England Journal of Medicine, 2010. 363(25): p. 2434-2443.
209. Sprenger, M. and K. Fukuda, *New mechanisms, new worries.* Science, 2016. 351(6279): p. 1263-1264.
210. Meredith, H.R., et al., *Collective antibiotic tolerance: mechanisms, dynamics and intervention.* Nat Chem Biol, 2015. 11(3): p. 182-188.
211. Eckhardt, S., et al., *Nanobio Silver: Its Interactions with Peptides and Bacteria, and Its Uses in Medicine.* Chemical Reviews, 2013. 113(7): p. 4708-4754.
212. Shen, M.-H., et al., *Exposure Medium: Key in Identifying Free Ag^+ as the Exclusive Species of Silver Nanoparticles with Acute Toxicity to Daphnia magna.* Sci. Rep., 2015. 5.
213. Leclerc, S. and K.J. Wilkinson, *Bioaccumulation of Nanosilver by*

Chlamydomonas reinhardtii—Nanoparticle or the Free Ion? Environmental Science & Technology, 2014. 48(1): p. 358-364.
214. Oberdörster, G., E. Oberdörster, and J. Oberdörster, *Nanotoxicology: An Emerging Discipline Evolving from Studies of Ultrafine Particles.* Environmental Health Perspectives, 2005. 113(7): p. 823-839.
215. Mostowfi, F., et al., *Asphaltene Nanoaggregates Studied by Centrifugation.* Energy & Fuels, 2009. 23(3): p. 1194-1200.
216. Kennedy, A.J., et al., *Fractionating Nanosilver: Importance for Determining Toxicity to Aquatic Test Organisms.* Environmental Science & Technology, 2010. 44(24): p. 9571-9577.
217. Mitrano, D.M., et al., *Silver nanoparticle characterization using single particle ICP-MS (SP-ICP-MS) and asymmetrical flow field flow fractionation ICP-MS (AF4-ICP-MS).* Journal of Analytical Atomic Spectrometry, 2012. 27(7): p. 1131-1142.
218. Pace, H.E., et al., *Single Particle Inductively Coupled Plasma-Mass Spectrometry: A Performance Evaluation and Method Comparison in the Determination of Nanoparticle Size.* Environmental Science & Technology, 2012. 46(22): p. 12272-12280.
219. Van Hyning, D.L. and C.F. Zukoski, *Formation Mechanisms and Aggregation Behavior of Borohydride Reduced Silver Particles.* Langmuir, 1998. 14(24): p. 7034-7046.
220. Michen, B., et al., *Avoiding drying-artifacts in transmission electron microscopy: Characterizing the size and colloidal state of nanoparticles.* Scientific Reports, 2015. 5: p. 9793.
221. Hendel, T., et al., *In Situ Determination of Colloidal Gold Concentrations with UV–Vis Spectroscopy: Limitations and Perspectives.* Analytical Chemistry, 2014. 86(22): p. 11115-11124.
222. Schneider, C.A., W.S. Rasband, and K.W. Eliceiri, *NIH Image to ImageJ: 25 years of image analysis.* Nat Meth, 2012. 9(7): p. 671-675.
223. Van Hyning, D.L., W.G. Klemperer, and C.F. Zukoski, *Silver Nanoparticle Formation: Predictions and Verification of the Aggregative Growth Model.* Langmuir, 2001. 17(11): p. 3128-3135.
224. Li, X., J.J. Lenhart, and H.W. Walker, *Aggregation Kinetics and Dissolution of Coated Silver Nanoparticles.* Langmuir, 2012. 28(2): p. 1095-1104.
225. Pfeiffer, C., et al., *Interaction of colloidal nanoparticles with their local environment: the (ionic) nanoenvironment around nanoparticles is different from bulk and determines the physico-chemical properties of the nanoparticles.* Journal of The Royal Society Interface, 2014. 11(96).
226. Baalousha, M., et al., *Effect of monovalent and divalent cations, anions and fulvic acid on aggregation of citrate-coated silver nanoparticles.* Science of the Total Environment, 2013. 454: p. 119-131.

227. Alexander, C.M., J.C. Dabrowiak, and J. Goodisman, *Gravitational sedimentation of gold nanoparticles.* Journal of Colloid and Interface Science, 2013. 396: p. 53-62.
228. Bonaccorso, F., et al., *Sorting Nanoparticles by Centrifugal Fields in Clean Media.* Journal of Physical Chemistry C, 2013. 117(25): p. 13217-13229.
229. Ostermeyer, A.K., et al., *Influence of Bovine Serum Albumin and Alginate on Silver Nanoparticle Dissolution and Toxicity to Nitrosomonas europaea.* Environmental Science & Technology, 2013. 47(24): p. 14403-14410.
230. Grimm, J., *Cancer nanomedicine: Therapy from within.* Nat Nano, 2015. 10(4): p. 299-300.
231. Hsueh, Y.-H., et al., *The Antimicrobial Properties of Silver Nanoparticles in Bacillus subtilis Are Mediated by Released Ag^+ Ions.* PLoS ONE, 2015. 10(12): p. e0144306.
232. Li, X. and J.J. Lenhart, *Aggregation and Dissolution of Silver Nanoparticles in Natural Surface Water.* Environmental Science & Technology, 2012. 46(10): p. 5378-5386.
233. Fujiwara, K., G.A. Sotiriou, and S.E. Pratsinis, *Enhanced Ag^+ Ion Release from Aqueous Nanosilver Suspensions by Absorption of Ambient CO2.* Langmuir, 2015. 31(19): p. 5284-5290.
234. Pokhrel, L.R., B. Dubey, and P.R. Scheuerman, *Impacts of Select Organic Ligands on the Colloidal Stability, Dissolution Dynamics, and Toxicity of Silver Nanoparticles.* Environmental Science & Technology, 2013. 47(22): p. 12877-12885.
235. Tejamaya, M., et al., *Stability of Citrate, PVP, and PEG Coated Silver Nanoparticles in Ecotoxicology Media.* Environmental Science & Technology, 2012. 46(13): p. 7011-7017.
236. Metreveli, G., A. Philippe, and G.E. Schaumann, *Disaggregation of silver nanoparticle homoaggregates in a river water matrix.* Science of the Total Environment, 2015. 535: p. 35-44.
237. Furtado, L.M., et al., *Environmental Fate of Silver Nanoparticles in Boreal Lake Ecosystems.* Environmental Science & Technology, 2015. 49(14): p. 8441-8450.
238. Cho, E.C., Q. Zhang, and Y.N. Xia, *The effect of sedimentation and diffusion on cellular uptake of gold nanoparticles.* Nature Nanotechnology, 2011. 6(6): p. 385-391.
239. Petersen, E.J., et al., *Adapting OECD Aquatic Toxicity Tests for Use with Manufactured Nanomaterials: Key Issues and Consensus Recommendations.* Environmental Science & Technology, 2015. 49(16): p. 9532-9547.
240. Andersen, J.B., et al., *New unstable variants of green fluorescent protein for studies of transient gene expression in bacteria.* Applied and Environmental Microbiology, 1998. 64(6): p. 2240-2246.
241. Sen, M., et al., *In vivo evolutionary engineering of a boron-resistant bacterium:*

Bacillus boroniphilus. Antonie Van Leeuwenhoek International Journal of General and Molecular Microbiology, 2011. 99(4): p. 825-835.
242. Bringmann, G. and R. Kühn, *Comparison of the toxicity thresholds of water pollutants to bacteria, algae, and protozoa in the cell multiplication inhibition test.* Water Research, 1980. 14(3): p. 231-241.
243. Andrews, J.M., *Determination of minimum inhibitory concentrations.* Journal of Antimicrobial Chemotherapy, 2001. 48(suppl 1): p. 5-16.
244. Van Hyning, D.L., W.G. Klemperer, and C.F. Zukoski, *Characterization of Colloidal Stability during Precipitation Reactions.* Langmuir, 2001. 17(11): p. 3120-3127.
245. Zhang, C., Z. Hu, and B. Deng, *Silver nanoparticles in aquatic environments: Physiochemical behavior and antimicrobial mechanisms.* Water Research, 2016. 88: p. 403-427.
246. Lv, J., et al., *Dissolution and Microstructural Transformation of ZnO Nanoparticles under the Influence of Phosphate.* Environmental Science & Technology, 2012. 46(13): p. 7215-7221.
247. Struempler, A.W., *Adsorption characteristics of silver, lead, cadmium, zinc, and nickel on borosilicate glass, polyethylene, and polypropylene container surfaces.* Analytical Chemistry, 1973. 45(13): p. 2251-2254.
248. West, F.K., P.W. West, and F.A. Iddings, *Adsorption of Traces of Silver on Container Surfaces.* Analytical Chemistry, 1966. 38(11): p. 1566-1570.
249. Sekine, R., et al., *Quantifying the adsorption of ionic silver and functionalized nanoparticles during ecotoxicity testing: Test container effects and recommendations.* Nanotoxicology, 2015. 9(8): p. 1005-1012.
250. Malysheva, A., et al., *Sorption of silver nanoparticles to laboratory plastic during (eco)toxicological testing.* Nanotoxicology, 2015: p. 1-6.
251. Udekwu, K.I., et al., *Functional relationship between bacterial cell density and the efficacy of antibiotics.* Journal of Antimicrobial Chemotherapy, 2009. 63(4): p. 745-757.
252. Abel zur Wiesch, P., et al., *Classic reaction kinetics can explain complex patterns of antibiotic action.* Science Translational Medicine, 2015. 7(287): p. 287ra73-287ra73.
253. Eckhardt, S., et al., *Nanobio Silver: Its Interactions with Peptides and Bacteria, and Its Uses in Medicine.* Chemical Reviews, 2013.
254. Lemire, J.A., J.J. Harrison, and R.J. Turner, *Antimicrobial activity of metals: mechanisms, molecular targets and applications.* Nature Reviews Microbiology, 2013. 11(6): p. 371-384.
255. Vijayaraghavan, K. and Y.-S. Yun, *Bacterial biosorbents and biosorption.* Biotechnology Advances, 2008. 26(3): p. 266-291.
256. Brauner, A., et al., *Distinguishing between resistance, tolerance and persistence to antibiotic treatment.* Nat Rev Micro, 2016. 14(5): p. 320-330.

257. Gordon, O., et al., *Silver Coordination Polymers for Prevention of Implant Infection: Thiol Interaction, Impact on Respiratory Chain Enzymes, and Hydroxyl Radical Induction.* Antimicrobial Agents and Chemotherapy, 2010. 54(10): p. 4208-4218.
258. Pradas del Real, A.E., et al., *Fate of Ag-NPs in Sewage Sludge after Application on Agricultural Soils.* Environmental Science & Technology, 2016. 50(4): p. 1759-1768.
259. Pourzahedi, L. and M.J. Eckelman, *Environmental Life Cycle Assessment of Nanosilver-Enabled Bandages.* Environmental Science & Technology, 2015. 49(1): p. 361-368.
260. Hsueh, Y.-H., et al., *The Antimicrobial Properties of Silver Nanoparticles in Bacillus subtilis Are Mediated by Released Ag^+ Ions.* PLoS ONE, 2015. 10(12): p. e0144306.
261. Stoyanov, J.V., D. Magnani, and M. Solioz, *Measurement of cytoplasmic copper, silver, and gold with a lux biosensor shows copper and silver, but not gold, efflux by the CopA ATPase of Escherichia coli.* Febs Letters, 2003. 546(2-3): p. 391-394.
262. Kang, F., P.J. Alvarez, and D. Zhu, *Microbial Extracellular Polymeric Substances Reduce Ag^+ to Silver Nanoparticles and Antagonize Bactericidal Activity.* Environmental Science & Technology, 2014. 48(1): p. 316-322.
263. Asiani, K.R., et al., *SilE is an intrinsically disordered periplasmic "molecular sponge" involved in bacterial silver resistance.* Molecular Microbiology, 2016. 101(5): p. 731-742.
264. Blount, Z.D., C.Z. Borland, and R.E. Lenski, *Historical contingency and the evolution of a key innovation in an experimental population of Escherichia coli.* Proceedings of the National Academy of Sciences, 2008. 105(23): p. 7899-7906.
265. Blair, J.M.A., et al., *Molecular mechanisms of antibiotic resistance.* Nat Rev Micro, 2015. 13(1): p. 42-51.
266. Lieberman, T.D., et al., *Parallel bacterial evolution within multiple patients identifies candidate pathogenicity genes.* Nat Genet, 2011. 43(12): p. 1275-1280.
267. Toprak, E., et al., *Evolutionary paths to antibiotic resistance under dynamically sustained drug selection.* Nat Genet, 2012. 44(1): p. 101-105.
268. Jorth, P., et al., *Regional Isolation Drives Bacterial Diversification within Cystic Fibrosis Lungs.* Cell Host & Microbe, 2015. 18(3): p. 307-319.
269. Lenski, R.E., et al., *Long-Term Experimental Evolution in Escherichia coli. I. Adaptation and Divergence During 2,000 Generations.* The American Naturalist, 1991. 138(6): p. 1315-1341.
270. Choi, L., J.D. Blume, and W.D. Dupont, *Elucidating the Foundations of Statistical Inference with 2 x 2 Tables.* PLoS ONE, 2015. 10(4): p. e0121263.
271. Belda, E., et al., *The revisited genome of Pseudomonas putida KT2440 enlightens its value as a robust metabolic chassis.* Environmental Microbiology,

2016.
272. Nelson, K.E., et al., *Complete genome sequence and comparative analysis of the metabolically versatile Pseudomonas putida KT2440.* Environmental Microbiology, 2002. 4(12): p. 799-808.
273. Rensing, C., et al., *CopA: An Escherichia coli Cu(I)-translocating P-type ATPase.* Proceedings of the National Academy of Sciences, 2000. 97(2): p. 652-656.
274. Orr, H.A., *Fitness and its role in evolutionary genetics.* Nat Rev Genet, 2009. 10(8): p. 531-539.
275. Wiser, M.J., N. Ribeck, and R.E. Lenski, *Long-Term Dynamics of Adaptation in Asexual Populations.* Science, 2013. 342(6164): p. 1364-1367.
276. Lenski, R.E., et al., *Sustained fitness gains and variability in fitness trajectories in the long-term evolution experiment with Escherichia coli.* Proceedings of the Royal Society of London B: Biological Sciences, 2015. 282(1821).
277. Wiser, M.J. and R.E. Lenski, *A Comparison of Methods to Measure Fitness in Escherichia coli.* PLoS ONE, 2015. 10(5): p. e0126210.
278. Barrick, J.E., et al., *Genome evolution and adaptation in a long-term experiment with Escherichia coli.* Nature, 2009. 461(7268): p. 1243-1247.
279. Barrick, J.E. and R.E. Lenski, *Genome dynamics during experimental evolution.* Nat Rev Genet, 2013. 14(12): p. 827-839.
280. Gullberg, E., et al., *Selection of Resistant Bacteria at Very Low Antibiotic Concentrations.* PLoS Pathog, 2011. 7(7): p. e1002158.
281. Lenski, R.E., *Phenotypic and Genomic Evolution during a 20,000-Generation Experiment with the Bacterium Escherichia coli*, in *Plant Breeding Reviews*. 2010, John Wiley & Sons, Inc. p. 225-265.
282. Weart, R.B. and P.A. Levin, *Growth Rate-Dependent Regulation of Medial FtsZ Ring Formation.* Journal of Bacteriology, 2003. 185(9): p. 2826-2834.
283. Heeb, S. and D. Haas, *Regulatory Roles of the GacS/GacA Two-Component System in Plant-Associated and Other Gram-Negative Bacteria.* Molecular Plant-Microbe Interactions, 2001. 14(12): p. 1351-1363.
284. Slauch, J.M., et al., *EnvZ functions through OmpR to control porin gene expression in Escherichia coli K-12.* Journal of Bacteriology, 1988. 170(1): p. 439-441.
285. Vollmer, W., D. Blanot, and M.A. De Pedro, *Peptidoglycan structure and architecture.* FEMS Microbiology Reviews, 2008. 32(2): p. 149-167.

7 Appendices

Appendix 1 Mutations in population in the pre-evolution experiment

Mutations in the population with the highest fitness after evolving for 465 generations in the pre-evolution experiment. Gene names and functions were obtained from the annotation in GenBank (RefSepq, NC_002947.4).

Gene name	Gene function	Mutation position	Reference	Effect	Codon change	Amino acid change
		178,396	A	Intergenic		
PP_0168	Putative surface adhesion protein	195,505	C	Synonymous	gcC/gcG	A337
PP_0168	Putative surface adhesion protein	195,559	C	Synonymous	acC/acA	T355
PP_0168	Putative surface adhesion protein	195,634	C	Synonymous	acC/acT	T380
PP_0168	Putative surface adhesion protein	196,459	C	Synonymous	acC/acA	T655
PP_0168	Putative surface adhesion protein	196,489	T	Synonymous	aaT/aaC	N665
PP_0168	Putative surface adhesion protein	196,672	G	Synonymous	aaG/aaA	K726
PP_0168	Putative surface adhesion protein	196,795	G	Synonymous	acG/acC	T767
PP_0168	Putative surface adhesion protein	196,927	A	Synonymous	acA/acC	T811
PP_0168	Putative surface adhesion protein	197,128	T	Synonymous	gaT/gaC	D878
PP_0168	Putative surface adhesion protein	197,572	G	Synonymous	aaG/aaA	K1026
PP_0168	Putative surface adhesion protein	197,590	T	Synonymous	gaT/gaC	D1032
PP_0168	Putative surface adhesion protein	197,632	T	Synonymous	acT/acC	T1046
PP_0168	Putative surface adhesion protein	197,695	G	Synonymous	acG/acC	T1067
gacS	Sensor protein GacS	1,843,901	C	Non Synonymous	cGc/cAc	R298H
		2,069,557	T	Intergenic		
		4,022,306	G	Intergenic		
		4,022,307	G	Intergenic		
fleQ	Transcriptional regulator Fleq	4,964,454	C	Non Synonymous	Gac/Aac	D302N
flgK	Flagellar hook-associated protein Flgk	4,974,437	CAG	Frame Shift	ctg/	L389
PP_4920	Lipoprotein	5,592,669	G	Synonymous	acG/acA	T205

Gene name	Gene function	Mutation position	Reference	Effect	Codon change	Amino acid change
		5,988,889	C	Intergenic		
		5,988,905	T	Intergenic		
		5,988,910	CA	Intergenic		

Appendix 2 Mutations in populations in main evolution experiment

List of mutations in the 15 populations after evolving for 500 generations in the main evolution experiment. The reads of the evolved populations were aligned with the *Pseudomonas putida* KT2440 reference genome (RefSepq, NC_002947.4, GenBank) and variants called as described in section 4.2.7. Gene names were obtained from the annotation of the reference genome. REF represents the reference genome. ALT represents the mutation. There were three types of population, evolved under different conditions: control (populations evolved without Ag stress); Ag^+ population (evolved in the presence of Ag^+); AgNP population (evolved in the presence of AgNPs). Mutations were only called when they passed quality thresholds: 0 refers to no mutation; 1 refers to mutation. Under each condition (control, Ag^+ treatment and AgNP treatment), there were five parallel population (C1-5). A modified Fisher's exact test was used to calculate the mid-p-values for association of mutation with treatment (see section 4.2.8). The cells with p-values smaller than 0.05 are highlighted in red.

Gene name	Mutation position	REF	ALT	Effect	Mutation call															Total number of parallel mutations			p-values for association		
					Control					Ag^+ population					AgNP population										
					C1	C2	C3	C4	C5	C1	C2	C3	C4	C5	C1	C2	C3	C4	C5	Control	Ag^+	AgNP	Ag^+ vs Control	AgNP vs Control	AgNP vs Ag^+
	172,966	A	G	Intergenic	1	1	1	1	1	1	1	1	1	0	0	1	1	1	1	5	4	4	0.50	0.5	1
	173,074	A	G	Intergenic	0	0	0	0	0	1	0	0	0	0	1	1	1	1	0	0	1	4	0.5	0.024	0.1071
	178,396	A	G	Intergenic	1	1	1	0	0	1	1	1	1	0	1	0	0	1	0	3	4	2	0.58	0.603	0.2857
	178,437	C	T	Intergenic	1	1	1	1	1	1	1	1	1	0	1	1	0	1	0	5	4	3	0.5	0.222	0.5833
	178,504	A	G	Intergenic	1	0	0	0	0	0	0	1	1	0	1	1	1	1	1	1	2	5	0.58	0.024	0.08333
PP_0168	195,406	C	T	Synonymous	0	0	0	0	1	0	0	0	0	0	0	1	0	1	0	1	0	2	0.5	0.583	0.2222
PP_0168	195,424	G	A	Synonymous	0	1	1	0	1	1	0	0	1	0	1	0	1	1	0	3	2	3	0.6	1	0.6032
PP_0168	195,449	G	A	Nonsynonymous	0	0	0	0	0	1	0	0	0	0	0	0	1	0	0	0	1	1	0.5	0.5	1
PP_0168	19,450	T	C	Nonsynonymous	0	0	0	0	0	1	0	1	0	1	0	0	0	0	0	0	3	0	0.08	1	0.08333
PP_0168	195,457	T	C	Synonymous	0	0	0	0	1	1	0	0	0	0	0	0	0	0	0	1	1	0	1	0.5	0.5
PP_0168	195,472	A	G	Synonymous	0	1	1	0	0	0	0	0	0	0	0	0	0	0	0	2	0	0	0.22	0.222	1
PP_0168	195,505	C	G	Synonymous	1	0	1	1	1	1	0	0	1	1	1	0	1	1	1	4	3	4	0.58	1	0.5833

Gene name	Mutation position	REF	ALT	Effect	Mutation call															Total number of parallel mutations			p-values for association		
					Control					Ag^+ population					AgNP population										
					C1	C2	C3	C4	C5	C1	C2	C3	C4	C5	C1	C2	C3	C4	C5	Control	Ag^+	AgNP	Ag^+ vs Control	AgNP vs Control	AgNP vs Ag^+
PP_0168	195,559	C	A	Synonymous	1	1	1	1	1	1	1	1	1	1	1	0	1	0	1	5	5	3	1	0.222	0.2222
PP_0168	195,568	T	C	Synonymous	0	0	0	0	0	0	0	0	1	0	0	0	0	0	0	0	1	0	0.5	1	0.5
PP_0168	195,589	T	C	Synonymous	0	0	1	0	1	0	1	1	1	1	1	1	1	1	1	2	4	5	0.29	0.083	1
PP_0168	195,628	C	T	Synonymous	1	1	1	1	1	1	0	1	0	0	0	1	0	1	0	5	2	2	0.08	0.083	1
PP_0168	195,629	A	G	Nonsynonymous	1	1	1	1	1	1	0	1	0	1	0	1	0	1	0	5	3	2	0.22	0.083	0.6032
PP_0168	195,634	C	T	Synonymous	1	1	1	1	1	1	1	1	1	1	1	0	1	1	1	5	5	4	1	0.5	0.5
PP_0168	195,685	T	C	Synonymous	1	0	1	0	0	0	1	1	1	1	1	1	0	1	1	2	4	4	0.29	0.286	1
PP_0168	195,724	A	G	Synonymous	0	0	0	0	0	1	0	1	0	0	1	0	0	0	0	0	2	1	0.22	0.5	0.5833
PP_0168	195,732	A	C	Nonsynonymous	1	1	1	0	1	0	1	1	1	1	1	1	1	1	1	4	4	5	1	1	1
PP_0168	195,766	G	C	Synonymous	0	1	0	0	0	1	0	0	0	0	0	0	0	0	1	1	1	1	1	1	1
PP_0168	195,769	T	C	Synonymous	0	1	1	0	1	1	0	0	0	0	0	0	1	0	1	3	1	2	0.29	0.603	0.5833
PP_0168	195,805	C	G	Synonymous	0	1	0	0	0	0	0	0	0	0	0	0	0	0	0	1	0	0	0.5	0.5	1
PP_0168	195,826	C	T	Synonymous	0	0	0	0	1	0	0	0	1	0	0	0	0	0	1	1	1	1	1	1	1
PP_0168	195,852	G	A	Nonsynonymous	0	1	1	1	1	1	0	0	0	0	0	1	0	0	0	4	1	1	0.11	0.107	1
PP_0168	195,877	G	A	Synonymous	0	0	0	1	0	0	0	0	0	0	0	0	0	0	0	1	0	0	0.5	0.5	1
PP_0168	195,929	A	G	Nonsynonymous	0	0	1	0	0	0	0	0	0	0	0	0	0	0	0	1	0	0	0.5	0.5	1
PP_0168	195,934	C	T	Synonymous	0	0	0	0	0	0	0	0	0	0	0	0	0	0	1	0	0	1	1	0.5	0.5
PP_0168	195,979	G	A	Synonymous	0	0	0	0	0	0	0	1	0	0	0	0	0	0	0	0	1	0	0.5	1	0.5
PP_0168	195,985	C	T	Synonymous	0	0	0	0	0	0	0	0	0	0	0	0	0	0	1	0	0	1	1	0.5	0.5
PP_0168	196,027	T	C	Synonymous	1	1	1	0	0	1	0	1	1	1	1	1	1	1	1	3	4	5	0.58	0.222	1
PP_0168	196,051	G	C	Synonymous	0	1	0	0	0	0	0	0	0	0	0	0	0	0	0	1	0	0	0.5	0.5	1
PP_0168	196,066	G	C	Synonymous	0	0	0	0	0	0	0	0	0	0	1	1	0	0	0	0	0	2	1	0.222	0.2222
PP_0168	196,069	T	C	Synonymous	0	0	1	0	0	0	0	0	1	0	0	1	0	0	0	1	1	1	1	1	1
PP_0168	196,132	G	C	Synonymous	0	0	1	0	1	1	1	0	1	1	1	1	1	1	1	2	4	5	0.29	0.083	1
PP_0168	196,159	G	A	Synonymous	1	0	1	0	1	1	0	0	1	1	0	0	1	1	1	3	3	3	1	1	1

Gene name	Mutation position	REF	ALT	Effect	Mutation call															Total number of parallel mutations			p-values for association		
					Control					Ag^+ population					AgNP population										
					C1	C2	C3	C4	C5	C1	C2	C3	C4	C5	C1	C2	C3	C4	C5	Control	Ag^+	AgNP	Ag^+ vs Control	AgNP vs Control	AgNP vs Ag^+
PP_0168	196,195	G	C	Synonymous	1	0	1	0	0	0	1	0	0	0	0	0	0	1	1	2	1	2	0.58	1	0.5833
PP_0168	196,234	T	C	Synonymous	1	0	1	1	1	1	1	1	1	0	1	1	1	1	1	4	4	5	1	1	1
PP_0168	196,285	T	C	Synonymous	1	0	0	0	1	1	1	1	1	0	0	1	0	1	1	2	4	3	0.29	0.603	0.5833
PP_0168	196,306	T	C	Synonymous	1	1	1	1	1	1	1	1	0	1	1	1	1	1	1	5	4	5	0.5	1	1
PP_0168	196,324	G	A	Synonymous	0	0	0	0	0	0	0	0	0	0	0	1	0	1	1	0	0	3	1	0.083	0.08333
PP_0168	196,327	A	C	Synonymous	1	1	1	1	1	1	1	1	1	0	1	1	1	1	1	5	4	5	0.5	1	1
PP_0168	196,351	C	G	Synonymous	1	1	1	1	1	1	1	1	0	1	1	1	1	1	1	5	4	5	0.5	1	1
PP_0168	196,366	C	G	Synonymous	0	0	0	0	0	0	0	0	0	0	0	1	0	0	0	0	0	1	1	0.5	0.5
PP_0168	196,369	C	T	Synonymous	0	0	0	0	0	0	0	0	0	0	0	1	0	0	0	0	0	1	1	0.5	0.5
PP_0168	196,372	A	G	Synonymous	1	1	1	1	1	1	1	1	1	1	1	1	1	1	1	5	5	5	1	1	1
PP_0168	196,390	T	C	Synonymous	1	1	1	0	1	0	1	1	0	1	1	0	1	1	1	4	3	4	0.58	1	0.5833
PP_0168	196,405	G	C	Synonymous	0	0	0	0	0	0	0	0	0	0	0	0	0	1	0	0	0	1	1	0.5	0.5
PP_0168	196,432	T	C	Synonymous	0	1	0	1	0	0	0	0	0	0	0	0	0	0	1	2	0	1	0.22	0.583	0.5
PP_0168	196,459	C	A	Synonymous	0	1	0	1	1	1	1	1	0	1	1	1	1	1	1	3	4	5	0.58	0.222	1
PP_0168	196,489	T	C	Synonymous	1	1	1	0	1	1	1	1	1	0	1	1	1	1	1	4	4	5	1	1	1
PP_0168	196,495	G	C	Synonymous	1	1	1	1	1	1	1	1	1	0	1	1	1	1	1	5	4	5	0.5	1	1
PP_0168	196,528	T	C	Synonymous	0	0	0	0	0	0	0	0	0	0	0	1	0	0	0	0	0	1	1	0.5	0.5
PP_0168	196,579	G	A	Synonymous	1	1	1	1	1	1	1	1	1	1	1	1	1	1	1	5	5	5	1	1	1
PP_0168	196,585	C	T	Synonymous	0	0	1	1	0	1	1	0	1	0	0	0	1	0	0	2	3	1	0.6	0.583	0.2857
PP_0168	196,606	T	C	Synonymous	0	0	0	1	0	0	0	0	1	0	0	0	0	0	0	1	1	0	1	0.5	0.5
PP_0168	196,624	G	A	Synonymous	0	0	0	1	1	0	0	0	1	0	0	0	0	0	0	2	1	0	0.58	0.222	0.5
PP_0168	196,627	A	C	Synonymous	1	1	1	1	1	1	1	1	1	1	0	1	1	1	1	5	5	4	1	0.5	0.5
PP_0168	196,672	G	A	Synonymous	1	0	0	0	1	0	1	0	0	0	1	0	0	0	0	2	1	1	0.58	0.583	1
PP_0168	196,705	G	C	Synonymous	1	1	1	0	0	0	1	1	0	0	0	0	0	1	1	3	2	2	0.6	0.603	1
PP_0168	196,752	A	G	Nonsynonymous	0	0	0	0	0	0	0	0	0	1	0	0	0	0	0	0	1	0	0.5	1	0.5

Gene name	Mutation position	REF	ALT	Effect	Mutation call															Total number of parallel mutations			p-values for association		
					Control					Ag^+ population					AgNP population										
					C1	C2	C3	C4	C5	C1	C2	C3	C4	C5	C1	C2	C3	C4	C5	Control	Ag^+	AgNP	Ag^+ vs Control	AgNP vs Control	AgNP vs Ag^+
PP_0168	196,759	T	C, A	Synonymous	1	1	1	0	1	1	1	1	0	1	1	1	0	1	1	4	4	4	1	1	1
PP_0168	196,795	G	C	Synonymous	0	0	0	0	1	0	0	1	0	0	0	1	0	0	0	1	1	1	1	1	1
PP_0168	196,828	T	C	Synonymous	0	1	0	0	0	0	0	0	0	0	0	1	0	0	0	1	0	1	0.5	1	0.5
PP_0168	196,829	G	A	Nonsynonymous	0	1	0	0	0	0	0	0	0	0	0	0	0	0	0	1	0	0	0.5	0.5	1
PP_0168	196,885	C	T	Synonymous	1	1	1	1	0	0	1	1	1	1	1	1	1	0	0	4	4	3	1	0.583	0.5833
PP_0168	196,906	T	C	Synonymous	0	0	1	0	0	0	0	0	0	0	0	0	0	0	0	1	0	0	0.5	0.5	1
PP_0168	196,924	G	A	Synonymous	0	0	0	1	0	0	0	0	0	0	0	0	0	0	0	1	0	0	0.5	0.5	1
PP_0168	196,927	A	C	Synonymous	1	1	1	1	1	1	1	1	1	0	1	1	1	1	1	5	4	5	0.5	1	1
PP_0168	196,972	G	A	Synonymous	1	1	1	1	1	1	1	0	1	0	1	1	1	1	0	5	3	4	0.22	0.5	0.5833
PP_0168	197,128	T	C	Synonymous	0	0	0	0	0	0	0	0	0	0	1	1	0	0	0	0	0	2	1	0.222	0.2222
PP_0168	197,129	G	A	Nonsynonymous	0	0	0	0	0	0	0	0	0	0	1	1	0	0	0	0	0	2	1	0.222	0.2222
PP_0168	197,179	A	G	Synonymous	1	1	1	1	0	1	1	1	1	1	1	1	1	1	1	4	5	5	1	1	1
PP_0168	197,185	C	T	Synonymous																0	0	0	1	1	1
PP_0168	197,206	T	C	Synonymous	0	0	0	0	0	0	0	0	1	0	0	0	0	0	0	0	1	0	0.5	1	0.5
PP_0168	197,224	A	G	Synonymous	1	0	0	0	0	1	0	1	1	1	1	0	0	0	1	1	4	2	0.11	0.583	0.2857
PP_0168	197,227	C	A	Synonymous	0	0	0	0	0	0	0	0	0	0	0	0	0	0	1	0	0	1	1	0.5	0.5
PP_0168	197,250	T	C	Nonsynonymous	0	0	0	0	1	0	0	0	0	0	0	0	0	0	0	1	0	0	0.5	0.5	1
PP_0168	197,257	T	C	Synonymous	1	0	0	0	0	0	0	0	0	1	1	0	0	0	0	1	1	1	1	1	1
PP_0168	197,326	T	C	Synonymous	0	0	0	0	0	0	0	0	0	1	0	0	0	0	0	0	1	0	0.5	1	0.5
PP_0168	197,395	G	C	Synonymous	0	0	1	0	0	1	0	0	0	0	0	0	0	0	0	1	1	0	1	0.5	0.5
PP_0168	197,479	G	A	Synonymous	0	1	1	0	0	0	0	0	0	0	0	0	0	0	0	2	0	0	0.22	0.222	1
PP_0168	197,496	T	C	Nonsynonymous	0	1	1	1	1	1	1	1	1	1	1	1	0	1	1	4	5	4	1	1	0.5
PP_0168	197,524	A	G	Synonymous	0	0	0	1	0	0	0	0	0	1	0	0	0	0	0	1	1	0	1	0.5	0.5
PP_0168	197,551	C	G	Synonymous	0	0	0	0	0	0	0	0	1	0	0	0	0	1	0	0	1	1	0.5	0.5	1

Gene name	Mutation position	REF	ALT	Effect	Mutation call															Total number of parallel mutations			p-values for association		
					Control					Ag^+ population					AgNP population										
					C1	C2	C3	C4	C5	C1	C2	C3	C4	C5	C1	C2	C3	C4	C5	Control	Ag^+	AgNP	Ag^+ vs Control	AgNP vs Control	AgNP vs Ag^+
PP_0168	197,572	G	A	Synonymous	1	1	0	1	1	1	1	1	1	1	1	1	1	1	0	4	5	4	1	1	0.5
PP_0168	197,590	T	C	Synonymous	1	0	0	1	1	1	1	1	1	1	1	1	0	1	0	3	5	3	0.22	1	0.2222
PP_0168	197,605	G	C	Synonymous	0	0	0	0	0	0	0	1	0	0	0	0	0	0	0	0	1	0	0.5	1	0.5
PP_0168	197,632	T	C	Synonymous	1	1	1	1	1	1	1	1	1	1	1	1	1	1	1	5	5	5	1	1	1
PP_0168	197,665	T	C	Synonymous	0	0	0	0	0	0	0	1	0	0	0	0	0	0	0	0	1	0	0.5	1	0.5
PP_0168	197,689	C	T	Synonymous	1	0	0	0	0	0	0	0	0	0	0	0	0	0	0	1	0	0	0.5	0.5	1
PP_0168	197,695	G	C	Synonymous	1	1	1	0	0	0	1	0	1	0	1	1	0	1	1	3	2	4	0.6	0.583	0.2857
PP_0168	197,715	C	A	Nonsynonymous	1	1	0	0	0	0	1	0	0	0	0	1	0	1	0	2	1	2	0.58	1	0.5833
PP_0168	197,834	T	C	Synonymous	1	1	1	1	1	1	1	1	0	0	1	1	1	1	1	5	3	5	0.22	1	0.2222
PP_0168	197,866	G	C	Synonymous	0	1	1	1	0	0	0	0	0	1	1	0	1	0	1	3	1	3	0.29	1	0.2857
PP_0168	197,869	T	C	Synonymous	0	1	1	1	0	1	1	0	0	1	1	1	1	0	0	3	3	3	1	1	1
PP_0168	197,872	A	G	Synonymous	0	0	0	0	0	0	0	0	0	0	0	1	0	0	0	0	0	1	1	0.5	0.5
PP_0168	197,926	C	T	Synonymous	0	0	0	1	0	0	0	0	0	1	0	0	0	0	0	1	1	0	1	0.5	0.5
PP_0168	198,400	C	G	Synonymous	0	0	0	1	0	0	0	0	0	0	0	0	0	0	0	1	0	0	0.5	0.5	1
PP_0168	199,318	T	G	Synonymous	0	0	0	1	0	1	0	0	0	0	0	0	0	0	0	1	1	0	1	0.5	0.5
PP_0168	199,480	T	C	Synonymous	0	0	0	0	0	0	0	0	0	0	1	0	0	0	0	0	0	1	1	0.5	0.5
PP_0168	199,550	T	C	Synonymous	0	0	0	0	0	0	0	0	0	0	1	0	0	0	1	0	0	2	1	0.222	0.2222
PP_0168	199,744	T	C	Synonymous	0	0	0	0	0	0	0	0	0	0	0	0	1	0	0	0	0	1	1	0.5	0.5
PP_0168	199,822	G	C	Synonymous	1	0	0	0	0	0	0	0	0	0	0	0	0	0	0	1	0	0	0.5	0.5	1
PP_0168	200,113	T	C	Synonymous	0	0	0	0	0	1	1	0	0	0	0	0	0	0	1	0	2	1	0.22	0.5	0.5833
PP_0168	200,164	T	C	Synonymous	0	0	1	1	0	0	0	0	0	0	0	0	0	0	1	2	0	1	0.22	0.583	0.5
PP_0168	200,338	G	C	Synonymous	0	0	0	0	0	0	0	0	0	1	0	0	0	0	0	0	1	0	0.5	1	0.5
PP_0168	200,473	T	C	Synonymous	0	0	1	0	0	0	1	0	1	0	0	0	0	0	0	1	2	0	0.58	0.5	0.2222
PP_0168	201,007	T	C	Synonymous	0	0	0	0	0	0	0	0	0	0	0	0	0	1	0	0	0	1	1	0.5	0.5
PP_0168	201,043	T	C	Synonymous	0	0	0	1	0	0	0	0	0	0	0	0	0	0	1	1	0	1	0.5	1	0.5

Gene name	Mutation position	REF	ALT	Effect	Mutation call															Total number of parallel mutations			p-values for association		
					Control					Ag^+ population					AgNP population										
					C1	C2	C3	C4	C5	C1	C2	C3	C4	C5	C1	C2	C3	C4	C5	Control	Ag^+	AgNP	Ag^+ vs Control	AgNP vs Control	AgNP vs Ag^+
PP_0168	201,100	T	C	Synonymous	0	0	0	0	0	0	0	0	0	0	0	1	0	0	0	0	0	1	1	0.5	0.5
PP_0168	201,175	T	C	Synonymous	1	0	1	0	0	0	0	0	0	0	0	0	0	0	0	2	0	0	0.22	0.222	1
PP_0168	201,622	C	G	Synonymous	0	0	0	0	0	0	0	0	0	0	0	1	0	0	0	0	0	1	1	0.5	0.5
PP_0168	201,652	G	C	Synonymous	0	0	0	0	0	0	0	0	0	0	0	1	0	0	1	0	0	2	1	0.222	0.2222
PP_0168	201,685	G	C	Synonymous	0	0	0	1	0	0	0	0	0	0	1	0	1	0	0	1	0	2	0.5	0.583	0.2222
PP_0168	201,715	T	C	Synonymous	0	0	0	0	0	1	0	0	0	0	0	0	0	0	0	0	1	0	0.5	1	0.5
PP_0168	201,798	T	C	Nonsynonymous	0	0	0	0	0	0	0	0	0	0	0	1	0	0	0	0	0	1	1	0.5	0.5
PP_0168	201,859	G	C	Synonymous	0	0	0	0	0	0	0	0	1	0	0	1	0	1	0	0	1	2	0.5	0.222	0.5833
PP_0168	201,997	T	C	Synonymous	0	0	0	0	0	0	0	0	0	0	0	1	0	0	0	0	0	1	1	0.5	0.5
PP_0168	202,111	G	A	Synonymous	0	1	0	0	0	0	0	0	0	0	0	0	0	0	0	1	0	0	0.5	0.5	1
PP_0168	202,117	T	C	Synonymous	0	1	0	0	0	0	0	0	0	0	0	0	0	0	0	1	0	0	0.5	0.5	1
PP_0168	202,321	T	C	Synonymous	0	0	1	0	0	0	0	0	0	0	0	0	0	0	0	1	0	0	0.5	0.5	1
PP_0168	203,227	C	G	Synonymous	0	0	0	0	0	1	0	0	0	0	0	0	0	0	0	0	1	0	0.5	1	0.5
PP_0168	203,422	T	C	Synonymous	0	0	0	0	1	0	0	0	1	1	0	0	1	0	0	1	2	1	0.58	1	0.5833
PP_0168	203,647	T	C	Synonymous	0	0	1	0	0	0	0	0	0	0	0	0	0	0	0	1	0	0	0.5	0.5	1
PP_0168	203,674	T	C	Synonymous	0	1	0	0	0	0	0	0	0	0	1	0	0	0	0	1	0	1	0.5	1	0.5
PP_0168	204,180	A	C	Nonsynonymous	0	0	0	0	0	0	0	0	0	0	0	1	0	0	0	0	0	1	1	0.5	0.5
PP_0168	204,532	T	C	Synonymous	0	0	1	0	0	0	0	0	0	0	0	0	0	0	0	1	0	0	0.5	0.5	1
PP_0168	205,120	A	T	Synonymous	0	0	0	0	0	0	0	0	0	0	0	0	1	0	0	0	0	1	1	0.5	0.5
PP_0168	205,327	C	G	Synonymous	0	0	1	0	0	0	0	0	0	0	0	1	0	0	0	1	0	1	0.5	1	0.5
PP_0168	205,672	T	C	Synonymous	0	1	0	0	0	0	0	0	0	0	0	0	0	0	0	1	0	0	0.5	0.5	1
PP_0168	205,789	C	T	Synonymous	0	1	0	0	0	0	0	0	0	0	0	0	0	0	0	1	0	0	0.5	0.5	1
PP_0168	205,912	G	C	Synonymous	0	0	1	0	0	0	0	0	0	0	0	0	0	0	0	1	0	0	0.5	0.5	1
PP_0168	206,143	A	G	Synonymous	0	1	0	0	0	0	0	0	0	0	0	0	0	0	1	1	0	1	0.5	1	0.5
PP_0168	206,311	G	C	Synonymous	0	0	0	0	0	0	0	0	0	0	0	1	0	0	0	0	0	1	1	0.5	0.5

Gene name	Mutation position	REF	ALT	Effect	Mutation call															Total number of parallel mutations			p-values for association		
					Control					Ag^+ population					AgNP population										
					C1	C2	C3	C4	C5	C1	C2	C3	C4	C5	C1	C2	C3	C4	C5	Control	Ag^+	AgNP	Ag^+ vs Control	AgNP vs Control	AgNP vs Ag^+
PP_0168	206,440	T	C	Synonymous	1	0	0	0	0	0	0	0	0	0	0	0	0	0	0	1	0	0	0.5	0.5	1
PP_0168	206,461	G	C	Synonymous	0	1	0	0	1	0	0	0	0	0	0	0	1	0	0	2	0	1	0.22	0.583	0.5
PP_0168	206,830	T	C	Synonymous	0	0	0	0	0	0	0	0	0	0	0	0	0	1	0	0	0	1	1	0.5	0.5
PP_0168	206,966	T	C	Synonymous	0	0	0	0	1	0	0	0	0	0	0	0	0	0	1	1	0	1	0.5	1	0.5
PP_0168	207,133	T	C	Synonymous	0	0	0	0	1	0	0	0	0	0	1	1	0	0	1	1	0	3	0.5	0.286	0.08333
PP_0168	207,136	C	G	Synonymous	0	0	0	0	0	0	0	0	0	0	0	1	0	0	0	0	0	1	1	0.5	0.5
PP_0168	207,235	G	A	Synonymous	0	0	1	0	0	0	0	0	0	0	0	1	0	0	0	1	0	1	0.5	1	0.5
PP_0168	207,370	G	T	Synonymous	0	1	0	0	0	0	0	0	0	0	0	0	0	0	0	1	0	0	0.5	0.5	1
PP_0168	207,796	G	C	Synonymous	1	0	0	0	0	0	0	0	0	0	0	0	0	0	0	1	0	0	0.5	0.5	1
PP_0168	208,015	A	G	Synonymous	0	0	1	0	0	0	0	0	0	0	0	0	0	0	0	1	0	0	0.5	0.5	1
PP_0168	208,027	T	C	Synonymous	0	0	1	0	0	0	0	0	0	0	0	0	0	0	0	1	0	0	0.5	0.5	1
PP_0168	208,030	T	G	Synonymous	0	0	1	0	0	0	0	0	0	0	0	0	0	0	0	1	0	0	0.5	0.5	1
PP_0168	208,150	T	C	Synonymous	0	0	1	1	0	0	0	0	0	0	0	0	0	1	0	2	0	1	0.22	0.583	0.5
PP_0168	208,399	T	C	Synonymous	0	0	0	0	0	0	0	0	0	0	0	0	1	0	0	0	0	1	1	0.5	0.5
PP_0168	208,456	C	G	Synonymous	0	0	1	0	0	0	0	0	0	0	0	0	0	0	0	1	0	0	0.5	0.5	1
PP_0168	208,564	A	G	Synonymous	0	0	0	0	0	1	0	0	0	0	0	0	0	0	0	0	1	0	0.5	1	0.5
PP_0168	208,675	G	A	Synonymous	0	0	1	0	0	0	0	0	0	0	0	0	0	0	0	1	0	0	0.5	0.5	1
PP_0168	209,404	T	C	Synonymous	0	1	0	0	0	1	0	0	0	0	0	0	0	0	1	1	1	1	1	1	1
PP_0168	209,638	T	C	Synonymous	0	0	0	0	0	1	0	0	0	0	0	0	0	0	0	0	1	0	0.5	1	0.5
PP_0168	209,782	T	C	Synonymous	0	0	0	0	0	0	0	0	1	0	0	0	0	0	0	0	1	0	0.5	1	0.5
PP_0168	209,942	T	C	Synonymous	0	0	0	1	0	0	0	0	0	0	0	0	0	0	0	1	0	0	0.5	0.5	1
PP_0168	210,088	A	G	Synonymous	0	0	0	0	1	0	0	0	0	0	0	0	0	0	0	1	0	0	0.5	0.5	1
PP_0168	210,121	T	C	Synonymous	0	0	0	0	0	0	0	0	0	0	0	0	0	0	1	0	0	1	1	0.5	0.5
PP_0168	210,271	T	C	Synonymous	0	1	0	0	0	0	0	0	0	0	0	0	0	0	0	1	0	0	0.5	0.5	1
PP_0168	210,691	T	C	Synonymous	0	0	0	0	0	0	0	0	0	0	0	0	1	0	0	0	0	1	1	0.5	0.5

Gene name	Mutation position	REF	ALT	Effect	Mutation call															Total number of parallel mutations			p-values for association		
					Control					Ag^+ population					AgNP population										
					C1	C2	C3	C4	C5	C1	C2	C3	C4	C5	C1	C2	C3	C4	C5	Control	Ag^+	AgNP	Ag^+ vs Control	AgNP vs Control	AgNP vs Ag^+
PP_0168	210,721	T	C	Synonymous	1	0	1	0	0	0	0	0	0	0	0	0	1	0	0	2	0	1	0.22	0.583	0.5
PP_0168	211,417	T	C	Synonymous	0	0	0	1	0	0	0	0	0	0	0	0	0	0	0	1	0	0	0.5	0.5	1
PP_0168	211,669	T	C	Synonymous	0	0	0	0	0	0	0	0	0	0	0	1	0	0	0	0	0	1	1	0.5	0.5
PP_0168	212,026	T	C	Synonymous	0	0	0	0	0	1	0	0	0	0	0	0	0	0	0	0	1	0	0.5	1	0.5
PP_0168	212,056	T	C	Synonymous	1	0	0	0	0	0	0	0	0	0	0	0	0	0	0	1	0	0	0.5	0.5	1
PP_0168	212,080	T	C	Synonymous	0	0	0	0	0	1	0	0	0	0	0	0	1	0	0	0	1	1	0.5	0.5	1
PP_0168	212,134	T	C	Synonymous	0	0	0	0	0	0	0	0	0	0	0	0	0	0	1	0	0	1	1	0.5	0.5
PP_0168	212,302	T	C	Synonymous	0	0	0	0	0	0	0	0	1	0	0	0	0	0	0	0	1	0	0.5	1	0.5
PP_0168	212,311	T	C	Synonymous	0	0	0	0	0	0	0	0	0	1	0	0	0	0	0	0	1	0	0.5	1	0.5
PP_0168	212,581	G	A	Synonymous	0	0	0	0	0	0	0	0	0	0	0	1	0	0	0	0	0	1	1	0.5	0.5
PP_0168	212,617	C	G	Synonymous	0	0	0	0	0	0	0	0	0	0	0	1	0	0	0	0	0	1	1	0.5	0.5
PP_0168	212,861	G	C	Nonsynonymous	0	0	1	0	0	0	0	0	0	0	0	0	0	0	0	1	0	0	0.5	0.5	1
PP_0168	212,941	C	G	Synonymous	0	0	0	0	0	1	0	0	0	0	0	0	0	0	0	0	1	0	0.5	1	0.5
PP_0168	213,028	G	C	Synonymous	0	0	0	0	0	0	0	0	0	0	0	0	0	0	1	0	0	1	1	0.5	0.5
PP_0168	213,415	A	G	Synonymous	0	0	0	0	0	0	0	0	0	0	0	1	0	0	0	0	0	1	1	0.5	0.5
PP_0168	213,619	T	C	Synonymous	0	0	0	0	1	0	0	0	0	0	0	0	0	0	0	1	0	0	0.5	0.5	1
PP_0168	213,874	T	G	Synonymous	0	0	0	0	0	1	0	0	0	0	0	0	1	0	0	0	1	1	0.5	0.5	1
PP_0168	213,918	C	T	Nonsynonymous	0	0	0	0	0	0	0	0	0	0	0	0	1	0	0	0	0	1	1	0.5	0.5
PP_0168	214,699	T	C	Synonymous	0	0	0	0	0	0	0	0	0	0	0	0	0	0	1	0	0	1	1	0.5	0.5
PP_0168	214,777	G	T	Synonymous	0	0	0	1	0	0	0	0	0	0	0	0	0	0	0	1	0	0	0.5	0.5	1
PP_0168	215,035	T	C	Synonymous	0	0	0	0	1	0	0	0	0	0	0	0	0	0	1	1	0	1	0.5	1	0.5
PP_0168	215,047	C	T	Synonymous	0	0	0	1	0	0	0	0	0	0	0	0	0	0	0	1	0	0	0.5	0.5	1
PP_0168	215,077	T	C	Synonymous	0	0	0	0	0	0	0	0	0	0	0	0	0	0	1	0	0	1	1	0.5	0.5
PP_0168	215,383	A	G	Synonymous	0	0	0	0	1	0	0	0	0	0	0	1	1	0	0	1	0	2	0.5	0.583	0.2222
PP_0168	215,897	C	T	Synonymous	0	0	0	0	0	0	0	0	0	0	0	0	0	0	1	0	0	1	1	0.5	0.5

Gene name	Mutation position	REF	ALT	Effect	Mutation call																Total number of parallel mutations			p-values for association		
					Control					Ag^+ population					AgNP population											
					C1	C2	C3	C4	C5	C1	C2	C3	C4	C5	C1	C2	C3	C4	C5	Control	Ag^+	AgNP	Ag^+ vs Control	AgNP vs Control	AgNP vs Ag^+
PP_0168	215,929	T	C	Synonymous	1	0	0	0	0	0	0	0	0	0	0	0	0	0	0	1	0	0	0.5	0.5	1
PP_0168	215,950	A	G	Synonymous	0	0	0	1	0	0	0	0	0	0	0	0	0	0	0	1	0	0	0.5	0.5	1
PP_0168	215,962	T	C	Synonymous	0	0	1	0	0	0	0	0	0	0	0	0	0	0	0	1	0	0	0.5	0.5	1
PP_0168	216,016	T	C	Synonymous	0	0	0	0	0	0	0	0	1	0	0	0	0	0	0	0	1	0	0.5	1	0.5
PP_0168	216,085	T	C	Synonymous	0	0	1	0	0	0	0	0	0	0	0	0	0	0	0	1	0	0	0.5	0.5	1
PP_0168	216,334	T	C	Synonymous	0	0	0	0	0	1	0	0	0	0	0	0	0	0	0	0	1	0	0.5	1	0.5
PP_0168	216,499	A	G	Synonymous	0	0	0	0	0	0	0	0	0	0	0	0	1	0	0	0	0	1	1	0.5	0.5
PP_0168	216,715	G	A	Synonymous	0	1	0	0	0	0	0	0	0	0	0	0	0	0	0	1	0	0	0.5	0.5	1
PP_0174	226,226	T	A	Nonsynonymous	0	0	0	0	0	0	0	0	1	0	0	0	0	0	0	0	1	0	0.5	1	0.5
	235,390	G	A	Intergenic	0	0	0	1	0	0	0	0	0	0	0	0	0	0	0	1	0	0	0.5	0.5	1
PP_0188	204,531	G	C	Nonsynonymous	1	0	0	0	0	0	0	0	0	0	0	0	0	0	0	1	0	0	0.5	0.5	1
PP_0188	240,536	G	C	Synonymous	1	0	0	0	0	0	0	0	0	0	0	0	0	0	0	1	0	0	0.5	0.5	1
	278,742	T	TA	Intergenic	1	1	1	1	1	1	1	1	1	1	1	1	1	1	1	5	5	5	1	1	1
tauB-II	287,067	G	C	Nonsynonymous	0	0	0	0	0	0	0	1	0	0	0	0	0	0	0	0	1	0	0.5	1	0.5
tauB-II	287,068	G	C	Nonsynonymous	0	0	0	0	0	0	0	1	0	0	0	0	0	0	0	0	1	0	0.5	1	0.5
envZ	302,935	G	C	Nonsynonymous	0	0	0	0	0	0	0	0	0	0	0	1	0	0	0	0	0	1	1	0.5	0.5
envZ	303,121	G	GGCT	Codon change/Codon insertion	0	0	0	0	0	0	0	0	0	0	1	1	1	0	0	0	0	3	1	0.083	0.08333
	308,738	C	T	Intergenic	0	1	0	0	1	0	0	0	0	0	0	0	0	0	0	2	0	0	0.22	0.222	1
	308,739	A	G	Intergenic	0	1	0	0	1	0	0	0	0	0	0	0	0	0	0	2	0	0	0.22	0.222	1
	336,298	T	A	Intergenic	0	0	0	0	0	0	0	1	0	0	0	0	0	0	0	0	1	0	0.5	1	0.5
	353,067	A	G	Intergenic	1	1	1	1	1	1	1	1	1	1	1	1	1	1	1	5	5	5	1	1	1

Gene name	Mutation position	REF	ALT	Effect	Mutation call															Total number of parallel mutations			p-values for association		
					Control					Ag^+ population					AgNP population										
					C1	C2	C3	C4	C5	C1	C2	C3	C4	C5	C1	C2	C3	C4	C5	Control	Ag^+	AgNP	Ag^+ vs Control	AgNP vs Control	AgNP vs Ag^+
	364,577	T	A	Intergenic	0	0	0	0	0	0	0	0	1	0	0	0	0	0	0	0	1	0	0.5	1	0.5
thiL	605,121	G	A	Nonsynonymous	0	0	0	0	0	0	0	1	0	0	0	0	0	0	0	0	1	0	0.5	1	0.5
thiL	605,126	A	T	Nonsynonymous	0	0	0	0	0	0	0	1	0	0	0	0	0	0	0	0	1	0	0.5	1	0.5
thiL	605,131	T	C	Synonymous	0	0	0	0	0	0	0	1	0	0	0	0	0	0	0	0	1	0	0.5	1	0.5
	661,588	C	T	Intergenic	0	0	0	0	0	0	1	0	0	0	0	0	0	0	0	0	1	0	0.5	1	0.5
	786,604	T	C	Intergenic	0	0	0	0	0	0	0	0	0	0	0	0	0	0	1	0	0	1	1	0.5	0.5
hemH	863,376	A	T	Synonymous	0	0	1	1	0	1	0	1	0	0	0	0	1	0	0	2	2	1	1	0.583	0.5833
	975,287	A	T	Intergenic	0	0	0	0	0	1	0	0	0	0	0	0	0	0	0	0	1	0	0.5	1	0.5
	975,288	A	T	Intergenic	0	0	0	0	0	1	0	0	0	0	0	0	0	0	0	0	1	0	0.5	1	0.5
PP_0861	999,625	C	G	Nonsynonymous	0	0	0	0	0	1	0	0	0	0	0	0	0	0	0	0	1	0	0.5	1	0.5
PP_0904	1,044,757	CAGCACGGCTGCCTGT	C	Codon change/Codon deletion	0	0	0	0	0	0	0	0	0	0	0	0	0	1	0	0	0	1	1	0.5	0.5

Gene name	Mutation position	REF	ALT	Effect	Mutation call															Total number of parallel mutations			p-values for association		
					Control					Ag^+ population					AgNP population										
					C1	C2	C3	C4	C5	C1	C2	C3	C4	C5	C1	C2	C3	C4	C5	Control	Ag^+	AgNP	Ag^+ vs Control	AgNP vs Control	AgNP vs Ag^+
		ATGGCA																							
	1,159,239	T	G	Intergenic	0	0	0	0	0	0	0	1	0	0	1	0	0	0	0	0	1	1	0.5	0.5	1
	1,184,536	GC	G	Intergenic	0	0	0	0	0	1	0	0	0	0	0	0	0	0	0	0	1	0	0.5	1	0.5
xcpY	1,202,854	A	C	Nonsynonymous	0	0	0	0	0	1	0	0	0	0	0	0	0	0	0	0	1	0	0.5	1	0.5
dtcD-II	1,221,046	C	A	Nonsynonymous	1	0	0	0	0	0	0	0	0	0	0	0	0	0	0	1	0	0	0.5	0.5	1
PP_16SE	1,326,938	G	A	Intragenic	1	0	0	0	0	1	1	1	1	1	0	0	0	0	0	1	5	0	0.02381	0.5	0.003968
PP_1175	1,350,104	C	A	Stop lost/Splice site region	0	0	0	0	0	1	0	0	0	0	0	0	0	0	0	0	1	0	0.5	1	0.5
PP_1175	1,350,119	A	G	Synonymous	0	0	0	1	0	0	0	0	0	0	0	0	0	0	0	1	0	0	0.5	0.5	1
PP_1195	1,370,775	GGGTCGAAAA	G	Codon change/Codon deletion	0	0	0	0	0	0	0	0	0	0	0	0	0	0	1	0	0	1	1	0.5	0.5
PP_1256	1,435,822	A	T	Nonsynonymous	0	0	0	0	0	0	0	0	1	0	0	0	0	0	0	0	1	0	0.5	1	0.5

Gene name	Mutation position	REF	ALT	Effect	Mutation call															Total number of parallel mutations			p-values for association		
					Control					Ag^+ population					AgNP population										
					C1	C2	C3	C4	C5	C1	C2	C3	C4	C5	C1	C2	C3	C4	C5	Control	Ag^+	AgNP	Ag^+ vs Control	AgNP vs Control	AgNP vs Ag^+
	1,499,497	T	TC	Intergenic	0	0	1	0	1	0	1	0	0	1	0	0	1	1	0	2	2	2	1	1	1
PP_1325	1,511,070	T	A	Nonsynonymous	0	0	0	0	0	0	0	0	0	0	0	0	1	0	0	0	0	1	1	0.5	0.5
ftsZ	1,503,160	C	T	Nonsynonymous	0	0	0	0	0	0	1	0	0	0	1	1	1	1	1	0	1	5	0.5	0.004	0.02381
ftsZ	1,530,173	A	C	Stop lost/Splice site region	1	1	1	1	1	1	1	1	1	1	0	0	0	0	0	5	5	0	1	0.004	0.003968
PP_1344	1,531,780	G	T	Nonsynonymous	0	0	0	0	0	0	0	0	0	0	0	0	1	0	0	0	0	1	1	0.5	0.5
	1,617,777	C	T	Intergenic	0	0	0	0	0	0	0	0	0	0	1	0	0	0	0	0	0	1	1	0.5	0.5
	1,617,782	C	G	Intergenic	0	0	0	0	0	0	0	0	0	0	1	0	0	0	0	0	0	1	1	0.5	0.5
	1,777,419	G	A	Intergenic	0	1	0	0	1	1	1	0	1	1	1	1	0	0	1	2	4	3	0.29	0.603	0.5833
	1,777,422	C	A	Intergenic	0	1	0	0	1	1	1	0	1	1	1	1	0	0	0	2	4	2	0.29	1	0.2857
	1,777,428	G	A	Intergenic	0	1	0	0	1	1	1	0	1	1	1	0	0	0	0	2	4	1	0.29	0.583	0.1071
	1,780,067	C	T	Intergenic	0	1	0	0	0	1	1	0	0	0	0	0	1	0	0	1	2	1	0.58	1	0.5833
	1,838,142	G	A	Intergenic	0	0	0	0	0	0	0	0	1	0	0	0	0	0	0	0	1	0	0.5	1	0.5
gacS	1,843,091	A	C	Nonsynonymous	1	1	1	0	1	1	1	1	1	1	0	0	0	0	1	4	5	1	1	0.107	0.02381
gacS	1,843,901	C	T	Nonsynonymous																0	0	0	1	1	1
gacS	1,844,166	T	A	Stop gained	0	0	0	0	0	0	1	0	0	0	1	1	1	1	0	0	1	4	0.5	0.02381	0.1071
PP_1666	1,863,240	T	A	Nonsynonymous	0	0	0	0	0	0	0	0	0	0	0	0	1	0	0	0	0	1	1	0.5	0.5
PP_1666	1,863,278	G	C	Nonsynonymous	0	0	1	0	0	0	0	0	0	0	0	0	0	0	0	1	0	0	0.5	0.5	1
PP_1703	1,901,761	A	T	Nonsynonymous	0	0	0	0	0	0	0	1	0	0	0	0	0	0	0	0	1	0	0.5	1	0.5
	2,051,065	T	A	Intergenic	1	0	0	0	0	0	1	1	1	0	0	0	0	0	0	1	3	0	0.29	0.5	0.08333
	2,063,185	C	G	Intergenic	0	0	0	0	0	1	0	0	0	0	0	0	0	0	0	0	1	0	0.5	1	0.5
	2,068,151	A	T	Intergenic	0	0	0	0	0	0	0	0	1	0	0	0	0	0	0	0	1	0	0.5	1	0.5
	2,068,152	A	T	Intergenic	0	0	0	0	0	0	0	0	1	0	0	0	0	0	0	0	1	0	0.5	1	0.5
	2,069,557	T	C	Intergenic	1	0	0	0	0	1	1	1	0	1	1	1	0	0	0	1	4	2	0.11	0.583	0.2857

Gene name	Mutation position	REF	ALT	Effect	Mutation call															Total number of parallel mutations			p-values for association		
					Control					Ag^+ population					AgNP population										
					C1	C2	C3	C4	C5	C1	C2	C3	C4	C5	C1	C2	C3	C4	C5	Control	Ag^+	AgNP	Ag^+ vs Control	AgNP vs Control	AgNP vs Ag^+
	2,087,422	C	T	Intergenic	0	0	0	0	0	0	1	0	0	0	0	0	0	1	0	0	1	1	0.5	0.5	1
	2,087,428	G	A	Intergenic	1	0	0	0	0	0	1	0	0	1	1	0	1	0	0	1	2	2	0.58	0.583	1
	2,087,439	G	A	Intergenic	0	0	0	0	0	0	1	0	0	0	0	0	0	0	0	0	1	0	0.5	1	0.5
	2,087,463	G	A	Intergenic	0	0	0	0	0	0	1	0	0	0	0	0	0	0	0	0	1	0	0.5	1	0.5
	2,087,635	T	C	Intergenic	0	0	0	0	1	1	0	1	0	0	0	0	1	0	0	1	2	1	0.58	1	0.5833
PP_5491	2,187,722	GT	G	Intergenic	0	0	0	0	0	0	1	0	0	0	0	0	0	0	0	0	1	0	0.5	1	0.5
	2,256,267	C	T	Intergenic	0	0	0	0	0	0	0	0	0	0	0	0	1	0	0	0	0	1	1	0.5	0.5
	2,256,290	C	T	Intergenic	0	0	0	0	0	0	0	0	0	0	0	0	1	0	0	0	0	1	1	0.5	0.5
PP_2068	2,354,379	T	G	Nonsynonymous	0	0	0	1	0	0	0	0	0	0	0	0	0	0	0	1	0	0	0.5	0.5	1
	2,414,802	C	G	Intergenic	0	0	0	0	0	0	0	0	0	0	0	0	1	0	0	0	0	1	1	0.5	0.5
	2,550,588	A	G	Intergenic	0	0	0	0	0	0	0	0	0	1	0	0	0	0	0	0	1	0	0.5	1	0.5
PP_2397	2,742,917	C	T	Nonsynonymous	0	0	0	0	0	1	0	0	0	0	0	0	0	0	0	0	1	0	0.5	1	0.5
PP_2397	2,742,918	A	G	Nonsynonymous	0	0	0	0	0	1	0	0	0	0	0	0	0	0	0	0	1	0	0.5	1	0.5
PP_2478	2,824,518	A	C	Nonsynonymous	0	0	0	0	1	0	0	0	0	0	0	0	0	0	0	1	0	0	0.5	0.5	1
	2,935,858	C	G	Intergenic	0	0	0	0	0	0	0	0	0	0	0	0	1	0	0	0	0	1	1	0.5	0.5
PP_2638	3,021,030	A	T	Nonsynonymous	0	0	1	0	0	0	0	1	0	0	1	0	0	1	0	1	1	2	1	0.583	0.5833
pp_2757	3,141,492	GT	G	Frame shift	0	0	0	0	0	0	0	0	0	0	0	1	0	0	0	0	0	1	1	0.5	0.5
PP_2758	3,142,272	C	T	Nonsynonymous	0	0	0	0	0	0	0	0	0	0	1	1	1	1	0	0	0	4	1	0.02381	0.02381
PP_3045	3,430,349	G	C	Synonymous	0	0	0	0	0	0	0	0	0	0	0	0	1	0	0	0	0	1	1	0.5	0.5
PP_3221	3,656,539	T	G	Synonymous	0	0	0	0	0	0	0	0	0	0	1	0	0	0	0	0	0	1	1	0.5	0.5
PP_5743/ PP_3334	3,774,247	C	G	Intragenic	1	0	0	0	0	1	0	0	0	0	0	0	0	0	0	1	1	0	1	0.5	0.5
oprN	3,881,829	A	T	Nonsynonymous	0	1	0	0	0	0	0	0	0	0	0	0	0	0	0	1	0	0	0.5	0.5	1

Gene name	Mutation position	REF	ALT	Effect	Mutation call															Total number of parallel mutations			p-values for association		
					Control					Ag^+ population					AgNP population										
					C1	C2	C3	C4	C5	C1	C2	C3	C4	C5	C1	C2	C3	C4	C5	Control	Ag^+	AgNP	Ag^+ vs Control	AgNP vs Control	AgNP vs Ag^+
	4,022,306	G	C	Intergenic	0	0	0	1	0	1	1	1	1	0	1	0	1	1	0	1	4	3	0.11	0.286	0.5833
	4,022,307	G	C	Intergenic	0	0	0	1	0	1	1	1	1	0	1	0	1	1	0	1	4	3	0.11	0.286	0.5833
	4,022,806	C	G	Intergenic	1	0	0	0	0	1	0	1	0	0	0	0	1	1	0	1	2	2	0.58	0.583	1
	4,022,807	C	G	Intergenic	1	0	0	0	0	1	0	1	0	0	1	1	1	1	0	1	2	4	0.58	0.107	0.2857
PP_3563	4,042,322	T	G	Nonsynonymous	0	0	0	0	0	0	1	0	0	0	0	0	0	0	0	0	1	0	0.5	1	0.5
PP_3573	4,053,476	A	T	Nonsynonymous	0	1	0	0	1	0	0	1	0	0	0	0	1	0	0	2	1	1	0.58	0.583	1
	4,293,218	G	C	Intergenic	0	0	0	0	0	0	0	0	0	0	1	0	0	0	0	0	0	1	1	0.5	0.5
yrpB	4,353,296	C	G	Nonsynonymous	0	0	0	0	0	0	0	1	0	0	1	0	0	0	0	0	1	1	0.5	0.5	1
clpA	4,518,633	C	T	Nonsynonymous	0	0	0	0	0	0	0	0	0	0	0	0	0	0	1	0	0	1	1	0.5	0.5
idh	4,522,716	G	A	Nonsynonymous	0	0	1	0	0	0	0	0	0	0	0	0	0	0	0	1	0	0	0.5	0.5	1
malQ	4,568,619	C	G	Synonymous	1	0	0	0	0	0	0	0	0	0	0	0	0	0	0	1	0	0	0.5	0.5	1
mccB	4,990,049	T	C	Nonsynonymous	0	0	0	0	0	0	0	0	0	0	1	0	0	0	0	0	0	1	1	0.5	0.5
uvrY	4,635,590	T	C	Nonsynonymous	1	1	1	1	1	1	1	1	1	1	0	0	0	0	1	5	5	1	1	0.02381	0.02381
PP_5662	4,741,229	A	C	Intergenic	1	1	1	0	1	1	1	1	1	0	1	1	1	1	1	4	4	5	1	1	1
PP_5662	4,741,231	C	G	Intergenic	1	1	1	0	1	1	1	1	0	0	1	1	1	1	1	4	3	5	0.58	1	0.2222
PP_5662	4,741,234	C	T	Intergenic	1	1	1	0	1	1	1	1	1	0	1	1	1	1	1	4	4	5	1	1	1
PP_5662	4,741,236	G	T	Intergenic	1	1	1	0	1	1	1	1	1	0	1	1	1	1	1	4	4	5	1	1	1
PP_5662	4,741,237	C	G	Intergenic	1	1	1	0	1	1	1	1	1	0	1	1	1	1	1	4	4	5	1	1	1
PP_5662	4,741,239	A	G	Intergenic	1	1	1	0	1	1	1	1	1	0	1	1	1	1	1	4	4	5	1	1	1
PP_5662	4,741,243	G	T	Intergenic	1	1	1	0	1	1	1	1	1	0	1	1	1	1	1	4	4	5	1	1	1
PP_5662	4,741,244	C	G	Intergenic	1	1	1	0	1	1	1	1	1	0	1	1	1	1	1	4	4	5	1	1	1
PP_5662	4,741,245	A	C	Intergenic	1	1	1	0	1	1	1	1	1	0	1	1	1	1	1	4	4	5	1	1	1
PP_5662	4,741,255	C	T	Intergenic	1	1	1	0	1	1	1	1	1	0	1	1	1	1	1	4	4	5	1	1	1
PP_5662	4,741,257	A	C	Intergenic	1	1	1	0	1	1	1	1	1	0	1	1	1	1	1	4	4	5	1	1	1
	4,741,260	C	G	Intergenic	1	1	1	0	1	1	1	1	1	0	1	1	1	1	1	4	4	5	1	1	1

Gene name	Mutation position	REF	ALT	Effect	Mutation call															Total number of parallel mutations			p-values for association		
					Control					Ag^+ population					AgNP population										
					C1	C2	C3	C4	C5	C1	C2	C3	C4	C5	C1	C2	C3	C4	C5	Control	Ag^+	AgNP	Ag^+ vs Control	AgNP vs Control	AgNP vs Ag^+
	4,741,261	A	C	Intergenic	1	1	1	0	1	1	1	1	1	0	1	1	1	1	1	4	4	5	1	1	1
	4,741,263	A	C	Intergenic	1	1	1	0	1	1	1	1	1	0	1	1	1	1	1	4	4	5	1	1	1
	4,741,272	A	G	Intergenic	1	1	1	0	1	1	1	1	1	0	1	1	1	1	1	4	4	5	1	1	1
	4,741,274	A	C	Intergenic	1	1	1	0	1	1	1	1	1	0	1	1	1	1	1	4	4	5	1	1	1
	4,741,276	G	C	Intergenic	1	1	1	0	1	1	1	1	1	0	1	1	1	1	1	4	4	5	1	1	1
	4,741,278	C	T	Intergenic	1	1	1	0	1	1	1	1	1	0	1	1	1	1	1	4	4	5	1	1	1
	4,741,283	C	CT	Intergenic	1	1	1	0	1	1	1	1	1	0	1	1	1	1	1	4	4	5	1	1	1
	4,741,289	C	G	Intergenic	1	1	1	0	1	1	1	1	1	0	1	1	1	1	1	4	4	5	1	1	1
	4,741,292	C	T	Intergenic	1	1	1	0	1	1	1	1	1	0	1	1	1	1	1	4	4	5	1	1	1
	4,741,294	C	G	Intergenic	1	1	1	0	1	1	1	1	1	0	1	1	1	1	1	4	4	5	1	1	1
	4,741,296	A	C	Intergenic	1	1	1	0	1	1	1	1	1	0	1	1	1	1	1	4	4	5	1	1	1
	4,741,298	C	T	Intergenic	1	1	1	0	1	1	1	1	1	0	1	1	1	1	1	4	4	5	1	1	1
	4,808,166	GAGCGCCGCCCGC	G	Intergenic	0	0	0	0	0	0	0	1	0	0	0	0	0	0	0	0	1	0	0.5	1	0.5

Gene name	Mutation position	REF	ALT	Effect	Mutation call															Total number of parallel mutations			p-values for association		
					Control					Ag^+ population					AgNP population										
					C1	C2	C3	C4	C5	C1	C2	C3	C4	C5	C1	C2	C3	C4	C5	Control	Ag^+	AgNP	Ag^+ vs Control	AgNP vs Control	AgNP vs Ag^+
		GA																							
	4,861,127	A	G	Intergenic	0	0	0	0	0	0	0	0	0	0	0	0	1	0	0	0	0	1	1	0.5	0.5
	4,861,219	C	T	Intergenic	0	0	0	0	0	1	1	0	0	0	1	0	0	1	0	0	2	2	0.22	0.222	1
ccmE	4,914,726	T	A	Nonsynonymous	0	0	0	0	0	0	0	0	0	0	1	0	0	0	0	0	0	1	1	0.5	0.5
	4,945,198	C	G	Intergenic	0	0	1	0	0	1	0	0	0	0	1	0	0	0	1	1	1	2	1	0.583	0.5833
	4,945,201	C	G	Intergenic	0	0	1	0	0	1	0	0	0	0	1	0	0	0	0	1	1	1	1	1	1
	4,945,389	G	C	Intergenic	1	0	0	0	0	0	1	0	0	0	0	1	0	0	0	1	1	1	1	1	1
	4,945,392	G	C	Intergenic	1	0	0	0	0	0	1	0	0	0	0	1	0	0	0	1	1	1	1	1	1
fliF	4,960,263	C	A	Nonsynonymous	0	0	0	0	0	0	0	0	0	0	0	0	0	0	1	0	0	1	1	0.5	0.5
flgK	4,974,437	CAG	AG	Frameshift																0	0	0	1	1	1
astB	5,087,105	A	T	Nonsynonymous	0	0	0	0	0	0	0	0	0	0	0	1	0	1	0	0	0	2	1	0.222	0.2222
	5,119,601	A	G	Intergenic	0	0	0	0	0	0	0	0	0	0	0	1	0	0	0	0	0	1	1	0.5	0.5
	5,257,856	T	C	Intergenic	0	0	0	0	0	1	0	0	0	0	0	0	0	0	0	0	1	0	0.5	1	0.5
	5,459,560	T	G	Intergenic	0	0	0	0	0	0	1	0	0	0	0	0	0	0	0	0	1	0	0.5	1	0.5
	5,459,561	C	A	Intergenic	0	0	0	0	0	0	1	0	0	0	0	0	0	0	0	0	1	0	0.5	1	0.5
	5,509,759	C	T	Intergenic	0	0	0	0	0	0	0	0	0	0	0	0	0	1	0	0	0	1	1	0.5	0.5
hisZ	5,559,943	T	A	Nonsynonymous	0	0	0	0	0	1	0	0	0	0	0	0	0	0	0	0	1	0	0.5	1	0.5
PP_4941	5,623,261	A	T	Nonsynonymous	0	0	0	0	0	0	0	0	0	0	1	0	0	0	0	0	0	1	1	0.5	0.5
	5,692,563	C	T	Intergenic	0	0	0	0	0	0	0	0	0	0	1	0	0	0	0	0	0	1	1	0.5	0.5
	5,743,331	G	A	Intergenic	0	0	0	0	0	0	0	0	0	0	0	1	0	0	0	0	0	1	1	0.5	0.5
	5,743,335	T	C	Intergenic	0	0	0	0	0	0	0	0	0	0	0	1	0	0	0	0	0	1	1	0.5	0.5
	5,743,390	G	A	Intergenic	0	0	0	0	0	1	0	0	0	0	0	0	0	0	0	0	1	0	0.5	1	0.5

Gene name	Mutation position	REF	ALT	Effect	Mutation call																Total number of parallel mutations			p-values for association		
					Control					Ag^+ population					AgNP population											
					C1	C2	C3	C4	C5	C1	C2	C3	C4	C5	C1	C2	C3	C4	C5	Control	Ag^+	AgNP	Ag^+ vs Control	AgNP vs Control	AgNP vs Ag^+
	5,743,394	T	C	Intergenic	0	0	0	0	0	1	0	0	0	0	0	0	0	0	0	0	1	0	0.5	1	0.5
metW	5,821,897	T	A	Nonsynonymous	1	0	0	0	0	0	0	0	0	0	0	0	0	0	0	1	0	0	0.5	0.5	1
ubiH	5,931,283	C	G	Nonsynonymous	0	0	0	0	0	0	0	0	0	0	0	0	0	0	1	0	0	1	1	0.5	0.5
	5,988,760	C	G	Intergenic	0	0	0	0	0	0	0	0	0	0	0	1	0	1	0	0	0	2	1	0.222	0.2222
	5,988,763	C	G	Intergenic	0	0	0	0	0	0	0	0	0	0	0	1	0	1	0	0	0	2	1	0.222	0.2222
	5,988,803	G	T	Intergenic	0	0	0	0	0	1	1	0	0	0	0	0	0	0	0	0	2	0	0.22	1	0.2222
	5,988,889	C	A	Intergenic	0	0	0	1	1	1	0	0	0	0	1	0	1	0	1	2	1	3	0.58	0.603	0.2857
	5,988,894	C	T	Intergenic	0	0	0	1	1	1	0	0	0	0	1	0	1	0	1	2	1	3	0.58	0.603	0.2857
	5,988,895	A	G	Intergenic	0	0	0	1	1	1	0	0	0	0	1	0	1	0	1	2	1	3	0.58	0.603	0.2857
	5,988,905	T	C	Intergenic	1	0	0	1	0	1	0	1	0	1	0	1	1	0	1	2	3	3	0.6	0.603	1
	5,988,910	CA	C	Intergenic	1	0	0	1	0	1	0	1	0	1	0	1	1	0	1	2	3	3	0.6	0.603	1
	5,988,951	G	C	Intergenic	0	1	1	1	1	1	1	1	0	0	1	1	0	1	1	4	3	4	0.58	1	0.5833
	5,988,954	G	C	Intergenic	0	1	1	1	1	1	1	1	0	0	1	1	1	1	1	4	3	5	0.58	1	0.2222
copA	6,132,511	C	T	Nonsynonymous	0	0	0	0	1	1	0	0	0	1	0	0	0	1	0	1	2	1	0.58	1	0.5833
copA	6,131,525	T	C	Nonsynonymous	0	0	0	0	0	1	0	0	1	0	1	0	1	1	0	0	2	3	0.22	0.083	0.6032
copA	6,132,542	A	G	Synonymous	0	0	0	0	0	0	0	0	0	0	1	0	0	0	0	0	0	1	1	0.5	0.5

Appendix 3 List of mutations in the coding regions for the populations in main evolution experiment

List of mutations in the coding regions for the 15 populations and corresponding gene products. The gene name, codon substrate and amino acid change were obtained by aligning the reads from the evolved populations to the *Pseudomonas putida* KT2440 reference genome [271, 272]. The annotations of product type, EC number and product were extracted from MicroScope platform [271]. The capitalized bases in the codon substrate are the changed nucleotides. The mutations called were marked in red. The p-values ≤0.05 are marked in red.

Gene name	Mutation Position	Product type	EC Number	Product	Codon substrate	Amino acid change	Mutation call														p-value for comparison of total mutant number		
							Control					Ag^+ population					AgNP population							
							C1	C2	C3	C4	C5	C1	C2	C3	C4	C5	C1	C2	C3	C4	C5	Ag^+ vs Control	AgNP vs Control	Ag^+ vs AgNP
PP_0174	226226	N/A	N/A	Conserved protein of unknown function	cTg/cAg	L151Q	0	0	0	0	0	0	0	0	1	0	0	0	0	0	0	0.5	1	0.5
PP_0188	240531	Putative enzyme	N/A	Putative uroporphyrin-III C-methyltransferase	Gcc/Ccc	A276P	1	0	0	0	0	0	0	0	0	0	0	0	0	0	0	0.5	0.5	1
PP_0188	240536	Putative enzyme	N/A	Putative uroporphyrin-III C-methyltransferase	ggG/ggC	G277	1	0	0	0	0	0	0	0	0	0	0	0	0	0	0	0.5	0.5	1
tauB-II	287067	Transporter	3.6.3.36	Taurine transporter subunit ; ATP-binding component of ABC superfamily	cCg/cGg	P19R	0	0	0	0	0	0	0	1	0	0	0	0	0	0	0	0.5	1	0.5
tauB-II	287068	Transporter	3.6.3.36	Taurine transporter subunit ; ATP-binding component of ABC superfamily	Ccg/Gcg	P19A	0	0	0	0	0	0	0	1	0	0	0	0	0	0	0	0.5	1	0.5
envZ	302935	Regulator	N/A	Osmolarity sensor protein EnvZ,sensory histidine kinase in two-component regulatory system with OmpR	gGt/gCt	G367A	0	0	0	0	0	0	0	0	0	0	0	1	0	0	0	1	0.5	0.5
envZ	303121	Regulator	N/A	Osmolarity sensor protein EnvZ,sensory histidine kinase in two-component regulatory system with OmpR	ccg/cTGCcg	P433LP	0	0	0	0	0	0	0	0	0	0	1	1	1	0	0	1	0.0833	0.0833

Gene name	Mutation Position	Product type	EC Number	Product	Codon substrate	Amino acid change	Mutation call															p-value for comparison of total mutant number		
							Control					Ag^+ population					AgNP population							
							C1	C2	C3	C4	C5	C1	C2	C3	C4	C5	C1	C2	C3	C4	C5	Ag^+ vs Control	AgNP vs Control	Ag^+ vs AgNP
thiL	605121	Enzyme	2.7.4.16	Thiamine monophosphate kinase	cGc/cAc	R145H	0	0	0	0	0	0	0	1	0	0	0	0	0	0	0	0.5	1	0.5
thiL	605126	Enzyme	2.7.4.16	Thiamine monophosphate kinase	Agc/Tgc	S147C	0	0	0	0	0	0	0	1	0	0	0	0	0	0	0	0.5	1	0.5
thiL	605131	Enzyme	2.7.4.16	Thiamine monophosphate kinase	ggT/ggC	G148	0	0	0	0	0	0	0	1	0	0	0	0	0	0	0	0.5	1	0.5
hemH	863376	Enzyme	4.99.1.1	Ferrochelatase	gcA/gcT	A170	0	0	1	1	0	1	0	1	0	0	0	0	1	0	0	1	0.5833	0.5833
PP_0861	999625	Receptor/putative transporter	N/A	Outer membrane ferric siderophore receptor/TonB-dependent siderophore receptor	gGc/gCc	G182A	0	0	0	0	0	1	0	0	0	0	0	0	0	0	0	0.5	1	0.5
PP_0904	1044757	ORF of unknown function	N/A	InaA protein	ggctgcctgtatggcaagcacgta/gta	GCLYGKHV156V	0	0	0	0	0	0	0	0	0	0	0	0	0	1	0	1	0.5	0.5
xcpY	1202854	N/A	N/A	Type II secretion pathway protein XcpY	cAg/cCg	Q228P	0	0	0	0	0	1	0	0	0	0	0	0	0	0	0	0.5	1	0.5
dtcD-II	1221046	Regulator	N/A	C4-dicarboxylate transport transcriptional regulatory protein	gGc/gTc	G87V	1	0	0	0	0	0	0	0	0	0	0	0	0	0	0	0.5	0.5	1
PP_16SE	1326938	N/A	N/A	16S ribosomal RNA			1	0	0	0	0	1	1	1	1	1	0	0	0	0	0	0.0238	0.5	0.0039
PP_1175	1350104	ORF or unknown function	N/A	Conserved protein of unknown function (fragment)	taG/taT	*32Y	0	0	0	0	0	1	0	0	0	0	0	0	0	0	0	0.5	1	0.5
PP_1175	1350119	ORF or unknown function	N/A	Conserved protein of unknown function (fragment)	agT/agC	S27	0	0	0	1	0	0	0	0	0	0	0	0	0	0	0	0.5	0.5	1
PP_1195	1370775	ORF of	N/A	Conserved exported protein of	gaaaaggtc	EKVE53	0	0	0	0	0	0	0	0	0	0	0	0	0	0	1	1	0.5	0.5

Gene name	Mutation Position	Product type	EC Number	Product	Codon substrate	Amino acid change	Mutation call															p-value for comparison of total mutant number		
							Control					Ag^+ population					AgNP population							
							C1	C2	C3	C4	C5	C1	C2	C3	C4	C5	C1	C2	C3	C4	C5	Ag^+ vs Control	AgNP vs Control	Ag^+ vs AgNP
		unknown function		unknown function	gag/gag	5E																		
PP_1256	1435822	Putative enzyme	1.2.1.26	Putative alpha-ketoglutarate semialdehyde dehydrogenase	Tgc/Agc	C48S	0	0	0	0	0	0	0	0	1	0	0	0	0	0	0	0.5	1	0.5
PP_1325	1511070	Lipoprotein	N/A	Putative lipoprotein	cAg/cTg	Q166L	0	0	0	0	0	0	0	0	0	0	0	0	1	0	0	1	0.5	0.5
ftsZ	1530160	Cell process	N/A	GTP-binding tubulin-like cell division protein	Cgt/Tgt	R395C	0	0	0	0	0	0	1	0	0	0	1	1	1	1	1	0.5	0.0039	0.0238
ftsZ	1530173	Cell process	N/A	GTP-binding tubulin-like cell division protein	tAa/tCa	*399S	1	1	1	1	1	1	1	1	1	1	0	0	0	0	0	1	0.0039	0.0039
PP_1344	1531780	ORF of unknown function	N/A	Conserved protein of unknown function	Ccc/Acc	P36T	0	0	0	0	0	0	0	0	0	0	0	0	1	0	0	1	0.5	0.5
gacS	1843091	N/A	2.7.13.3	Sensor protein GacS	gTg/gGg	V568G	1	1	1	0	1	1	1	1	1	1	0	0	0	0	1	1	0.1071	0.0238
gacS	1844166	N/A	2.7.13.3	Sensor protein GacS	Aag/Tag	K210*	0	0	0	0	0	0	1	0	0	0	1	1	1	1	0	0.5	0.0238	0.1071
PP_1666	1863240	ORF of unknown function	N/A	Conserved exported protein of unknown function	cTg/cAg	L309Q	0	0	0	0	0	0	0	0	0	0	0	0	1	0	0	1	0.5	0.5
PP_1666	1863278	ORF of unknown function	N/A	Conserved exported protein of unknown function	Gcg/Ccg	A322P	0	0	1	0	0	0	0	0	0	0	0	0	0	0	0	0.5	0.5	1
PP_1703	1901761	Enzyme	1.7.99.4	Assimilatory nitrate reductase/sulfite reductase	gAc/gTc	D787V	0	0	0	0	0	0	0	1	0	0	0	0	0	0	0	0.5	1	0.5
PP_5491	2187722	ORF of unknown function	N/A	Conserved protein of unknown function with SEC-C motif domain			0	0	0	0	0	0	1	0	0	0	0	0	0	0	0	0.5	1	0.5
PP_2068	2354379	N/A	N/A	Putative Multidrug efflux MFS	aaA/aaC	K51N	0	0	0	1	0	0	0	0	0	0	0	0	0	0	0	0.5	0.5	1

Gene name	Mutation Position	Product type	EC Number	Product	Codon substrate	Amino acid change	Mutation call															p-value for comparison of total mutant number		
							Control					Ag^+ population					AgNP population							
							C1	C2	C3	C4	C5	C1	C2	C3	C4	C5	C1	C2	C3	C4	C5	Ag^+ vs Control	AgNP vs Control	Ag^+ vs AgNP
				membrane fusion protein																				
PP_2397	2742917	N/A	N/A	EF hand domain protein	Cac/Tac	H5Y	0	0	0	0	0	1	0	0	0	0	0	0	0	0	0	0.5	1	0.5
PP_2397	2742918	N/A	N/A	EF hand domain protein	cAc/cGc	H5R	0	0	0	0	0	1	0	0	0	0	0	0	0	0	0	0.5	1	0.5
PP_2478	2824518	N/A	N/A	Putative Isoquinoline 1-oxidoreductase, beta subunit	gAg/gCg	E44A	0	0	0	0	1	0	0	0	0	0	0	0	0	0	0	0.5	0.5	1
PP_2638	3021030	N/A	N/A	Putative Cellulose synthase operon C protein	cAg/cTg	Q523L	0	0	1	0	0	0	0	1	0	0	1	0	0	1	0	1	0.5833	0.5833
PP_2757	3141492	N/A	N/A	Putative Sugar-binding protein, similar to periplasmic binding protein/LacI transcriptional regulator	gtc/	V137	0	0	0	0	0	0	0	0	0	0	0	1	0	0	0	1	0.5	0.5
PP_2758	3142272	N/A	N/A	Putative Ribose ABC transporter, periplasmic ribose-binding protein	gCg/gTg	A74V	0	0	0	0	0	0	0	0	0	0	1	1	1	1	0	1	0.0238	0.0238
PP_3045	3430349	N/A	N/A	Putative ClpP protease	tcG/tcC	S189	0	0	0	0	0	0	0	0	0	0	0	0	1	0	0	1	0.5	0.5
PP_3221	3656539	N/A	N/A	ABC transporter, permease protein	ccA/ccC	P253	0	0	0	0	0	0	0	0	0	0	1	0	0	0	0	1	0.5	0.5
PP_5743 /PP_3334	3774247	Putative membrane component/putative regulator	N/A	Putative TonB-dependent receptor protein/putative lysR family transcriptional regulator (fragment)			1	0	0	0	0	1	0	0	0	0	0	0	0	0	0	1	0.5	0.5
oprN	3881829	N/A	N/A	Multidrug efflux RND outer membrane protein OprN	cAg/cTg	Q163L	0	1	0	0	0	0	0	0	0	0	0	0	0	0	0	0.5	0.5	1
PP_3563	4042322	ORF of unknown function	N/A	Conserved exported protein of unknown function	cTc/cGc	L137R	0	0	0	0	0	0	1	0	0	0	0	0	0	0	0	0.5	1	0.5

Gene name	Mutation Position	Product type	EC Number	Product	Codon substrate	Amino acid change	Mutation call															p-value for comparison of total mutant number		
							Control					Ag^+ population					AgNP population							
							C1	C2	C3	C4	C5	C1	C2	C3	C4	C5	C1	C2	C3	C4	C5	Ag^+ vs Control	AgNP vs Control	Ag^+ vs AgNP
PP_3573	4053476	N/A	N/A	Putative monooxygenase/ similar to FAD-dependent oxidoreductase	cAg/cTg	Q17L	0	1	0	0	1	0	0	1	0	0	0	0	1	0	0	0.5833	0.5833	1
yrpB	4353296	Enzyme	1.13.12.16	2-nitropropane dioxygenase	cCg/cGg	P141R	0	0	0	0	0	0	0	1	0	0	1	0	0	0	0	0.5	0.5	1
clpA	4518633	Enzyme	3.4.21.92	ATP-dependent serine protease, chaperone activity/class III stress response-related ATPase, AAA+ superfamily	gGc/gAc	G296D	0	0	0	0	0	0	0	0	0	0	0	0	0	0	1	1	0.5	0.5
idh	4522716	Enzyme	1.1.1.-	Isocitrate dehydrogenase	Gca/Aca	A189T	0	0	1	0	0	0	0	0	0	0	0	0	0	0	0	0.5	0.5	1
malQ	4568619	Enzyme	2.4.1.25	4-alpha-glucanotransferase	gcC/gcG	A183	1	0	0	0	0	0	0	0	0	0	0	0	0	0	0	0.5	0.5	1
mccB	4590049	Enzyme	6.4.1.4	Methylcrotonyl-CoA carboxylase biotin-containing subunit beta	gTc/gCc	V244A	0	0	0	0	0	0	0	0	0	0	1	0	0	0	0	1	0.5	0.5
uvrY	4635590	Regulator	N/A	Two-componenent system BarA/UvrY - regulatory subunit	Aaa/Gaa	K56E	1	1	1	1	1	1	1	1	1	1	0	0	0	0	1	1	0.0238	0.0238
ccmE	4914726	Factor	N/A	Cytochrome c-type biogenesis protein CcmE	cAg/cTg	Q142L	0	0	0	0	0	0	0	0	0	0	1	0	0	0	0	1	0.5	0.5
fliF	4960263	Structure	N/A	Flagellar M-ring protein	Ggc/Tgc	G70C	0	0	0	0	0	0	0	0	0	0	0	0	0	0	1	1	0.5	0.5
astB	5087105	Enzyme	3.5.3.23	N-succinylarginine dihydrolase	cTg/cAg	L73Q	0	0	0	0	0	0	0	0	0	0	0	1	0	1	0	1	0.2222	0.2222
hisZ	5559946	Enzyme	2.4.2.17	Histidyl-tRNA synthetase-like component of ATP phophoribosyltransferase	cAg/cTg	Q185L	0	0	0	0	0	1	0	0	0	0	0	0	0	0	0	0.5	1	0.5
PP_4941	5623261	ORF or unknown function	N/A	Conserved exported protein of unknown function	caT/caA	H159Q	0	0	0	0	0	0	0	0	0	0	1	0	0	0	0	1	0.5	0.5

Gene name	Mutation Position	Product type	EC Number	Product	Codon substrate	Amino acid change	Mutation call															p-value for comparison of total mutant number		
							Control					Ag^+ population					AgNP population							
							C1	C2	C3	C4	C5	C1	C2	C3	C4	C5	C1	C2	C3	C4	C5	Ag^+ vs Control	AgNP vs Control	Ag^+ vs AgNP
metW	5821897	Enzyme	N/A	Methionine biosynthesis protein MetW	cTg/cAg	L173Q	1	0	0	0	0	0	0	0	0	0	0	0	0	0	0	0.5	0.5	1
ubiH	5931283	Enzyme	1.14.-.-	2-octaprenyl-6-methoxyphenol hydroxylase, FAD/NAD(P)-binding	Gtt/Ctt	V263L	0	0	0	0	0	0	0	0	0	0	0	0	0	0	1	1	0.5	0.5
copA	6132511	Transporter	N/A	Copper resistance protein A	Ggc/Agc	G448S	0	0	0	0	1	1	0	0	0	1	0	0	0	1	0	0.5833	1	0.5833
copA	6131525	Transporter	N/A	Copper resistance protein A	gAg/gGg	E443G	0	0	0	0	0	1	0	0	1	0	1	0	1	1	0	0.2222	0.0833	0.6032
copA	6132542	Transporter	N/A	Copper resistance protein A	gaT/gaC	D437	0	0	0	0	0	0	0	0	0	0	1	0	0	0	0	1	0.5	0.5